Mixtures of ultracold fermions in optical potentials

Oleksandr Fialko

Lehrstuhl für Theoretische Physik II
Universität Augsburg

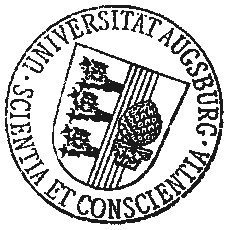

Augsburg, April 2010

Erstgutachter:	Prof. Dr. Klaus Ziegler
Zweitgutachter:	Prof. Dr. Gert-Ludwig Ingold
Tag der mündlichen Prüfung:	11 Juni 2010

Contents

Chapter 1

Introduction

The experimental achievement of the Bose-Einstein condensation in ultracold dilute gases has opened a new chapter in atomic and molecular physics [6,19,25]. The end of the last century was enlightened by the study of these weakly interacting Bose gases [70,84,86]. In recent years, the attention of experimentalists and theorists was devoted to the study of strongly interacting atoms either in free space or in an optical potential [18]. Ultracold atoms loaded to a periodic optical potential can simulate the condensed matter phenomena or the solid state theory free of any imperfections [49]. In chapter 2 we review the basic physics of the Bose-Einstein condensation and briefly sketch the physics of two-body scattering at low energies. We end up the chapter by explaining what an optical potential is. There the Bose-Hubbard model is introduced, which describes the physics of a Bose gas confined in an optical lattice.

The classical example of theoretical treatment of the Bose-Einstein condensation is the Gross-Pitaevskii equation, which is valid for the weakly interacting dilute Bose gas in free space. This nonlinear equation has proven capable of accounting for many experimentally measured quantities in Bose-Einstein condensed gases. It describes not only the ground state but also quasiparticle excitations around it. It is introduced in chapter 3. Here, as an example, we apply this equation to attractive particles confined in a ring geometry and see that for large attractions the solution of the Gross-Pitaevskii equation does not represent an appropriate approximation to the exact ground state. As explained further, in order to describe strongly interacting bosons one has to resort to other methods and models.

Everything in nature is made of fermions. They interact via exchanging bosons. This is the basic of the so called Standard model. The playground of this view spreads far beyond quantum field theory of interactions. For instance, the explanation of superconductivity of metals relies on the pic-

ture where two electrons are constituents of a composite boson, called a Cooperon [14]. So, bosons themselves can be represented as composite particles, made of two fermions with different internal degrees of freedom. It appears that such tightly bound fermions behave as hard-core bosons due to the Pauli exclusion principle and thus are strongly interacting. It is thus tempting to study attractive fermions and, in the limit where there are no single fermions but all of them are paired up to form bosonic molecules, they can serve as an attempt to the study of strong interactions, which are missing in the Gross-Pitaevskii equation as mentioned above. Thus, attractive fermions may serve as a platform to study two apparently distinctive physics (governed by their distinct statistics) of bosons and fermions on the unified background. In chapter 4 we study a model of tightly bound fermionic pairs in an optical lattice. We solve it by means of powerful field theoretical functional integral approach. We draw a mean-field ground state phase diagram, which comprises of empty, condensed and Mott insulating states. We further investigate the fate of quantum fluctuations around the ground state in order to calculate the spectral properties of these states. We calculate the excitation spectrum of quasiparticles, an experimentally accessible structure factor and the superfluid density. Then, we derive an effective Gross-Pitaevskii equation in the weakly interacting regime. To relate our system to experimental investigations we also study interference pattern across the superfluid-Mott insulator transition in the trap, which is sensitive to the fourth order correlations among fermions. In the end, we set a connection between our model and the quantum XY model as well as with the Heisenberg model.

The quantum statistics at low temperatures plays a major role in the behavior of ultracold atoms. This was the main motivation for experimentalists and theorists to orient towards the study of Fermi gases shortly after the advent of the Bose gases had started [48]. By means of the magnetic Feshbach resonance it became possible to tune interaction among Fermi atoms at will [31]. There is a smooth crossover between weakly attracting fermions in two hyperfine internal states (spin-1/2 fermions) in the BCS state and tightly bound fermions in the BEC phase in free space (BCS-BEC crossover). In chapter 5 we introduce a model to study attractive spin-1/2 fermions in a lattice. In the strongly attractive limit we reproduce the paired fermions model considered in chapter 4. We set a connection between our lattice model and the model of the BCS-BEC crossover in free space introduced in the literature. We study the ground state properties for equal as well as unequal spin populations of fermions. We calculate density profiles of this system superimposed by a harmonic trapping potential. To this end we derive nonlinear field equations and solve them

numerically by the relaxation method. Further, we investigate quantum fluctuations and calculate an experimentally accessible spectral function.

In chapter 6 we consider a mixture of repulsive fermions with unequal masses in two dimensions. The light atoms tunnel in an optical lattice and are scattered from the heavy atoms localized on lattice sites. The distribution of the heavy atoms can be controlled by the interaction strength between two species and temperature. By varying them, the system may undergo the celebrated Anderson localization transition of the light atoms [7]. To study this scenario we apply the transfer matrix numerical approach and calculate the localization length as well as critical exponents.

The appendices at the end of the thesis contain the details of the calculations, made in the main text.

Chapter 2

Physics of ultracold quantum gases

In this chapter we consider the generic phenomenon, which is the key to understanding of other phenomena occurring in nature (e.g. superfluidity and superconductivity), the Bose-Einstein condensation. The two-body elastic scattering at low energies and the physics in an optical potential are then briefly discussed.

2.1 Bose-Einstein condensation

When matter is cooled down to very low temperature new and rich physics emerges. The approach into the Kelvin regime was rewarded with the discovery of superconductivity of ^{80}Hg in 1911 and of superfluidity of ^{4}He in 1938. Cooling into the microkelvin range revealed superfluidity of ^{3}He in 1972. Recently, the invention of laser cooling and subsequent evaporative cooling has helped achieving the nanokelvin regime where quantum-degenerate gases, such as Bose-Einstein condensates of alkali gases, were explored experimentally in 1995. A brief overview of these developments can be found in Ref. [10].

It turns out that in all these seemingly different phenomena the particle statistics, effects of quantum mechanics and their interactions rather than the study of single atoms play the major role. These are many-body systems and their collective nature gives rise to the effects observed in the experiments mentioned above. From modern point of view the core ingredient of explanation is the phenomenon of Bose-Einstein condensation.

Particle statistics: The particle statistics emerges as a consequence of the famous theorem of the quantum field theory, which states that the total wave function of any many-particle system must be even under the interchange

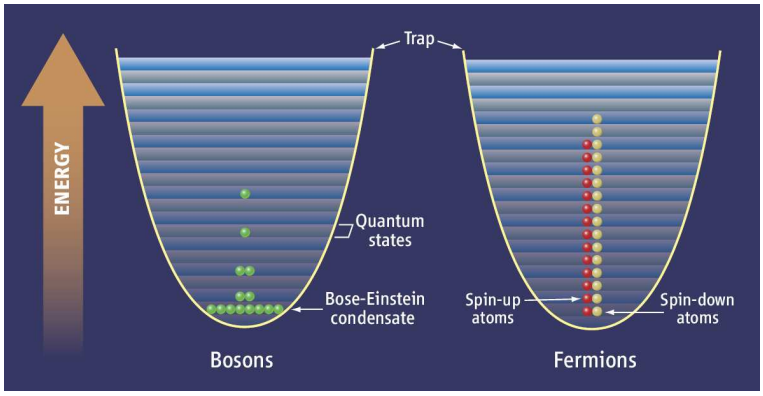

Figure 2.1: Trapped bosons and fermions. While bosons may condense, fermions form the Fermi sea. Taken from [24].

of all the coordinates of any two bosons of identical type, and odd under interchange of any two identical fermions. Being seemingly innocent, this result has profound effect on the behavior of quantum many-body systems consisting of bosons or fermions. It turns out that in the special case of non-interacting particles that can occupy one of the energy levels denoted by $\epsilon_{\mathbf{k}}$ and are in thermal equilibrium, the above statement leads to a single particle distribution [65]:

$$n(\epsilon_{\mathbf{k}}, T, \mu) = \frac{1}{e^{\beta(\epsilon_{\mathbf{k}}-\mu)} \pm 1}, \tag{2.1}$$

where μ is the chemical potential, which controls the total number of particles, N, via the condition $\sum_{\mathbf{k}} n(\epsilon_{\mathbf{k}}, T, \mu) = N$. Sign $+(-)$ refers to fermions (bosons). The minus sign (i.e., the case of bosons) plays a crucial role. In this case A. Einstein predicted the occurrence of the phase transition when a macroscopic fraction of atoms condense into the ground state of the system below a critical temperature T_c [32]. This is quite different from the case of fermions: There are at most two fermions with different spin states (we assume the total spin of a fermion is $1/2$) per each energy level up to Fermi level, ϵ_{F}, at zero temperature due to Pauli exclusion principle. The two cases are shown in Fig. 2.1.

The critical temperature of condensation for bosons with mass m and density n in three dimensions reads [68]:

$$k_{\mathrm{B}} T_c \approx 3.31 n^{2/3} \hbar^2 / m, \tag{2.2}$$

while in a symmetric harmonic trap with frequency ω_0 also in three di-

mensions it is

$$k_{\mathrm{B}}T_c \approx 0.94N^{1/3}\hbar\omega_0. \tag{2.3}$$

It is interesting that in both cases T_c is of the order of the corresponding Fermi temperature $\sim \epsilon_{\mathrm{F}}/k_{\mathrm{B}}$. This apparent coincidence is the effect of the quantum mechanics [68,71].

Quantum mechanics: The novelty brought by quantum mechanics to our understanding of the world is the necessity to ascribe particle-wave attributes, which are given by the celebrated de Broglie relation

$$\lambda = h/p, \tag{2.4}$$

where λ is the wavelength of a particle with momentum p [65]. Like optics can be divided into geometrical optics with wavelength of an electromagnetic wave being much smaller than device measuring it and physical optics with wavelength comparable to the device, the particle or wave nature can reveal itself depending on λ given above. If $\lambda > d$, where d is a separation between atoms in a gas, then wave-like picture arises and quantum mechanics aspects enter the scene of the consideration. In thermal equilibrium we write $p \approx (2mk_{\mathrm{B}}T)^{1/2}$. Approximating $d \sim n^{-1/3}$ we get the condition

$$k_{\mathrm{B}}T < n^{2/3}\hbar^2/m \tag{2.5}$$

for the wave nature to prevail. We see that Eq. (2.5) and Eq. (2.2) give the same order for the critical temperature. The similar lines of arguments can be applied for the trapped condensate by noticing that by energetics $k_{\mathrm{B}}T$ should be less than the separation between levels in that trap, i.e. $k_{\mathrm{B}}T < \hbar\omega_0$.

In most experiments with trapped BEC, densities ranges between 10^{-14} and 10^{-15} cm^{-3}. Substituting the mass m of ^{87}Rb or ^{23}Na to the above equation implies the temperature, which lies in the nanokelvin regime.

Interactions: Interactions between atoms play an important role. They lead to a plethora of phenomena not seen in the non-interacting case. Bose gas is sensible to the sign of the interaction. If the latter is attractive, then the system is unstable and the condensate may turn into a fragmented condensate, where few single energy levels are macroscopically populated, or even collapses. On the other hand, repulsive interaction favors condensation and even increases the critical temperature. Moreover, interactions make BEC a rich many-body system which displays phenomena such as superfluidity. In the case of fermions, as it is well known, attraction leads to the formation of Cooper pairing, which leads in turn to superconductivity. When repulsive atoms are superimposed by an optical lattice, they

may form a Mott insulating state, which is a result of interactions rather than a filled Bloch band. We thus turn to the consideration of the two-body scattering at low temperatures.

2.2 Two-body scattering at low temperatures

Here again, we distinguish the effect of quantum mechanics from the effect of quantum statistics. The effect of quantum mechanics amounts to considering the low energy scattering. The latter is substantiated by the fact that the temperature is small and thus the kinetic energy of particles is small. We consider the scattering of two particles of masses m_1 and m_2 in a central potential $\hat{V}$. We assume that particles have no internal degrees of freedom and are distinguishable. We transform the two coordinates of the two particles into the center-of-mass and relative coordinates, respectively. Then the wave function is the product of the plane wave of the center-of-mass motion and that of the relative motion, which satisfies the Schrödinger equation with the reduced mass $m = m_1 m_2/(m_1 + m_2)$. The scattering is described by the latter as the sum of an incoming wave and a scattered wave, which is an outgoing spherical wave at large interatomic separation [65]:

$$\psi(r, \theta) = e^{ikz} + f(\theta)\frac{e^{ikr}}{r}. \tag{2.6}$$

Due to the spherical symmetry the scattering amplitude $f(\theta)$ depends only on the scattering angle θ. At very low energies it is sufficient to consider only s-wave scattering. In this case, there is no dependence on angle θ and the scattering amplitude becomes a constant, which we denote as $f(\theta) = -a_s$, where a_s is the scattering length. Physically, there is no enough energy to excite partial waves with $l > 0$ and the available state with $l = 0$ is spherically symmetric.

The scattering amplitude defines the cross section, i.e. the ratio of the total number of particles scattered, $\int \hbar k/mr^2 |f(\theta)|^2 dS_r$ (S_r is the cross section of the sphere with radius r), to the incident flux of particles, $\hbar k/m$,

$$\sigma = 4\pi a_s^2. \tag{2.7}$$

The cross section is used to express the likelihood of interaction among particles and has the dimension of area. We see that for very low temperatures, atoms effectively behave as hard-core spheres with radius a_s: There the cross section is also given by Eq. (2.7) [64].

The effect of quantum statistics amounts in considering of identical particles. The wave function must be symmetric under the interchange

of coordinates for bosons, and antisymmetric for fermions. We thus arrive at the symmetrized wave function [84]

$$\psi(r,\theta) = e^{ikz} \pm e^{-ikz} + (f(\theta) \pm f(\pi-\theta))\frac{e^{ikr}}{r}. \tag{2.8}$$

Here $+$ sign stands for bosons and $-$ sign stands for fermions. We immediately see that in the case of s-wave scattering the total cross section is $8\pi a^2$ for identical bosons and 0 for identical fermions. In words, at low temperatures identical fermions do not interact.

We denote the second term in Eq. (2.6) as ψ_{sc} (the subscript "sc" means "scattered") and the first term as ψ_{in} (here "in" means "incoming"). If we plug Eq. (2.6) into the Schrödinger equation, we can solve it for ψ_{sc}. The solution reads [84]

$$\psi_{sc} = \hat{G}_0 \hat{T} \psi_{in}, \tag{2.9}$$

where $\hat{G}_0$ is the free Green's matrix, while the scattering matrix $\hat{T}$ satisfies the Lippmann-Schwinger equation

$$\hat{T} = \hat{V} + \hat{V}\hat{G}_0\hat{T}. \tag{2.10}$$

At zero temperature it turns out that $\psi_{sc}(r) = -mT(0,0)/4\pi\hbar^2 r$ ($\hat{T}$ is expressed in momentum representation, $T(\mathbf{k},\mathbf{k}')$). From this it follows that the scattering length is $a_s = m/4\pi\hbar^2 T(0,0)$. For the contact potential $V(\mathbf{r}) = U\delta(\mathbf{r})$ we get the following equation for the scattering length

$$\frac{4\pi a_s \hbar^2}{m} = \left[\frac{1}{U} + \sum_{\mathbf{k}} \frac{1}{2\epsilon_{\mathbf{k}}}\right]^{-1}. \tag{2.11}$$

We emphasize that $V(\mathbf{r})$ is an effective potential, which reproduces a correct value of the scattering length of a true interatomic potential (the relation of the scattering length to a true interatomic potential is given in [51]).

In dilute gases usually the second term in the square bracket is ignored (as U is supposed to be small) and this is called the Born approximation. In this approximation we can express the scattering potential as

$$V(\mathbf{r}-\mathbf{r}') = \frac{4\pi a_s \hbar^2}{m}\delta(\mathbf{r}-\mathbf{r}'). \tag{2.12}$$

The scattering length can be tuned by the magnetic field. This effect is called the Feshbach resonance [18, 31]. This is one of the major tools of manipulation in the modern experiments on ultracold gases. The interaction can be tuned at will: it can be made effectively repulsive ($a_s > 0$) or attractive ($a_s < 0$).

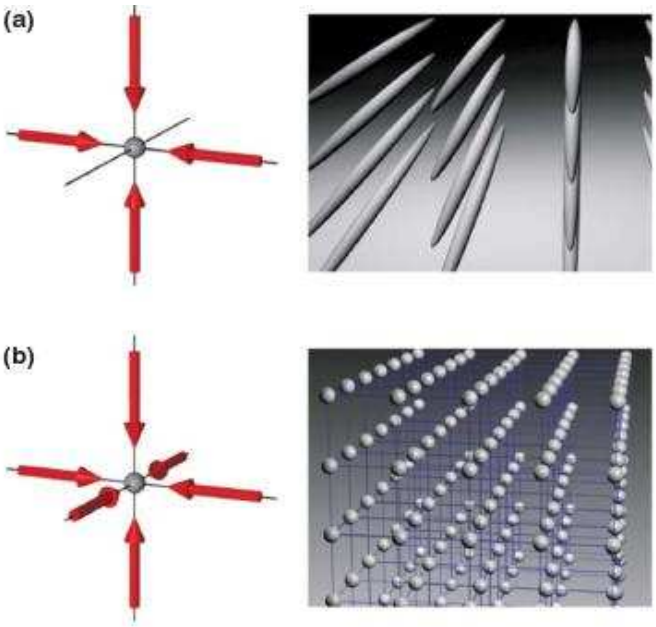

Figure 2.2: 2D and 3D optical lattices. Taken from [18].

2.3 Optical potentials

An optical potential is a useful tool to confine cold atoms by means of laser light. This can be an optical trap or a periodic lattice. The physical origin of the confinement in both cases is the dipole force. When atom is placed in an electric field its levels are shifted due to the Stark effect [65]. The atom acquires a dipole moment, which is proportional to the electric field, $\mathbf{p}(\mathbf{r}) = \alpha\mathbf{E}(\mathbf{r})$. Polarizability α can be calculated by means of quantum mechanics. What we are interested in here is that this dipole feels the force if placed in the electric field:

$$\mathbf{F} = \alpha\nabla|\mathbf{E}(\mathbf{r})|^2. \tag{2.13}$$

Usually, the electric field oscillates in time with frequency ω_l. If the time scale for the center-of-mass motion of the atom is much slower than ω_l^{-1}, then only the time averaged $|\mathbf{E}(\mathbf{r})|^2$ is taken and $\alpha \sim (\omega_0 - \omega_l)^{-1}$, where $\hbar\omega_0$ is the energy needed to excite the atom. If the trapping potential has the form of a parabola

$$V_{\mathrm{trap}}(\mathbf{r}) = \alpha|\mathbf{E}(\mathbf{r})|^2 \equiv \frac{\omega_{\mathrm{trap}}^2}{2}r^2, \tag{2.14}$$

then, for $\omega_0 > \omega_l$, the atom feels the attractive force towards the center (node) of the trap $\mathbf{F} \sim \alpha\mathbf{r}$. A typical value of trapping frequencies ω_{trap} in modern experiments is up to 100 kHz.

A periodic potential is generated by two counterpropagating laser beams. Due to their interference an optical standing wave is formed. A 3D optical lattice created by three perpendicular laser beams parallel to the coordinate axes is of the general form [18]

$$V_{\mathrm{latt}}(\mathbf{r}) = V_x \sin^2(q_x x) + V_y \sin^2(q_y y) + V_z \sin^2(q_z z), \tag{2.15}$$

where the amplitudes V_i are proportional to the intensity of the laser field and $q_i = 2\pi/\lambda_j$ with λ_j being the wavelength of the lasers. A 2D lattice (e.g. for $V_x = 0$, $V_y, V_z \neq 0$) has the form of parallel running tubes (cf. Fig. 2.2) and a 1D lattice (e.g. for $V_x = V_y = 0, V_z \neq 0$) has the form of parallel planes.

In the second quantization formalism the particles confined in a deep optical lattice are well described by the Bose-Hubbard Hamiltonian [58]

$$\hat{H} = -J \sum_{\langle i,j \rangle} \hat{b}_i^\dagger \hat{b}_j^\dagger + \sum_i \epsilon_i \hat{n}_i + \frac{1}{2} U \sum_i \hat{n}_i(\hat{n}_i - 1), \tag{2.16}$$

where the annihilation and creation operators $\hat{b}_i$ and $\hat{b}_i^\dagger$ obey the canonical commutation relations $[\hat{b}_i, \hat{b}_j^\dagger] = \delta_{ij}$. The first term describes the tunneling of bosons between adjacent sites, the second one corresponds to the onsite energy caused by the trapping potential (optical lattice) and the third one is responsible for the onsite pairwise interaction among bosons. Though there are some limits on the range of parameters in which the effective Hamiltonian takes the single-band Hubbard form [102]. The phase diagram is depicted in Fig. 4.2 [41]: There is a transition from a Mott insulator with integer number of bosons per lattice site to a superfuid phase with nonzero condensed density.

Chapter 3

Weakly interacting bosons

In this chapter we introduce the Gross-Pitaevskii equation for the weakly interacting Bose gas in free space. We also consider quasiparticle excitations derived from this equation. This will be needed for the next chapter, where the effect of strong interaction will be considered and thus compared to that of the weak interaction elucidated in this chapter. Finally, as an example, we present an attractive Bose gas confined in a ring. The latter was the subject of a project lead by Dr. Ofir E. Alon at the Minerva summer school [1].

3.1 Gross-Pitaevskii equation

In the current experiments on the Bose-Einstein condensation, a Bose gas is prepared at extremely low densities in order to prevent it from liquefaction or solidification. Thus the gas is dilute and weakly interacting. For the latter to be true the following condition must be satisfied

$$na_s^3 \ll 1, \tag{3.1}$$

where n is the density and a_s is the scattering length. Physically, this condition states that the interparticle separation in the gas is much larger than the scattering length. There are two commonly used approaches to describe a weakly interacting Bose gas. These are the Bogoliubov theory and the Gross-Pitaevskii theory. We would like to mention here that the Gross-Pitaevskii theory is the limit of the Bogoliubov theory, where terms of the order $(na_s^3)^{1/2}$ can be neglected [67]. We will need to derive the condensed density and the excitation spectrum in the dilute Bose gas and the Gross-Pitaevskii theory suffices for this purpose, since the results agree with the

[1] www.mpipks-dresden.mpg.de/∼lmi07/

corresponding results of the Bogoliubov theory in this limit (see [94] on the Bogoliubov theory).

The condensation means that all bosons reside in a single particle state and thus this state is macroscopically occupied. The condensate can be thus described by a macroscopic wave function $\Psi(\mathbf{r}, t)$ normalized to the total number of particles

$$\int d\mathbf{r}|\Psi(\mathbf{r})|^2 = N. \tag{3.2}$$

Here $|\Psi(\mathbf{r})|^2$ measures the density of the condensate. The Gross-Pitaevskii equation for the dynamics of such condensate of bosons with mass m with the pairwise interaction as in Eq. (2.12) reads [84]

$$i\hbar\frac{\partial\Psi(\mathbf{r},t)}{\partial t} = -\frac{\hbar^2}{2m}\nabla^2\Psi(\mathbf{r},t) + V_{\text{ext}}\Psi(\mathbf{r},t) + \frac{4\pi a_s\hbar^2}{m}|\Psi(\mathbf{r},t)|^2\Psi(\mathbf{r},t). \tag{3.3}$$

This equation is similar to the Schrödinger equation. The only difference is the presence of the last term, which describes the two-particle interaction. The effect of many particles is described by the macroscopic wave function $\Psi(\mathbf{r}, t)$. On the other hand, the equation looks like a nonlinear Schrödinger equation of a single particle. This is an example when the wave function has a classical significance, since it is macroscopic and its effects can be seen on a large scale (e.g. by direct visualization of the density profile [8]).

We would like to find a stationary solution $\Psi_0(\mathbf{r}, t)$ by setting

$$\Psi_0(\mathbf{r}, t) = e^{-i\mu t/\hbar}\Psi_0(\mathbf{r}). \tag{3.4}$$

Moreover, we consider small fluctuations around the stationary solution to study dynamical effects near equilibrium

$$\Psi(\mathbf{r}, t) = \Psi_0(\mathbf{r}, t) + \delta\Psi(\mathbf{r}, t). \tag{3.5}$$

It is convenient to seek an oscillatory solution $\delta\Psi(\mathbf{r}, t) = e^{-i\mu t/\hbar}[u(\mathbf{r})e^{-i\omega t} + v(\mathbf{r})e^{i\omega t}]$. Substituting Eq. (3.5) into Eq. (3.3) we get

$$\hbar\omega\sigma_3\vec{u}(\mathbf{r}) = [(\hat{H}_0 + 2\gamma n_0(\mathbf{r}))\sigma_0 + \gamma n_0(\mathbf{r})\sigma_1]\vec{u}(\mathbf{r}), \tag{3.6}$$

where $\vec{u}(\mathbf{r}) = (u(\mathbf{r}), v(\mathbf{r}))^{\mathrm{T}}$, $\hat{H}_0 = -\hbar^2/2m\nabla^2 + V_{\text{ext}}$, $\gamma = 4\pi a_s\hbar^2/m$, $n(\mathbf{r}) = |\Psi_0(\mathbf{r})|^2$. Assuming that for the stationary solution $n(\mathbf{r}) = n_0 = \text{const.}$ and looking for a wave solution by setting $\vec{u}(\mathbf{r}) \sim e^{i\mathbf{kr}}$, we arrive at the Bogoliubov spectrum

$$\hbar\omega = \sqrt{\epsilon_{\mathbf{k}}(\epsilon_{\mathbf{k}} + 2\gamma n_0)} \tag{3.7}$$

with $\epsilon_{\mathbf{k}} = \hbar^2 k^2/2m$. The condensate density n_0 should be calculated for a given external potential V_{ext}. If $V_{ext} = 0$, then $n_0 = \frac{\mu}{\gamma}$.

For small momentum $\hbar\omega \approx c_{\text{sound}} k$, where $c_{\text{sound}} = \sqrt{\hbar^2 \gamma n_0/m}$ is the sound velocity. It is called "sound" since it describes small density fluctuations with linear spectrum like for the sound waves in the air. The profound difference here from the non-interacting Bose gas is its spectrum, which is quadratic $\hbar\omega = \epsilon_{\mathbf{k}}$. Seemingly innocent difference in the spectrum leads to profound consequences. One of them is the effect of superfluidity.

Superfluidity is the most fascinating manifestation of collective phenomena displayed by condensed matter system. The most famous example is the helium liquids, which can flow up the walls of a vessel or propagate through porous media. Now we follow arguments given by L.Landau. Consider a flow of a fluid through a pipe with a uniform velocity $\mathbf{V}$ and kinetic energy E. We perform Galilean transformation into its own rest frame. Suppose the friction between the liquid and the walls creates excitations with energy $\tilde{\epsilon}_{\mathbf{k}}$ with respect to the rest frame. Transforming back to the laboratory frame, the energy of the fluid is

$$E \to E + \mathbf{kV} + \tilde{\epsilon}_{\mathbf{k}}. \tag{3.8}$$

So the creation of excitations is energetically favorable if the velocity of the fluid is large, $\mathbf{kV} + \tilde{\epsilon}_{\mathbf{k}} < 0$ or when $V > \{\tilde{\epsilon}_{\mathbf{k}}/k\}_{\min} \equiv V_c$. If $\tilde{\epsilon}_{\mathbf{k}} \sim k^2$ then $V_c = 0$ and the fluid is unstable towards creation of excitations and energy losses. If $\tilde{\epsilon}_{\mathbf{k}} \sim k$, $V_c \neq 0$ and at $V < V_c$ the fluid is superfluid. Thus a non-interacting gas is not superfluid while interactions lead to superfluidity.

3.2 Particles confined in a ring

The Gross-Pitaevskii equation (Eq. (3.3)) describes an interacting gas, which is Bose-Einstein condensed. The natural questions arise: a) whether a Bose-Einstein condensate occurs in an interacting system at all and b) whether the Gross-Pitaevskii equation can be used for strong interactions. There are strong qualitative arguments in favor of the occurrence, when the interparticle interactions are repulsive. On the other hand, if they are attractive the condensate is unstable. It may form a so called fragmented condensate. In this case not a single but several single particle states are macroscopically occupied. Moreover, it appears that the Gross-Pitaevskii equation gives wrong results for large interactions. Here we present an example of a situation when it can not describe a true ground state and gives rise to fragmentation. The problem was considered analytically in [59] and numerically in [2].

We consider bosons with mass m in a ring. This is a one-dimensional problem. The Gross-Pitaevskii equation reads (we set $\Psi(\theta,t)=\sqrt{N}\psi(\theta,t)$ in Eq. (3.3))

$$i\hbar\frac{\partial\psi(\theta,t)}{\partial t}=-\frac{\hbar^2}{2m}\frac{\partial^2\psi(\theta,t)}{\partial\theta^2}+\gamma N|\psi(\theta,t)|^2\psi(\theta,t), \tag{3.9}$$

where now the wave function depends on angle $\theta\in(0,2\pi]$, $\gamma=4\pi a_s\hbar/m$, N is the total number of particles such that the wave function is normalized as $\int_0^{2\pi}|\psi|d\theta=1$. Moreover, it is subjected to obvious boundary conditions $\psi(0)=\psi(2\pi)$. In the following we set $\hbar=1$ and we are looking for the stationary solution

$$\mu\psi_0(\theta)=-\frac{\hbar^2}{2m}\frac{\partial^2\psi_0(\theta)}{\partial\theta^2}+\gamma N|\psi_0(\theta)|^2\psi_0(\theta). \tag{3.10}$$

This is a nonlinear equation and we solve it as follows. We define a grid on the ring such that the kinetic energy is represented as a tridiagonal matrix $\hat{\mathbf{T}}$ and the wave function is represented as a vector $\vec{\psi}_0$. We also define a diagonal matrix $\hat{\mathbf{P}}$ whose diagonal element j is $|\vec{\psi}_0^j|^2$. Then we solve the following eigenvalue problem recursively

$$[\hat{\mathbf{T}}+2\pi\gamma\hat{\mathbf{P}}_{n-1}]\vec{\psi}_{0,n}=\mu\vec{\psi}_{0,n}, \tag{3.11}$$

starting from some initial $\vec{\psi}_{0,0}$ until $|\vec{\psi}_{0,n}-\vec{\psi}_{0,n-1}|^2$ becomes some small number. Here $\hat{\mathbf{P}}_{n-1}$ is made of $\vec{\psi}_{0,n-1}$ and we rescale $\gamma\to N\gamma/2\pi$. The total energy can be calculated as

$$E_{GP}=\vec{\psi}_0^T[\hat{\mathbf{T}}+\pi\gamma\hat{\mathbf{P}}]\vec{\psi}_0, \tag{3.12}$$

where the first term is the kinetic energy while the second term is the potential energy. In Fig. 3.1 the energies are calculated versus interaction strength γ. We see that at $\gamma=0.5$ something profound happens: There are kinks at this point. We calculate also eigenfunctions and plot them in Fig. 3.2. Here we see that for $\gamma<0.5$ the wave function possesses the axial symmetry of the ring geometry and this solution is an eigenfunction of the angular momentum with eigenvalue 0. But for $\gamma>0.5$ this symmetry is broken. Consequently, the solution does not present a good approximation for the ground state. To remedy this problem, a continuous configuration-interaction approach is applied. Within this approach the many-body ground state is approximated as [2]

$$\Phi(\vec{\theta})\sim\int_0^{2\pi}d\phi C(\phi)\Psi(\vec{\theta}-\phi) \tag{3.13}$$

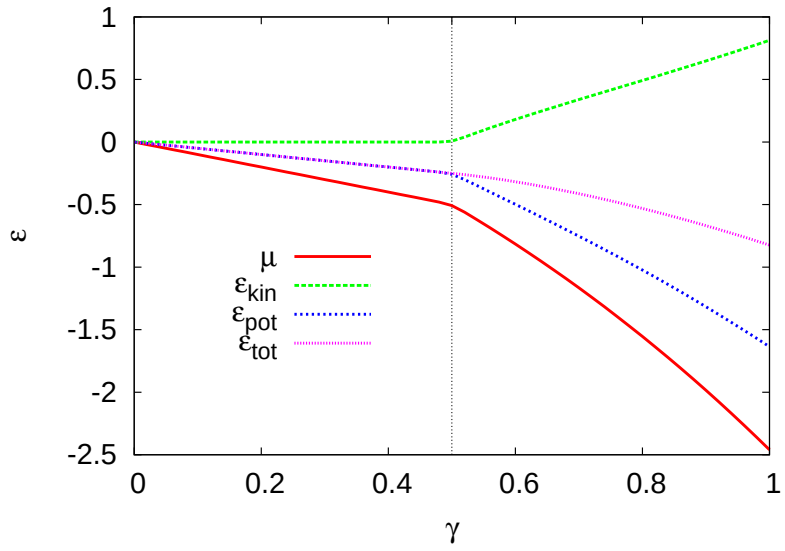

Figure 3.1: The chemical potential, the kinetic, the potential and the total energies. In each case a kink at $\gamma = 0.5$ is seen.

with $\Psi(\vec{\theta} - \phi) = \prod_i \psi_0(\theta_i - \phi)$, where ψ_0 are orbitals of the Gross-Pitaevskii equation. It turns out that for $C(\phi) = e^{il\phi}$ such an ansatz represents the solution with correct symmetry of the ground state. Then it appears that for large particle number we can define the probability p_l of occupation of a state with specific momentum l

$$p_l = |a_l|^2, \quad a_l = \frac{1}{2\pi} \int_0^{2\pi} d\theta \psi_0(\theta) e^{il\theta}. \tag{3.14}$$

We plot this quantity in Fig. 3.3. We clearly see that $\gamma = 0.5$ separates pure condensed state and fragmented states, where not only the state with $l = 0$ is occupied but states with higher l are occupied as well. This is the effect of fragmentation.

In summary, the Gross-Pitaevskii equation is appropriate for describing the Bose-Einstein condensation, if the interactions among particles is not strong. For larger interactions other methods and approaches are needed as, for example, the continuous configuration-interaction approach in a ring geometry explained briefly above or the Bogoliubov approximation for a repulsively interacting Bose gas. The reason is that the Gross-Pitaevskii theory does not give the depletion of the condensate, i.e. the relative difference between the condensed density and the total density of

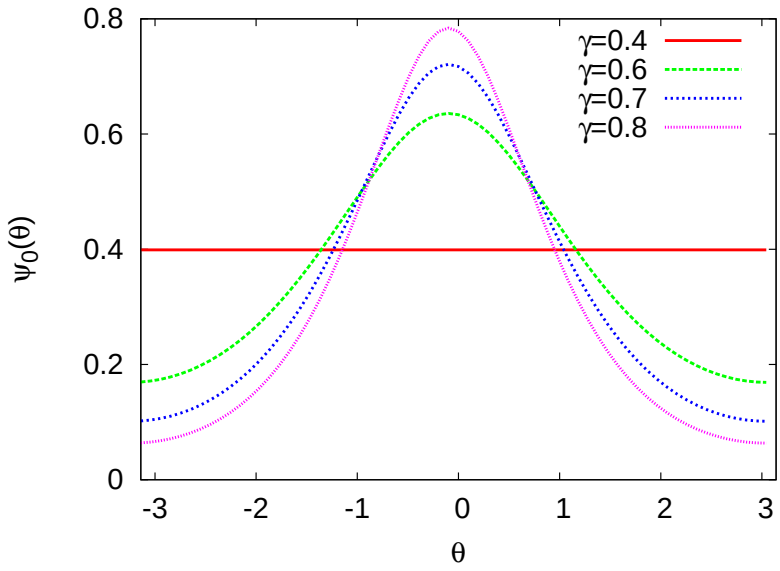

Figure 3.2: The solution of the Gross-Pitaevskii equation. For $\gamma > 0.5$ it does not possess the axial symmetry of the ring.

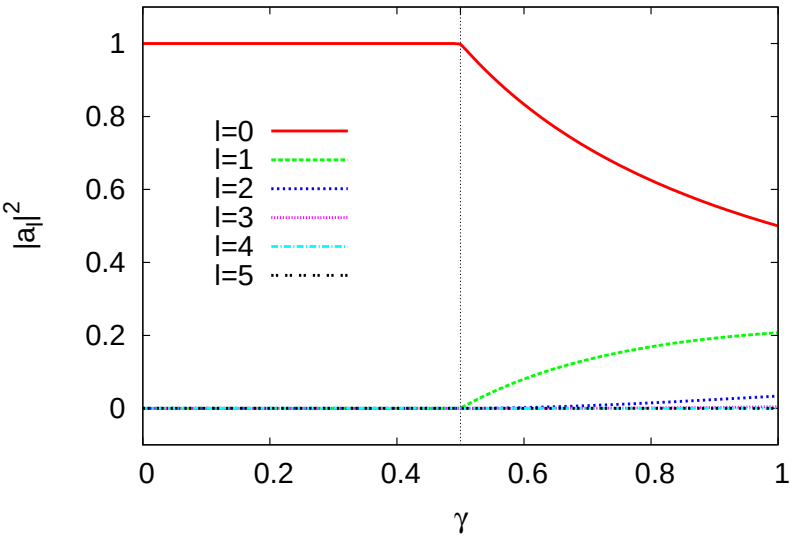

Figure 3.3: Occupations of the orbitals. Fragmentation occurs for $\gamma > 0.5$.

bosons caused by the interactions between bosons. On the other hand, the Bogoliubov approach does reveal the depletion provided it is small compared to 1. The Bogoliubov theory describes "more interacting" bosons than the Gross-Pitaevskii theory does. If placed in an optical lattice, strongly interacting bosons form a Mott insulating phase with one or more integer numbers of particles per each lattice site. This feature can not be explained within the Bogoliubov theory. A strongly interacting Bose gas in an optical lattice is the subject of the next chapter.

Chapter 4

Paired fermions

In this chapter we consider a dense Bose gas with hard-core interaction in an optical lattice. We study the phase diagram in terms of a special mean-field theory that describes Bose-Einstein condensate and a Mott insulator with a single particle per lattice site for zero as well as for nonzero temperature. We calculate the densities, the excitation spectrum, and the static structure factor for each of these phases. Partly, these results were published in Refs. [37, 38, 40, 76].

4.1 Model

The advent of optical lattices has opened an exciting field of physics. One of the consequences of the lattice is formation of lattice-commensurate ground states like the Mott insulating phase. For the latter the effect of strong interactions is crucial. The superfluid-Mott insulator transition in cold atoms in an optical lattice was theoretically proposed in [58] and experimentally observed in Ref. [50].

To describe the superfluid-Mott insulator transition, the Bose-Hubbard model presented in Eq. (2.16) is suitable. The two regimes, weak interaction and strong interaction regimes, require different approaches. In the former case the Bogoliubov approach is applicable, in the latter case the treatment is provided by the strong coupling expansion, i.e. by a perturbative expansion in t/U of Eq. (2.16). The both approaches are explained in Ref. [72].

We intend to construct a lattice model, which allows to be treated by a single approach and reveals the physics of a weakly interacting as well as strongly interacting Bose gas. Some approaches suitable for describing such systems have been considered in Ref. [76]. The extension of this model will be described in the next chapter and connected to the BCS-BEC

Figure 4.1: Paired-fermions in an optical lattice.

crossover of fermions in a lattice.

A hard-core boson can be represented by a pair of locally coupled spin-1/2 fermions (see Fig. 4.1). A creation operator of such a boson on lattice site i thus can be written as

$$\hat{b}_i^\dagger = \hat{c}_{i\uparrow}^\dagger \hat{c}_{i\downarrow}^\dagger, \tag{4.1}$$

where $\hat{c}_{i\sigma}^\dagger$ creates a fermion with spin σ on lattice site i and satisfies the following algebra

$$[\hat{c}_{j\sigma}, \hat{c}_{i\sigma'}^\dagger]_+ = \delta_{i,j}\delta_{\sigma,\sigma'}, \;\; [\hat{c}_{j\sigma}^\dagger, \hat{c}_{i\sigma'}^\dagger]_+ = [\hat{c}_{j\sigma}, \hat{c}_{i\sigma'}]_+ = 0. \tag{4.2}$$

It is easy to check that if all fermions are paired up, then hard-core Bose operators $\hat{b}_i^\dagger$ obey the Pauli spin-1/2 commutation relations, namely $[\hat{b}_i, \hat{b}_j^\dagger] = (1 - 2\hat{n}_i)\delta_{ij}$, $[\hat{b}_i, \hat{b}_j] = 0$, $(\hat{b}_i^\dagger)^2 = (\hat{b}_i)^2 = 0$, $\hat{b}_i^\dagger \hat{b}_i + \hat{b}_i \hat{b}_i^\dagger = 1$ and $\hat{n}_i = \hat{b}_i^\dagger \hat{b}_i$. These operators commute for different sites and anticommute on the same lattice site. The hard-core condition allows only one boson per lattice site. So we see that the operators $\hat{b}_j^\dagger$ possess the properties of bosons.

The Hamiltonian of the desired model reads [37]

$$\hat{H} = -\frac{J}{2d} \sum_{\langle r,r' \rangle} \hat{b}_r^\dagger \hat{b}_{r'} - \mu \sum_r \sum_{\sigma=\uparrow,\downarrow} \hat{c}_{r\sigma}^\dagger \hat{c}_{r\sigma}, \tag{4.3}$$

where J describes the rate of hopping of bosons through the lattice, μ is the chemical potential for fermions. It controls the number of particles in the grand canonical ensemble. The latter is given by the partition function

$$Z = \mathrm{Tr} e^{-\beta \hat{H}}. \tag{4.4}$$

The partition function can also be written in terms of a Grassmann integral as

$$Z = \int e^{-A(\bar{\psi},\psi)} \mathcal{D}[\bar{\psi}, \psi] \tag{4.5}$$

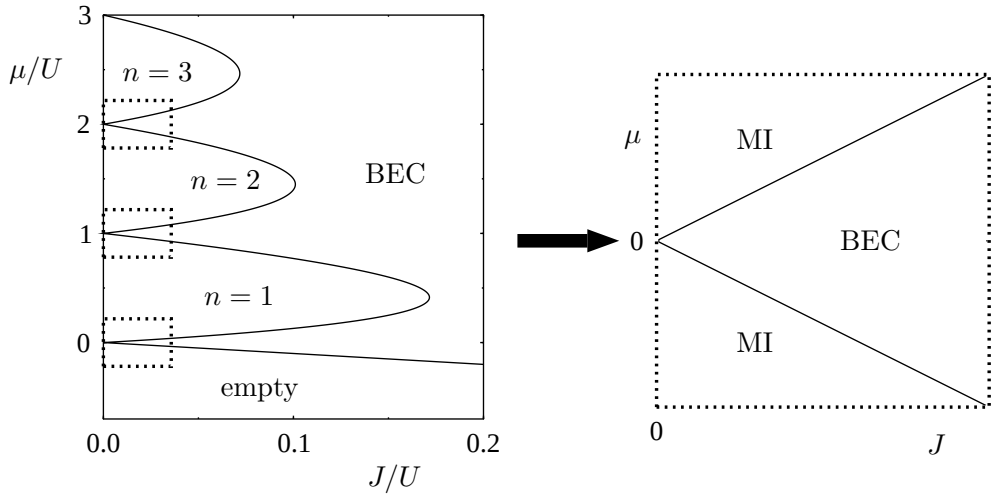

Figure 4.2: Right: the phase diagram of the Bose-Hubbard model. Left: paired-fermions model describes the point where two Mott lobes meet [37].

with imaginary time-dependent Grassmann fields $\psi, \bar{\psi}$ and the action

$$A = \int_0^\beta d\tau \left[\sum_r (\bar{\psi}_{r\tau\uparrow}\partial_t\psi_{r\tau\uparrow} + \bar{\psi}_{r\tau\downarrow}\partial_t\psi_{r\tau\downarrow}) - \mu \sum_r (\bar{\psi}_{r\tau+\delta\uparrow}\psi_{r\tau\uparrow} + \bar{\psi}_{r\tau+\delta\downarrow}\psi_{r\tau\downarrow}) \right.$$
$$\left. - \frac{J}{2d} \sum_{\langle r,r'\rangle} \bar{\psi}_{r\tau+\delta\uparrow}\psi_{r'\tau\uparrow}\bar{\psi}_{r\tau+\delta\downarrow}\psi_{r'\tau\downarrow} \right] \quad (4.6)$$

where δ should be sent to $+0$ at the end of calculations, τ is the imaginary time, the symbol $\partial_\tau\psi_\tau$ denotes the formal $\lim_{\delta\to+0}(\psi_{\tau+\delta} - \psi_\tau)$, $\beta \equiv (k_B T)^{-1}$ is the inverse temperature. It is expected that our hard-core bosons model corresponds to the Bose-Hubbard model (2.16) with on-site interaction U sent to ∞ as depicted in Fig. 4.2. But it allows us to study the phase transition within the same mean-field calculations, while at least two approaches are needed within the Bose-Hubbard model. We will return to this point later on.

4.2 Phase diagram

The action in Eq. (4.6) is expressed in terms of anticommuting Grassmann fields. Here we perform a Hubbard-Stratonovich transformation to ex-

press it in terms of complex fields. The Hubbard-Stratonovich transformation is not unique and should be chosen based on a particular physical problem under consideration. In Eq. (4.3) the fourth order term is the kinetic energy of bosons and we would like to decouple it into $\hat{b}_r^\dagger$ and $\hat{b}_{r'}$. We use the identity

$$\exp\left(\frac{J}{2d}\sum_{\langle r,r'\rangle}\bar{\psi}_{r\tau+\delta\uparrow}\psi_{r'\tau\uparrow}\bar{\psi}_{r\tau+\delta\downarrow}\psi_{r'\tau\downarrow}\right) = \int\mathcal{D}[\phi,\chi]\exp\left[-\sum_{r,r'}\bar{\phi}_{r\tau}\hat{v}^{-1}_{r,r'}\phi_{r'\tau}\right.$$
$$\left.-\frac{1}{S}\sum_r\bar{\chi}_{r\tau}\chi_{r\tau}-\sum_r(i\phi_{r\tau}+\chi_{r\tau})\bar{\psi}_{r\tau+\delta\uparrow}\bar{\psi}_{r\tau+\delta\downarrow}-\sum_r(i\bar{\phi}_{r\tau}+\bar{\chi}_{r\tau})\psi_{r\tau\uparrow}\psi_{r\tau\downarrow}\right] \quad (4.7)$$

In this formula, we have introduced new complex fields ϕ and χ. The physical nature of these fields will become clear in the next chapter, where we will generalize our model to that which describes BCS-BEC crossover in a lattice. Formally the auxiliary field χ and a free parameter S are needed to make the hopping matrix positive definite in order to perform Gaussian integration in Eq. (4.7). The expression

$$\hat{v}_{r,r'} = \frac{J}{2d}\delta_{|r-r'|,1} + S\delta_{r,r'} \quad (4.8)$$

has been introduced. The free parameter S is not physical and we will show that it disappears in the final results.

Substituting expression in Eq. (4.7) into Eq. (4.6) and integrating out Grassmann fields, we arrive at an effective but so far an exact action in terms of complex fields:

$$A_{\text{eff}} = \int_0^\beta d\tau\left\{\sum_{r,r'}\bar{\phi}_{r\tau}\hat{v}^{-1}_{r,r'}\phi_{r'\tau}+\frac{1}{S}\sum_r\bar{\chi}_{r\tau}\chi_{r\tau}-\log\det\hat{\mathbf{G}}^{-1}\right\}. \quad (4.9)$$

Here the matrix $\hat{\mathbf{G}}$ gives an effective boson-boson interaction as we will see later on and it is expressed in the so called Nambu-Gorkov representation as

$$\hat{\mathbf{G}}^{-1} = \begin{pmatrix} -i\phi-\chi & \partial_\tau+\mu \\ \partial_\tau-\mu & i\bar{\phi}+\bar{\chi}\end{pmatrix}. \quad (4.10)$$

From now onwards the partition function reads

$$Z = \int e^{-A_{\text{eff}}(\phi,\chi)}\mathcal{D}[\phi,\chi]. \quad (4.11)$$

The Hamiltonian of the system (Eq. (4.3)) is invariant with respect to a global gauge transformation $\hat{c}_{\sigma,i}\rightarrow e^{i\theta}\hat{c}_{\sigma,i}$, which is the consequence of

conservation of the total number of particles. The effective bosonic action possesses also this symmetry, namely it is invariant under $\phi \to e^{i\theta}\phi$, $\chi \to e^{i\theta}\chi$. A conventional phase transition is characterized by the breaking of a particular symmetry of the Hamiltonian. We will apply a saddle-point approximation to break the above gauge invariance, known also as the $U(1)$ symmetry, to get a phase transition (see also [94] on this account).

In the following, we make the replacement $\mu \to \mu/2$, such that μ plays the role of the chemical potential of the molecules. We can perform a saddle-point integration to calculate physical quantities. From a physical point of view we have to minimize our action to get the classical trajectory (the macroscopic wavefunction) of our system. It will appear also that the Free energy of the system will be minimazied as well, which is required by the thermodynamics as long as we consider a many-body problem. This approach proved to be fruitful in a wide range of applications [3]. Fluctuations around this solution are also important and they describe quasiparticle excitations above a ground state. In order to proceed within a mean-field approximation, we assume that quantum fluctuations are small and postpone the consideration of fluctuations till the next section.

Minimization of the action gives us two coupled linear equations between the complex fields ϕ and χ:

$$\delta A_{\text{eff}} = 0 \;\; \Rightarrow \;\; \left\{ \begin{array}{l} \phi = (J+S)G(\phi - i\chi) \\ \chi = -iSG(\phi - i\chi) \end{array} \right. , \tag{4.12}$$

where

$$G = \frac{1}{\beta}\sum_{\omega_n} \frac{1}{|\phi|^2 J^2/(J+S)^2 + \mu^2/4 + \omega_n^2} \tag{4.13}$$

with $\omega_n = (2n+1)\pi/\beta$ being Matsubara frequencies of the fermions. A solution of the above equations is

$$G = \frac{1}{J}, \;\; \chi = \frac{-iS\phi}{J+S}. \tag{4.14}$$

We wrote "a" solution and not "the" solution, because we fixed the phases of the complex fields. Different phases would corresponds to different solutions but with the same energy. So a particular lowest state is not unique and it does not obey the gauge symmetry (we fix the phase). So it said that the symmetry is broken once a particular solution for the ground state has been chosen [106].

We make the rescaling $4|\phi|^2 J^2/(J+S)^2 \to |\phi|^2$. Summing over the

Matsubara frequencies in Eq. (4.13), we arrive at

$$J = \sqrt{\mu^2 + |\phi|^2} \left(\frac{e^{\beta\sqrt{\mu^2+|\phi|^2}/2} + 1}{e^{\beta\sqrt{\mu^2+|\phi|^2}/2} - 1} \right). \tag{4.15}$$

This is an implicit equation for the rescaled order parameter $|\phi|^2$.

Within the saddle-point integration we obtain the expression for the local density:

$$n = \frac{1}{\beta\mathcal{N}} \frac{\partial \log Z}{\partial \mu} = \frac{1}{2} + \frac{1}{2} \frac{\mu}{\sqrt{\mu^2 + |\phi|^2}} \left(\frac{e^{\beta\sqrt{\mu^2+|\phi|^2}/2} - 1}{e^{\beta\sqrt{\mu^2+|\phi|^2}/2} + 1} \right). \tag{4.16}$$

We obtain the expression for the condensed density by using the definition introduced by Yang in 1962 [104]:

$$n_0 = \lim_{|r-r'|\to\infty} \langle \hat{b}_r^\dagger \hat{b}_{r'} \rangle. \tag{4.17}$$

Hence the occurrence of the BEC is connected to the presence in the system of off-diagonal long-range order. Since the Bose-Einstein condensate is described by a single macroscopic wave function, every two points are correlated, regardless how far they reside from each other. The above definition reflects this property. Within our mean-field we obtain

$$n_0 = \frac{|\phi|^2}{4J^2}. \tag{4.18}$$

At zero temperature the above expression is equal to $(J^2 - \mu^2)/4J^2$ for $J > |\mu|$ and is zero otherwise. We see that this model gives three phases as depicted in Figs. 4.3 and 4.4. It can describe both the dilute regime and the dense regime. As a consequence we have the empty phase along with the MI phase, where there are one boson per each lattice site. To properly identify the phases which we have obtained, we need to consider quantum fluctuations around the saddle-point results. We shall do this in the next section.

A few words about the type of the phase transitions. Near the phase transition the order parameter is small, so that we may apply a perturbative expansion :

$$A_{\text{eff}} = \underbrace{\frac{1}{J}\frac{|\phi|^2}{9} - \frac{1}{\beta}\sum_{\omega_n} \frac{1}{\mu^2 + \omega_n^2}\frac{|\phi|^2}{9}}_{\text{can be negative}} + \underbrace{\frac{1}{2\beta}\sum_{\omega_n} \frac{1}{(\mu^2 + \omega_n^2)^2}\frac{|\phi|^4}{81}}_{>0} + O(|\phi|^6) \tag{4.19}$$

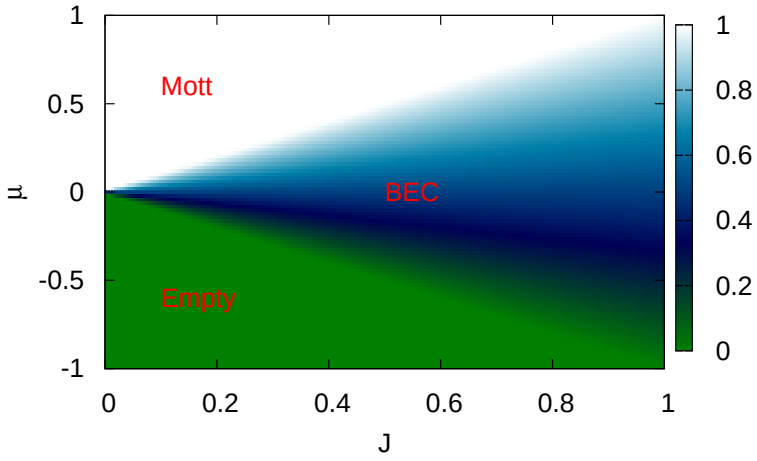

Figure 4.3: Phase diagram for $k_BT = 0$. μ and J are in arbitrary energy units.

Figure 4.4: Phase diagram for $k_BT = 0.05J$. μ and J are in arbitrary energy units.

The first term can be negative, such that the order parameter may differ from zero. The order parameter vanishes continuously indicating that we have a second order phase transition. The above expression resembles the ϕ_2^4 theory of scalar fields in quantum field theory [106]. It means it is in the same universality class as XY model. Indeed in Sec. 4.7.1 we map our hard-core Bosons to the XY model.

4.3 Collective excitations

The complex fields ϕ and χ are expected to fluctuate about the saddle-point solution due to thermal and quantum effects. Here we expand the action to the second order to study elementary excitations in the system. We will also expand it to the fourth order in the next chapter to take into account their interactions.

We denote $\Delta = i\phi + \chi$ and $\bar{\Delta} = i\bar{\phi} + \bar{\chi}$, then the Green's matrix in Eq. (4.10) can be written as

$$\hat{\mathbf{G}}^{-1} = \hat{\mathbf{G}}_0^{-1} + \begin{pmatrix} -\delta\Delta & 0 \\ 0 & \delta\bar{\Delta} \end{pmatrix}, \tag{4.20}$$

where

$$\hat{\mathbf{G}}_0^{-1} = \begin{pmatrix} -\Delta_0 & \partial_\tau + \mu \\ \partial_\tau - \mu & \bar{\Delta}_0 \end{pmatrix} \tag{4.21}$$

with $\Delta_0 = i\phi_0 + \chi_0$ being the saddle-point result. Applying the Taylor expansion $\ln(1+x) = x - x^2/2 + ...$ yields

$$\begin{aligned} \log\det\hat{\mathbf{G}}^{-1} &= \mathrm{tr}\ln\hat{\mathbf{G}}^{-1} = \mathrm{tr}\ln\left[\hat{\mathbf{G}}_0^{-1} + \begin{pmatrix} -\delta\Delta & 0 \\ 0 & \delta\bar{\Delta} \end{pmatrix}\right] \\ &\approx \mathrm{tr}\ln\hat{\mathbf{G}}_0^{-1} - \frac{1}{2}\mathrm{tr}\left[\hat{\mathbf{G}}_0\begin{pmatrix} -\delta\Delta & 0 \\ 0 & \delta\bar{\Delta} \end{pmatrix}\right]^2. \end{aligned} \tag{4.22}$$

Calculating the trace in $p = \{q, \omega\}$ representation we arrive at

$$Z \sim \int D[\delta\phi, \delta\chi] \exp\left[-\delta A_{\text{eff}}\right], \tag{4.23}$$

where δA_{eff} is given in Appendix A.1. The latter is expressed in terms of an inverse Green's matrix $\mathcal{G}^{-1}(i\omega_n, q)$ with imaginary time for quasiparticles which are described by fields $\delta\phi$. By applying the spectral representation of the Green's matrix (or Lehmann representation [3]), we can identify the poles of the matrix $\mathcal{G}(i\omega_n, q)$ with the excitation spectrum of the quasiparticles as $\epsilon_q = i\omega_n$.

BEC. The exact solution in the condensed phase is

$$\epsilon_q = \sqrt{g_q(J^2 - \mu^2) + g_q^2\mu^2}. \tag{4.24}$$

In the dilute regime, where $\mu + J$ is small, and for small momenta q we compare this spectrum with the spectrum which we have gotten within the Gross-Pitaevskii equation (cf. Eq. (3.7)). As a result we get the Bogoliubov spectrum with sound velocity $\approx \sqrt{2J\tilde{\mu}}$. Here $\tilde{\mu} = J + \mu$ is an effective chemical potential. Indeed, in the dilute regime $n_0 = \tilde{\mu}/2J$. For the dilute Bose gas within the Gross-Pitaevskii theory we have $n_0 = \mu/\gamma$ (cf. Eq. (3.7) and remarks below it). So we can identify in our theory in the dilute regime $\gamma \approx 2J$ and $m = d/J$ (we set $\hbar = 1$).

More generally the sound velocity is defined by the compressibility $\partial P/\partial n$ according to

$$c_{\text{sound}} = \left(\frac{1}{m}\frac{\partial P}{\partial n}\right)^{1/2}. \tag{4.25}$$

The pressure P can be defined through the free energy $P = \partial F/\partial V$. In our case the role of the volume plays the number of sites $\mathcal{N}$. One can calculate the free energy within the mean-field and get

$$\frac{\partial P}{\partial n} = \frac{\partial P}{\partial \mu}\frac{\partial \mu}{\partial n} = J + \mu. \tag{4.26}$$

It follows that$c_{\text{sound}} = \sqrt{(\mu + J)/m}$. Comparing this with $\sqrt{(J^2 - \mu^2)/2d}$ implies the expression for an effective mass of bosons:

$$m = \frac{2d}{J - \mu}. \tag{4.27}$$

In the dilute regime we reproduce $m \approx d/J$. In the dense regime the mass m diverges as $1/(J - \mu)$, where $\mu \to J$. This can be understood physically as if bosons become locked approaching the Mott insulating phase, therefore their mass becomes large.

Now we can infer the static structure factor without explicit lengthly calculations. The static structure factor can be directly measured in experiments [96]. It is defined through the density-density correlation function as [86]

$$S(q) = \frac{1}{N}(\langle \rho_q \rho_{-q} \rangle - |\langle \rho_q \rangle|^2). \tag{4.28}$$

It can be expressed via celebrated Feynman relation which is valid for small energies, i.e. for small momenta, as [35]

$$\epsilon_q = \frac{\hbar q^2}{2mS(q)}. \tag{4.29}$$

Using Eqs. (4.24) and (4.27) yields

$$S(q) \approx \frac{J^2 - \mu^2}{J^2 n} \frac{J g_q}{\epsilon_q}. \tag{4.30}$$

So the static structure factor vanishes at the BEC-MI transition. The above expression has been also calculated in [37].

In order to understand better the spectrum in Eq. (4.24), we separate the amplitude and the phase fluctuations of the order parameter. As it is shown in Appendix A.1, we arrive at the Green's matrix in Eq. (A.14). If the amplitude mode is not active but the phase mode is active, the Green's matrix in Eq. (A.14) has a pole at

$$\epsilon_q = J\sqrt{g_q}. \tag{4.31}$$

If the phase mode is not active but the amplitude mode is active, then the pole is at

$$\epsilon_q = \sqrt{J^2 - \mu^2 + \mu^2 g_q}, \tag{4.32}$$

which represents a massive mode with the mass $J^2 - \mu^2$. The Bogoliubov spectrum is then obtained by multiplying the both expressions. We notice that the two modes are coupled in general.

Mott insulator. In the empty phase and in the MI phase the excitations are with a gap:

$$\epsilon_q = |\mu| - J + J g_q. \tag{4.33}$$

The symmetric form of the results for the MI phase and for the empty phase is due to the particle-hole symmetry of our model. In order to apply the Landau criterion on superfluidity we should be careful here. In Eq. (3.8) $\epsilon_q \sim J/(2d)q^2$ not $|\mu| - J + J/(2d)q^2$, such that the criterion gives $V_c = 0$ and there is no superfluidity.

In previous calculations, performed on the Bose-Hubbard model, each phase requires its own specific mean-field approach [73, 100] or a single one close to the phase boundary [4, 54]. In the MI phase our expression for the excitation spectrum agrees with the branch of the excitation spectrum, which corresponds to creation of holes in the first Mott lobe of the Bose-Hubbard model, taking the limit of a large interaction. However, the second branch, which corresponds to formation of doubly occupied sites, does not exist in our model since we can create only holes in the singly occupied lattice to excite our system and not additional particles due to the hard-core condition. This is possible in the grand canonical ensemble, where only the average number is fixed but the number of particles fluctuates.

Within a Bogoliubov approximation to the Bose-Hubbard model the quasiparticle spectrum in the BEC phase was found as [73, 100]

$$\epsilon_q = \sqrt{J^2 g_q^2 + 2U n_0 J g_q}, \tag{4.34}$$

where U is the interaction parameter and n_0 is the condensate density. In contrast to this expression, we found for the spectrum the expression in Eq. (4.24). These expressions do not agree in the limit $U \to \infty$. Thus our hard-core Bose gas cannot be described within the Bogoliubov approximation to the Bose-Hubbard model by simply sending U to infinity. On the other hand, our results are in good agreement with a variational Schwinger-boson mean-field approach to the Bose-Hubbard model, which describe the phases near the phase transition, by sending U to infinity [54].

Our model thus correctly describes the physics of strongly interacting bosons in an optical lattice near the points where two Mott lobes meet (cf. Fig. 4.2). On top of that it allows us to describe the three phases within the unique mean-field approximation.

4.4 Superfluid density

As we mentioned above, the Bose-Einstein condensation and superfluidity do not depend on each other. For example, at zero temperature the whole ^{4}He is superfluid but only 7.25×10^{-2} part of it is condensed, while the ideal Bose gas is condensed but it is not superfluid. Superfluidity of the 1D Bose gas was studied in Ref. [91], while BEC is not possible in 1D. A jump in the superfluid fraction was obtained at the transition point. This is expected since Bose-Hubbard model, studied in [91] belongs to the universality class of the 2D XY spin model [41, 92] and the jump corresponds to the Kosterlitz-Thouless critical point [63].

We have gotten the Bogoliubov spectrum for the paired fermion model and the system is superfluid due to the Landau criterion. The system undergoes the density-driven SF-MI phase transition. It is thus interesting to calculate the superfluid density and compare it to the condensed density calculated within the paired fermion model. The superfluidity arises by disturbing a phase of an order parameter:

$$\mathbf{V}_s(\mathbf{r}) = \frac{\hbar}{m} \nabla \theta(\mathbf{r}). \tag{4.35}$$

We thus apply the phase twist to the order parameters $\theta(\mathbf{r}) = \mathbf{Q} \cdot \mathbf{r}$:

$$\phi(x) \to \phi(x) e^{i\mathbf{Q}\cdot\mathbf{r}}, \;\; \chi(x) \to \chi(x) e^{i\mathbf{Q}\cdot\mathbf{r}}. \tag{4.36}$$

To remove the phase from the fields in the matrix $\hat{\mathbf{G}}^{-1}$ in Eq. (4.9) we apply the unitary transformation $\hat{\mathbf{U}}^{-1}\hat{\mathbf{G}}^{-1}\hat{\mathbf{U}}$ with

$$\hat{\mathbf{U}} = \begin{pmatrix} 0 & e^{i\mathbf{Q}\cdot\mathbf{r}/2} \\ e^{-i\mathbf{Q}\cdot\mathbf{r}/2} & 0 \end{pmatrix}. \tag{4.37}$$

This transformation causes

$$v_p^{-1} \to v_{p-Q}^{-1}, \;\; \hat{\mathbf{G}}^{-1}(Q) \to \begin{pmatrix} -\Delta_0 & \partial_\tau + \mu \\ \partial_\tau - \mu & \bar{\Delta}_0 \end{pmatrix}. \tag{4.38}$$

The superfluid density is given through the response of the free energy to the twist [68]:

$$\delta F = F(Q) - F(0) \approx \frac{Q^2}{2}\left(\frac{\partial^2 F(Q)}{\partial Q^2}\right)_{Q\to 0} = \frac{1}{2}\rho_s m V_s^2. \tag{4.39}$$

Here $\rho_s m$ is the superfluid mass density. Using Eq. (4.35) we get

$$\rho_s = m\left(\frac{\partial^2 F(Q)}{\partial Q^2}\right)_{Q\to 0}. \tag{4.40}$$

Then the only place where Q is stored is inside the matrix v_{q-Q}^{-1}, and on the mean-field level (setting $q = 0$) we get

$$\delta F = \frac{J|\phi_0|^2}{2d(J+S)^2}Q^2 \;\; \Rightarrow \;\; \rho_s = m\frac{|\phi_0|^2}{d(J+S)^2} = \frac{mJn_0}{d}. \tag{4.41}$$

If we substitute here $m \approx 2d/(J-\mu)$ (cf. Eq. 4.27), we obtain that the superfluid density is equal to the total particle density. This is in a good agreement with the two-fluid model for superfluid Helium, where it is also the case at $T = 0$ [68]. Within the standard BCS theory one also gets the same result [3]. In the MI there should be no superfluidity. We thus have gotten a jump of the superfluid density at the transition.

4.5 Renormalized Gross-Pitaevskii equation

If we superimpose our system by a harmonic trap, we can not consider a homogeneous solution obtained above. Here we extend our theory for the slowly varying field ϕ_r in real space. Firstly, we would like to properly account for the lattice spacing a to reproduce the continuum limit by sending it to zero. It amounts to changing the tunneling rate $J/(2d)$ to

$J/(2da^2) - J/a^2$. Physically, we want to reproduce the kinetic energy in the continuum limit which is given as a nabla operator and scales as a^{-2}. This changes the matrix $\hat{v}_{\mathbf{r},\mathbf{r}'}$ as

$$\hat{v} = S\hat{1} + (\hat{J} - J\hat{1})/a^2, \tag{4.42}$$

where $\hat{J}$ is the hopping matrix with $J/(2d)$. For the slowly varying fields we approximate

$$\hat{v}^{-1}\phi \approx S^{-1}\phi - S^{-2}(\hat{J} - J\hat{1})\phi/a^2. \tag{4.43}$$

The second term, which is $\sim \nabla^2\phi$, is small for slowly varying fields ϕ. The above approximation is valid up to the second order. To show this we multiply the above equation by $\hat{v}$:

$$\phi \approx \left[S\hat{1} + (\hat{J} - J\hat{1})/a^2\right]\left[S^{-1}\hat{1} - S^{-2}(\hat{J} - J\hat{1})/a^2\right]\phi = \phi - S^{-2}(J\hat{1} - \hat{J})^2\phi/a^2. \tag{4.44}$$

The second term is of the second order and our approximation is justified.

The results should not depend on S. But once we have made the expansion for $\hat{v}^{-1}$ in Eq. (4.43) we should restrict it as

$$S \geq \frac{J}{2d}\frac{|\phi''|}{|\phi|} \tag{4.45}$$

in order to validate the approximation in Eq. (4.43). However, we will see in the next chapter that numerical investigation of the resulting equations reveals no dependence on S in the wide range.

For small a we perform a continuum approximation

$$\sum_{r'}\left(J\delta_{rr'} - \hat{J}_{rr'}\right)\phi_{r'}/a^2 = -\frac{J}{2d}\sum_{j=1}^{d}\frac{\phi_{r+ae_j} - 2\phi_r + \phi_{r-ae_j}}{a^2} \approx -\frac{J}{2d}\nabla^2\phi(r). \tag{4.46}$$

For small order parameters ϕ and χ we expand the action in Eq. (4.9) to the quartic order. The mathematical procedure is involved and the details of the calculations are shown in Appendix A.2. Here we state the result

$$i\frac{\partial}{\partial t}\phi(\mathbf{r},t) = -\frac{1}{2m_{\mathrm{R}}}\nabla^2\phi(\mathbf{r},t) + \mu_{\mathrm{R}}\phi(\mathbf{r},t) + g_{\mathrm{R}}|\phi(\mathbf{r},t)|^2\phi(\mathbf{r},t). \tag{4.47}$$

This is the Gross-Pitaevskii equation (cf. Eq. (3.3)) with the mass $m_{\mathrm{R}} \approx d/J$, the chemical potential $\mu_{\mathrm{R}} \approx \tilde{\mu}$ and the coupling $g_{\mathrm{R}} \approx 2J$.

Here we notice an important observation. Despite that field ϕ appears as an auxiliary field after the Hubbard-Stratonovich transformation,

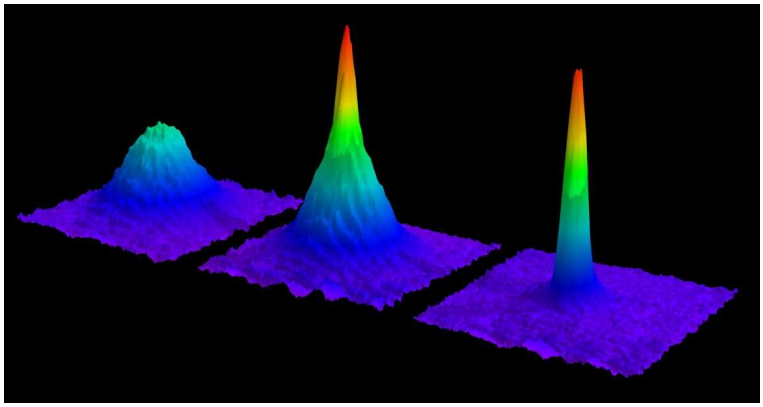

Figure 4.5: Shown is absorption vs. two spatial dimensions after 6 msec time of flight. The sharp peak is the Bose-Einstein condensate. The left picture shows an expanding cloud cooled to $T > T_c$, the middle one shows at $T \approx T_c$, the right one shows almost pure condensate at $T << T_c$. Taken from Alkali Quantum Gases at MIT.

being thus of a pure mathematical origin, it satisfies, nevertheless, the Gross-Pitaevskii equation in the dilute regime. Due to the time and spatial derivatives in Eq. (4.47), this field possesses full dynamics as would be in the case of usual physical field originating from a microscopic bosonic theory. It is said that Eq. (4.47) represents an effective low energy field theory of a Bose gas in the dilute regime to our microscopic fermionic model given in Eq. (4.3).

4.6 Noise correlations

4.6.1 Density distribution after time-of-flight

One of the most spectacular manifestations of BEC in Bose gases is the appearance of the peak in the density distribution after time of flight after realizing it from the trap below critical temperature, $T < T_c$ (see [9] and Fig. 4.5). To explain this appearance, we calculate the density distribution of the Bose gas after time of flight (see also [5]). We also assume that the gas after expansion in non-interacting. In the Heisenberg picture the field operator satisfies

$$\frac{\partial}{\partial t}\hat{\psi}^\dagger(r,t) = \frac{i}{\hbar}[\hat{H}, \hat{\psi}^\dagger(r,t)]. \tag{4.48}$$

The Hamiltonian consists only of the kinetic energy and thus

$$\hat{H} = \int d^d r' \hat{\psi}^\dagger(r', t) \left[-\frac{\hbar^2}{2m} \nabla^2 \right] \hat{\psi}(r', t). \tag{4.49}$$

Substituting Eq. (4.49) into Eq. (4.48) we arrive at

$$\frac{\partial}{\partial t} \hat{\psi}^\dagger(r, t) = -\frac{i\hbar}{2m} \nabla^2 \hat{\psi}^\dagger(r, t). \tag{4.50}$$

The above equation has the solution $\hat{\psi}^\dagger(r, t) = e^{-t\frac{i\hbar}{2m}\nabla^2} \hat{\psi}^\dagger(r, 0)$.

If we denote the ground state of the gas in the trap before the expansion as $|\Phi\rangle$, then we obtain for the density distribution the following expression (within the Heisenberg picture)

$$\langle \hat{n}(r) \rangle_t = \langle \Phi | \hat{\psi}^\dagger(r, t) \hat{\psi}(r, t) | \Phi \rangle. \tag{4.51}$$

We express the field operators as a sum over eigenstates ϕ_n of the harmonic potential, i.e. $\hat{\psi}^\dagger(r, 0) = \sum_n \phi_n^*(r) \hat{b}_n^\dagger$. Moreover, we demand the state $|\Phi\rangle$ be the condensed state, so $|\Phi\rangle = (\hat{b}_0^\dagger)^{N_0} |0\rangle$. Here N_0 is the number of condensed atoms. Then it is straightforward to show that

$$\langle \hat{n}(r) \rangle_t = N_0 \left| e^{-t\frac{i\hbar}{2m}\nabla^2} \phi_0(x) \right|^2. \tag{4.52}$$

In the momentum space $\phi_0(k) = 1/(\pi m \hbar \omega)^{3/4} e^{-\hbar k^2/(2m\omega)}$ and we obtain $\langle \hat{n}(r) \rangle_t \propto N_0 \left| \int d^d k e^{-\frac{\hbar k^2}{2m\omega}(1 - i\omega t) - ikr} \right|^2$, which for large ωt reduces to

$$\langle \hat{n}(r) \rangle_t \propto N_0 \left(\frac{m}{\hbar t} \right)^3 e^{-r^2/(a\omega t)^2}. \tag{4.53}$$

Here $a^2 = \hbar/(m\omega)$ is the width of the wave function of the harmonic oscillator. We notice that the above expression can also be expressed via the momentum distribution, $\langle \hat{n}(r) \rangle_t \propto \left(\frac{m}{\hbar t} \right)^3 \langle \hat{n}(k) \rangle$, where $\langle \hat{n}(k) \rangle = N_0 |\phi_0(k)|^2$ and $k = mr/(\hbar t)$. Indeed, it can be shown rigorously that the density distribution after a fixed time-of-flight is related to the momentum distribution of particles trapped before the expansion via

$$\langle \hat{n}(r) \rangle_t = \left(\frac{m}{\hbar t} \right)^3 \langle \hat{n}(k) \rangle. \tag{4.54}$$

This is valid at large times. In the case of the harmonic trap with frequency ω, t should be much larger than $1/\omega$.

The state with $n = 0$ is macroscopically occupied and has the width a. Above the critical temperature the width is $\sim (k_B T/(m\omega^2))^{1/2}$ and thus is much larger. Then, Eq. (4.53) shows the occurrence of the peak around the center when the system is cooled below the critical temperature, which is consistent with what is shown in Fig. 4.5. In case the gas is realized from an optical lattice, the resulting density distribution shows many peaks located on positions corresponding to the reciprocal lattice vector [45, 50].

If particles are trapped in an optical lattice before expansion, the field operator $\hat{\psi}_\sigma(r)$ is expanded in a basis of Wannier functions [62] as

$$\hat{\psi}(r) = \sum_{i,n} w_n(r - R_i)\hat{b}_{i,n}. \tag{4.55}$$

Here, $\hat{b}_{i,n}$ is the annihilation operator for particles in the Wannier state n at lattice site R_i. For a deep optical lattice only the lowest Wannier state is taken into account with $\hat{b}_i \equiv \hat{b}_{i,0}$. Since the Wannier function is a periodic function, we Fourier transform it as $w_0(r) = \sum_k e^{ikr}\tilde{\omega}_0(k)$. In this case Eq. (4.54) is also valid and is applicable for times t much larger than $1/\omega$ with ω being the frequency of a lattice well in an optical lattice.

4.6.2 Density-density correlations after time-of-flight

In a typical experiment with ultra-cold atoms it is not easy to identify the spin projection. Therefore, the detected fermion density should be described by a superposition of both spin projections. For this purpose we introduce the spin-independent fermionic density $\hat{n} = \hat{n}_\uparrow + \hat{n}_\downarrow$. Then the truncated density-density correlation function in a time-of-flight experiment is given under the assumption that the atoms expand freely after they have been released from the optical lattice as [18, 40] (cf. Eq. (4.54))

$$C_{r,r'} \equiv \langle \hat{n}(r)\hat{n}(r')\rangle - \langle \hat{n}(r)\rangle\langle \hat{n}(r')\rangle = \left(\frac{m}{\hbar t}\right)^{2d} \langle \hat{n}(k)\hat{n}(k')\rangle - \langle \hat{n}(r)\rangle\langle \hat{n}(r')\rangle. \tag{4.56}$$

Here k is related to r by $k = mr/\hbar t$ with the mass of atoms $m \propto \hbar/J$. Free expansion assumes that atoms evolve independently. This can be achieved by switching off an optical lattice as well as by switching the magnetic field to values far from the strongly attractive regime suddenly before the expansion [5, 21]. The above formula is widely used to analyze ground state properties of ultra-cold atoms trapped by an optical lattice [20, 55].

The partition function of a grand canonical ensemble of fermions with chemical potential μ at inverse temperature β can be expressed in terms of

an integral over a fermionic (Grassmann) field ψ and complex molecular fields ϕ, χ as

$$Z = \int e^{-\int_0^\beta d\tau \mathcal{L}} \mathcal{D}[\psi, \phi, \chi] \tag{4.57}$$

with the Lagrangian

$$\mathcal{L} = \sum_{i,j} \bar{\phi}_i \hat{v}_{i,j}^{-1} \phi_j + \frac{1}{2J} \sum_i \bar{\chi}_i \chi_i - \sum_{i,j} \hat{\mathcal{C}}_i^\dagger \hat{\mathbf{G}}_{ij}^{-1} \hat{\mathcal{C}}_j \ , \tag{4.58}$$

where we have used the notation $\hat{\mathcal{C}}^\dagger = (\psi_\uparrow, \bar{\psi}_\downarrow)$ and $\hat{\mathcal{C}} = (\psi_\downarrow, \bar{\psi}_\uparrow)^T$, and with the inverse fermionic Green's matrix $\hat{\mathbf{G}}^{-1}$ given in Eq. (4.10). Here $\hat{v}_{i,j} = \frac{J}{2d}\delta_{|i-j|,1}$.

Now we use the expansion of Eq. (4.55) to express the density-density correlation of Eq. (4.56) in terms of the coordinates of the underlying optical lattice as

$$C_{r,r'} = \left(\frac{M}{\hbar t}\right)^{2d} |\tilde{w}(k)|^2 |\tilde{w}(k')|^2 \sum_{i,i',j,j'} e^{ik(R_i - R_{i'}) + ik'(R_j - R_{j'})} \langle \hat{c}_{i\alpha}^\dagger \hat{c}_{j\beta}^\dagger \hat{c}_{j'\beta} \hat{c}_{i'\alpha} \rangle + \langle \hat{n}(r) \rangle \delta(r - r') - \langle \hat{n}(r) \rangle \langle \hat{n}(r') \rangle \tag{4.59}$$

where $\tilde{w}$ is a Fourier transform of the Wannier function.

Using the saddle-point approximation of the complex fields (ϕ, χ) we can evaluate $\langle \hat{c}_{i\alpha}^\dagger \hat{c}_{j\beta}^\dagger \hat{c}_{j'\beta} \hat{c}_{i'\alpha} \rangle$. Since the fermion field appears in a quadratic form in Eq. (4.58), the integration are given by a Wick contraction of pairs of fermions:

$$\langle \hat{c}_{i\alpha}^\dagger \hat{c}_{j\beta}^\dagger \hat{c}_{j'\beta} \hat{c}_{i'\alpha} \rangle = \langle \hat{c}_{i\alpha}^\dagger \hat{c}_{i'\alpha} \rangle \langle \hat{c}_{j\beta}^\dagger \hat{c}_{j'\beta} \rangle - \langle \hat{c}_{i\alpha}^\dagger \hat{c}_{j'\beta} \rangle \langle \hat{c}_{j\beta}^\dagger \hat{c}_{i'\alpha} \rangle + \langle \hat{c}_{i\alpha}^\dagger \hat{c}_{j\beta}^\dagger \rangle \langle \hat{c}_{j'\beta} \hat{c}_{i'\alpha} \rangle \tag{4.60}$$

The fermionic expectation values on the right-hand side are matrix elements of the fermionic Green's function $\hat{\mathbf{G}}$ of Eq. (4.10):

$$\langle \hat{c}_{i\uparrow}^\dagger \hat{c}_{j\uparrow} \rangle = \langle \hat{c}_{i\downarrow}^\dagger \hat{c}_{j\downarrow} \rangle = \frac{1}{\beta} \sum_n \mathbf{G}_{ij}^{12}(\omega_n) \tag{4.61}$$

and

$$\langle \hat{c}_{i\downarrow}^\dagger \hat{c}_{j\uparrow}^\dagger \rangle = \frac{1}{\beta} \sum_n \mathbf{G}_{ij}^{11}(\omega_n), \ \ \langle \hat{c}_{i\uparrow} \hat{c}_{j\downarrow} \rangle = \frac{1}{\beta} \sum_n \mathbf{G}_{ij}^{22}(\omega_n), \tag{4.62}$$

where we have summed over Matsubara frequencies ω_n. These expressions include also quantum fluctuations of the bosonic molecules when

we take into account Gaussian fluctuations around the saddle-point solutions. For instance, we can integrate over these fluctuations to evaluate the correlation function

$$\langle \hat{c}^\dagger_{i\alpha}\hat{c}^\dagger_{j\beta}\hat{c}_{j'\beta}\hat{c}_{i'\alpha}\rangle - \langle \hat{c}^\dagger_{i\alpha}\hat{c}^\dagger_{j\beta}\rangle\langle \hat{c}_{j'\beta}\hat{c}_{i'\alpha}\rangle. \tag{4.63}$$

The density-density correlations reduces to

$$C_{r,0} = \langle \hat{n}(r)\rangle\delta(r) + 2\left(\frac{M}{\hbar t}\right)^{2d}|\tilde{w}(k)|^2|\tilde{w}(0)|^2$$
$$\times\left[-\left|\sum_i e^{ikR_i}\langle \hat{c}^\dagger_{i\uparrow}\hat{c}_{i\uparrow}\rangle\right|^2 + \left|\sum_i e^{ikR_i}\langle \hat{c}_{i\uparrow}\hat{c}_{i\downarrow}\rangle\right|^2 + \mathcal{S}(k)\right] \tag{4.64}$$

The first two terms constitute the density-density correlation function for fermions [18], whereas the third and the fourth terms account for the presence of the condensed molecules. In particular, the fourth term describes the effect of quantum fluctuations and can be expressed as a momentum distribution of the molecules [37]

$$\mathcal{S}(k) = \sum_{i,j} e^{k(R_i-R_j)}(\langle \hat{b}^\dagger_i\hat{b}_j\rangle - \langle \hat{b}^\dagger_i\rangle\langle \hat{b}_j\rangle) \tag{4.65}$$

with $\hat{b}^\dagger_i = \hat{c}^\dagger_{i\downarrow}\hat{c}^\dagger_{i\uparrow}$. Phase fluctuations can destroy these terms, for instance, in the case of a MI state of the molecules. It is important to notice that fermionic terms contribute with a negative sign in Eq. (4.64), in contrast to the phase-coherent molecules, which contribute with a positive sign. This indicates a competition of the fermionic and the molecular contribution to the density-density correlation function. This provides a concept for measuring the properties of a strongly interacting Fermi gas.

The expressions $\langle \hat{c}^\dagger_{i\uparrow}\hat{c}_{i\uparrow}\rangle$ and $\langle \hat{c}_{i\uparrow}\hat{c}_{i\downarrow}\rangle$ are constant due to translational invariance:

$$C_{r,0} \propto N^2\delta_{k,G}\left(-1 + \frac{N_0\mathcal{N}}{N^2}\right) + \mathcal{S}(k), \tag{4.66}$$

where we have denoted $2N = 2\sum_i\langle \hat{c}^\dagger_{i\uparrow}\hat{c}_{i\uparrow}\rangle$ as the total number of fermions and $N_0\mathcal{N} = |\sum_i\langle \hat{c}_{i\uparrow}\hat{c}_{i\downarrow}\rangle|^2 \propto \mathcal{N}^2|i\phi + \chi|^2$. $\mathcal{N}$ is the number of lattice sites. The ratio $n_0 = N_0/N$ is the condensate fraction, i.e. the relative contribution of condensed molecules.

BEC.– For momenta close to the reciprocal lattice vectors G the main contribution in the BEC comes from the term $\mathcal{S}(k)$, since it is singular for $\epsilon_k \sim 0$:

$$C_{r,0} \propto \mathcal{S}(k) \approx \frac{4Jn_0 + Jg_k}{\epsilon_k}(1 - 2g_k)\ . \tag{4.67}$$

This results connects the density-density correlation function with the spectrum of the molecular condensate given in Eq. (4.24). The infrared divergence of the momentum distribution is a general property of a BEC at $T = 0$ [86]. The related 2D plot of the correlation function is shown in Fig. 4.6.

MI.– For larger densities the phase coherence in the molecular state is destroyed and a MI state with one bosonic molecule (i.e., a pair of fermions) appears. Due to strong phase fluctuations the second term in Eq. (4.66) vanishes, and the correlation function becomes

$$C_{r,0} \propto -N^2 \delta_{k,G} + \mathcal{S}(k) \tag{4.68}$$

with the non-singular term

$$\mathcal{S}(k) \approx \frac{J^2}{4\mu^2}(1 - 2g_k). \tag{4.69}$$

Since the number of fermions N is large in Eq. (4.68), the contribution of $\mathcal{S}(k)$ is negligible in time-of-flight experiments of the MI. Thus the MI state is characterized by sharp *dips* in contrast to the singular *peaks* in the BEC, which appear on positions corresponding to the reciprocal lattice vectors G, similar to a Bragg diffraction pattern. However, in contrast to the latter, where the diffraction pattern is created by light scattering on atoms of a crystal, here the pattern is created by the atomic state itself in the expansion process of the cloud.

Eq. (4.69) describes the bosonic nature of the molecules in the MI state: There are hole excitations in the MI phase (particle excitations are suppressed by the hard-core nature of the bosons) and their dynamics contributes to the interference pattern via the factor $\propto g_{\mathbf{k}}$. A similar situation was observed experimentally in the case of bosonic Mott insulator in Ref. [47]. The 2D plot of the correlation function is shown in Fig. 4.7.

The density-density correlation function of an expanding cloud provides a clear picture of the state when it was still trapped by an optical lattice. It consists of four different contributions in Eq. (4.64), two of them are related to the fermionic nature of the atoms. The second term leads to a fermionic dip in the density-density correlation function in the MI state. A third term measures the condensate fraction in the case of condensed bosonic molecules and together with the singular fourth term leads to the sharp peaks. Even though the third term can compete with the second term, the singular term is the most relevant in the BEC phase.

The competing behavior of the fermionic dips and the condensate peaks in the density-density correlation function are a result of the anticommut-

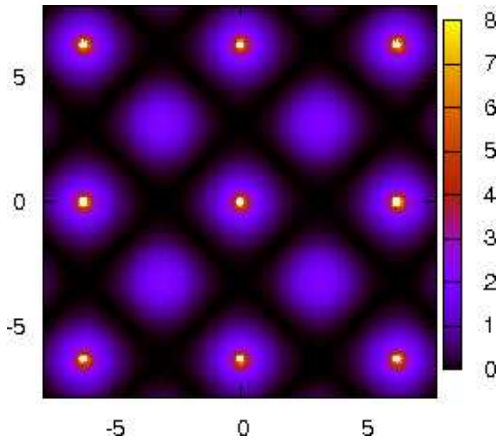

Figure 4.6: Density-density correlation function in units of $(\hbar t/Ma)^{-2d}$ of a strongly attractive spin-1/2 Fermi gas in an optical lattice with $J = 1$, $\mu = 0.4$, $k_BT = 0$, where the gas forms a BEC. The singular behavior at the positions corresponding to the reciprocal lattice vectors is due to long range phase coherence of the condensed molecules. There is also small modulation due to the tunneling of molecules. The axes are given in units of $\hbar t/Ma$, where a is a lattice spacing [40].

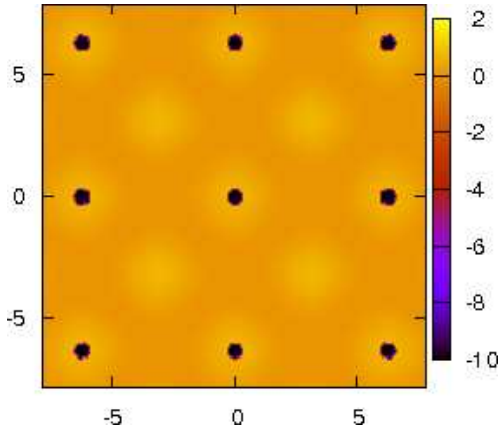

Figure 4.7: Density-density correlation function as in Fig. 4.6 but with $J = 1$, $\mu = 0.6$, $k_BT = 0$. The singular behavior in Fig. 4.6 is replaced by dips here. This is due to the anticommuting nature of fermionic operators and thus reflects the fermionic nature of the MI state [40].

ing properties of the fermionic operators. This provides a simple concept to distinguish different states in a cloud of attractively interacting fermions. This behavior is rather different in a bosonic cloud, where all atoms contribute with the same sign to density-density correlation function because the bosonic operators commute [44, 46].

In conclusion, we have studied an expanding cloud of strongly interacting spin-1/2 fermions after its release from an optical lattice. The properties are described in terms of the density-density correlation function. At lower densities a BEC is formed by the paired fermions, visible in the density-density correlation function as sharp peaks. At higher densities a Mott-insulating phase appears, characterized by dips in the density-density correlation function. This distinct behavior can be used in future experiments to distinguish between these two phases in a gas of strongly attractive spin-1/2 fermions in an optical lattice.

4.7 Spin analogues

4.7.1 Mapping to the XY model

The Hamiltonian in Eq. (4.3) can be rewritten in terms of spin operators

$$\hat{H} = -\frac{J}{2d}\sum_{\langle r,r'\rangle}\hat{S}_r^+\hat{S}_{r'}^- - h_z\sum_r \hat{S}_r^z \tag{4.70}$$

with

$$\hat{S}_r^+ = (\hat{S}_r^-)^\dagger = \hat{c}_{r\uparrow}^\dagger\hat{c}_{r\downarrow}^\dagger,\ \ \hat{S}_r^z = \frac{1}{2}(\hat{n}_{r\uparrow}+\hat{n}_{r\downarrow}-1),\ \ h_z = 2\mu. \tag{4.71}$$

These operators obey the commutation relations

$$[\hat{S}_r^\alpha, \hat{S}_{r'}^\beta] = 2i\epsilon^{\alpha\beta\gamma}\hat{S}_r^\gamma\delta_{r,r'} \tag{4.72}$$

where $\hat{S}_r^\pm = \hat{S}_r^x \pm i\hat{S}_r^y$. In other words, we have obtained the XY model in the transverse magnetic field:

$$\hat{H} = -\frac{J}{2d}\sum_{\langle r,r'\rangle}(\hat{S}_r^x\hat{S}_{r'}^x + \hat{S}_r^y\hat{S}_{r'}^y) - h_z\sum_r\hat{S}_r^z. \tag{4.73}$$

Let us consider this model for $h_z = 0$. It has been proven that the quantum XY model in a hypercubic lattice has long-range order in the ground state for all values of spins and all dimensions greater than one [60]. This state

corresponds to our superfluid state or BEC of paired fermions. If now we increase the value of the magnetic field h_z, at some point we get a paramagnetic phase with all spins aligned along the magnetic field, which corresponds to the Mott insulating phase of paired fermions. The mapping of hard-core bosons to the spin-1/2 operators is well known [110].

4.7.2 Mapping to the Heisenberg model

The tightly-bound fermions can be also described by the negative-U Fermi-Hubbard model

$$\hat{H} = -t \sum_{\langle r,r' \rangle} \sum_{\sigma} \hat{c}^{\dagger}_{r\sigma} \hat{c}_{r'\sigma} - U \sum_{r} (\hat{n}_r - 1)^2 - \mu \sum_{r} \hat{n}_r \tag{4.74}$$

with $t/U \ll 1$. Here t is the tunneling rate of fermions, U is the interaction strength. Physically, for large attraction the fermions become locally paired.

By applying a particle-hole transformation on the down-spin fermions the model can be mapped to a positive-U Fermi-Hubbard model [13], which in the limit of large interaction U becomes the Heisenberg spin Hamiltonian

$$\hat{H} = \tilde{J} \sum_{\langle r,r' \rangle} \sum_{\alpha=x,y,z} \hat{S}^{\alpha}_{r} \hat{S}^{\alpha}_{r'} - h \sum_{r} \hat{S}^{z}_{r} \tag{4.75}$$

with $\tilde{J} = 4t^2/U$ and magnetic field $h = 2\mu$. For $h = 0$ (i.e., at half-filling) we get an antiferromagnet. The spin-wave excitations of the antiferromagnet are bosonic excitations with a linear spectrum for small momenta $\sim \tilde{J}q$. This is to be compared with the elementary excitations in the BEC phase of the paired-fermions model at half-filling, which are given in Eq. (4.24) and also display a linear behavior $\sim Jq$.

4.8 Comparison with the N-component hard-core Bose gas

A grand canonical system of N-component hard-core bosons, subject to thermal fluctuations in a lattice, was studies in Refs. [76,77,107,108]. The hard-core bosons were not represented by paired fermions or by Grassmann fields in the field theoretical treatment, but by so called nilpotent fields. Here we digress from the paired fermions model and try to treat Eq. (4.3) from a different perspective.

Hard-core bosons are described by the operators $\hat{b}_i^\dagger$, $\hat{b}_i$ with the following algebra

$$[\hat{b}_i, \hat{b}_j^\dagger] = \delta_{ij}, \;\; (\hat{b}_i^\dagger)^2 = \hat{b}_i^2 = 0. \tag{4.76}$$

Instead of complex fields in the case of ordinary bosons or Grassmann fields in the case of fermions, the nilpotent fields η_i^1, η_i^2 are introduced for hard-core bosons such that for $\sigma = 1, 2$

$$(\eta_i^\sigma)^2 = 0, \;\; \eta_i^\sigma \eta_j^{\sigma'} = \eta_j^{\sigma'} \eta_i^\sigma. \tag{4.77}$$

The action in a discrete space-time domain $x = (\tau, r)$ is written as

$$S(\{\eta_x^\sigma\}) = -N \sum_{x,x'} (\delta_{xx'} + \zeta \hat{\omega}_{x,x'}) \eta_x^1 \eta_{x'}^2, \tag{4.78}$$

where $\zeta = e^{\delta\mu}$ and the matrix $\hat{\omega}_{x,x'}$ is nonzero for $\tau' = \tau + 1$ in the time domain and in the space domain its elements read

$$\hat{\omega}_{x,x'} = \begin{cases} -\delta J/2d, & r, r' \text{ are nearest neighbors} \\ 1 - \delta J, & r = r' \\ 0, & \text{otherwise} \end{cases} . \tag{4.79}$$

In these formulas δ should be send to $+0$ at the end of calculations.

The nilpotent variables can be replaced by products of Grassmann variables as $\eta_x^\sigma \to (-1)^\sigma \psi_x^\sigma \bar{\psi}_x^\sigma$. After this we can introduce a Hubbard-Stratonovich transformation similar to that, which we have done within the paired fermion model and proceed calculating. The calculations have been performed in Ref. [76]. It appears that the homogeneous density of bosons and the condensed density for $\mu \geq 0$ can be calculated as

$$n = \frac{1}{N} \int \frac{d^d q}{(2\pi)^d} \Phi_2(q) + n_0, \tag{4.80}$$

$$n_0 = -\frac{2}{N} \int \frac{d^d q}{(2\pi)^d} \left[\Phi_1(q) + \Phi_2(q) \right], \tag{4.81}$$

where

$$\Phi_1(q) = -\frac{\mu}{2\sqrt{2\mu J g_q + J^2 g_q^2}} \coth \left(\frac{\beta \sqrt{2\mu J g_q + J^2 g_q^2}}{2} \right), \tag{4.82}$$

$$\Phi_2(q) = -\Phi_1(q) \left(1 + \frac{J g_q}{\mu} \right) - \frac{1}{2}. \tag{4.83}$$

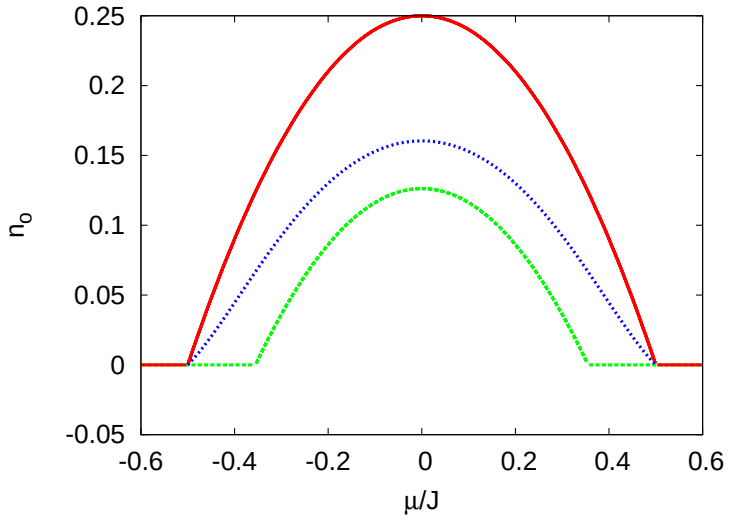

Figure 4.8: Condensed density. The solid, dotted and dashed lines show the mean-field result at $k_BT = 0$, the influence of the quantum fluctuations at $k_BT = 0$ to the mean-field result and the mean-field result at $k_BT = 0.2J$, respectively. μ and J are in arbitrary energy units [37].

Here g_q is given in Appendix A.1. This approach reveals the phase transition from the empty phase ($\mu \leq 0$) to the BEC phase ($\mu > 0$) and does not reveal the MI phase.

For small chemical potential and for small temperatures the above formulas give

$$n_0 \approx \frac{\mu}{N} \int \frac{d^d k}{(2\pi)^3} \frac{1}{J g_q} - \frac{1}{N} \left(\frac{k_B T}{J} \right)^{3/2} \int \frac{d^d k}{(2\pi)^3} \frac{1}{e^{g_q} - 1}. \tag{4.84}$$

This result is in good agreement with the similar result from the weakly interacting Bose gas if we set $N = 1$ [87]. More general expression, obtained within the paired fermion model, valid not only nearby the phase boundaries and for large temperatures, is given in [37]. We plot the result in Fig. 4.8. There are quantum as well as thermal fluctuations. We see that both fluctuations lead to a depletion of the condensate, but the quantum depletion alone does not change the transition points.

The reason why the N-component hard-core Bose gas is weakly interacting lies in the fact that a boson can occupy one of N different states at each lattice sites. Bosons can avoid the interaction during the tunneling process by choosing an unoccupied state. Since N is large the system is

effectively weakly interacting. In Ref. [109] it was shown that generalizing the N-component bosons to so called colored bosons reinforces interaction to be strong even for $N \to \infty$ and the phase diagram contains the Mott insulating state.

In conclusion, we have presented a model of strongly interacting bosons composed of two tightly bound fermions in an optical lattice. We have calculated the phase diagram, which includes the BEC and the MI. Including Gaussian fluctuations, we have found that the dispersion of quasiparticles is gapless in the BEC phase but has a gap in the MI phase. We have calculated the total density, the condensate density, and the static structure factor. We have shown that the quantum fluctuations as well as thermal fluctuations lead to a depletion of the condensate, but the former do not change the critical points. We have calculated the superfluid density and have shown that at the BEC-MI transition it has a jump from a finite value in the BEC to zero in the MI. In the dilute regime we have derived an effective Gross-Pitaevskii equation for bosons.

Chapter 5

BCS-BEC crossover in a lattice

In this chapter we consider a generalized model compared to the model introduced in the previous chapter. We include the possibility of single fermions to tunnel, as well as an on-site attractive interaction between them. We will show that this model can be applied to the BCS-BEC crossover in a lattice. The bosonic aspects have been studied in detail within the paired fermions model, therefore we concentrate here on fermions. Partly, these results were published in Refs. [36,38].

5.1 BCS-BEC crossover

Interaction between Fermi atoms may lead to the formation of a two-particle bound state. This may happen if the attraction is strong enough to bind the atoms. Moreover, an attractive interaction between many fermions always leads to the formation of Cooper pairs as a many-body effect, even though a two-particle potential does not lead to a bound state. This was shown by Bardeen, Cooper and Schrieffer in their theory of superconductivity in metals [14].

If the attraction is small we get a usual BCS theory of weakly interacting fermions. In this case not all fermions form Cooper pairs and the size of these pairs is large compared to the mean distance between fermions. In the opposite limit of large attraction all fermions can form bound states. This is the BEC limit. The size of molecules is very small and they can be considered as point-like bosons. If we increase attraction, the BCS limit goes smoothly into the BEC limit without any symmetry breaking as it has been pointed out phenomenologically in [69], and based on the microscopic calculations in [27,28,79]. The strength of the pair-wise interaction (its scattering length) can be controlled by the magnetic field by means of

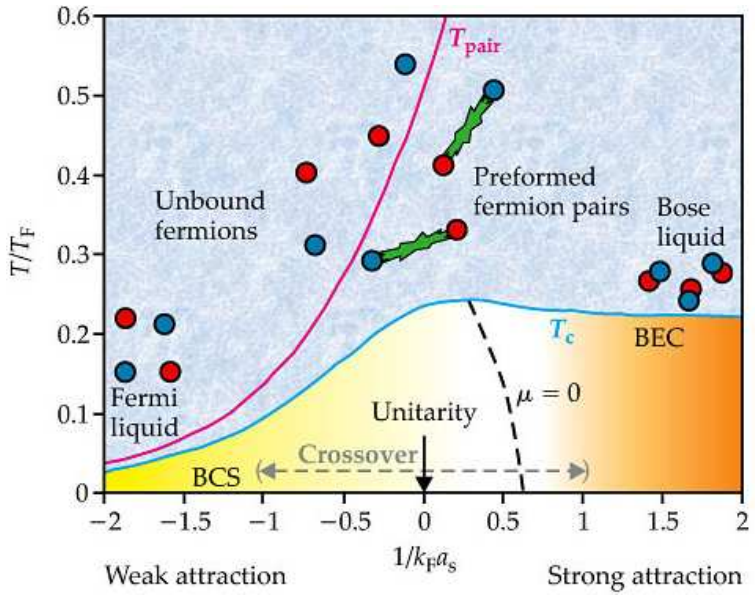

Figure 5.1: Phase diagram of fermions with attractive interaction. Taken from [26].

Feshbach resonance (see for example [99])

$$a_s = a_{bg}\left(1 + \frac{const.}{B_0 - B}\right), \tag{5.1}$$

such that a_s diverges at $B = B_0$. Here a_{bg} is the background (nonresonant) scattering length, which accounts for the nonresonant background interaction U_{bg} (see Eq. (2.11)).

The standard BCS Hamiltonian ($na_0^3 \gg 1$) with small positive U

$$\hat{H} = \sum_{k\sigma}(\epsilon_k - \mu)\hat{c}^\dagger_{k\sigma}\hat{c}_{k\sigma} - U\sum_{k,k'}\hat{c}^\dagger_{k\uparrow}\hat{c}^\dagger_{-k\downarrow}\hat{c}_{-k'\downarrow}\hat{c}_{k'\uparrow} \tag{5.2}$$

can thus be generalized to the strong coupling regime ($na_0^3 \ll 1$) with large U. Here, a_0 denotes the spatial extent of Cooper pairs or bound pairs and n is the density of fermions. In the weak coupling limit, the bound pairs overlap and fermions exchange are dominant. The ground state reads

$$\sim \prod_k (u_k + v_k\hat{c}^\dagger_{k,\uparrow}\hat{c}^\dagger_{-k,\downarrow})|0\rangle. \tag{5.3}$$

In the strong coupling regime, the creation of pairs is described by creation

operator

$$\hat{b}_q^\dagger = \sum_k \phi_k \hat{c}_{k+q/2,\uparrow}^\dagger \hat{c}_{-k+q/2,\downarrow}^\dagger, \tag{5.4}$$

where ϕ_k characterizes the internal structure of a pair. Then the ground state can be represented as a coherent state

$$\sim \exp[\sqrt{N_q}\hat{b}_0^\dagger]|0\rangle, \quad N_q = N/2, \tag{5.5}$$

where N_q is the number of pairs and N is the number of fermions. In this regime, the pairs are point-like ($a_0 \sim 0$) and the exchange interaction between fermions is negligible, so that the exclusion principle plays a minor role.

It turns out, that the ground state changes continuously as the system crosses over from one limit to other. The two limits of the ground state can be described by the same wave function in Eq. (5.3). For strong couplings, $v_k \ll 1$ and we recover Eq. (5.5). The mean-field approach describes equally well both the weak and the strong coupling limits. The chemical potential of fermions changes from $-\epsilon_0$ (bound energy) to k_F^2/m (twice a BCS gap).

The critical temperature in both regimes accounts for two distinct processes. In the weak coupling regime it is controlled by breaking up the Cooper pairs. In the strong coupling regime it is controlled by a Bose-Einstein condensation into a lowest quantum state with the center of mass momentum $q = 0$ of bound pairs. There is a higher temperature in this regime, which corresponds to breaking up the tightly bound pairs. This scenario is shown in Fig. 5.1.

At the Feshbach resonance, the scattering length becomes indefinite and the BCS model is not longer applicable (the interaction is not definite). The condition for perturbative approach, $na_s^3 \ll 1$, is not valid as well. The two-channel model with the coupling to bosonic molecules has been introduced in [53] and further developed in [80,81]. The Hamiltonian reads

$$\begin{aligned}\hat{H} = \sum_{k\sigma} \epsilon_k \hat{c}_{k\sigma}^\dagger \hat{c}_{k\sigma} \quad &+ \quad \sum_q (E_q^0 + 2\nu)\hat{b}_q^\dagger \hat{b}_q - U_{bg} \sum_{k,k'} \hat{c}_{k\uparrow}^\dagger \hat{c}_{-k\downarrow}^\dagger \hat{c}_{-k'\downarrow} \hat{c}_{k'\uparrow} \\ &+ \quad \sum_{k,q} [\hat{b}_q^\dagger \hat{c}_{-k+q/2\downarrow} \hat{c}_{k+q/2\uparrow} + \hat{b}_q \hat{c}_{k+q/2\uparrow}^\dagger \hat{c}_{-k+q/2\downarrow}^\dagger],\end{aligned} \tag{5.6}$$

where $\hat{c}_{k\sigma}^\dagger$ creates a fermion with the spin σ and kinetic energy $\epsilon_k = \hbar^2 k^2/2m$, $\hat{b}_q^\dagger$ creates a boson with kinetic energy $E_q^0 = \hbar^2 q^2/2M$. 2ν describes the detuning from the Feshbach resonance. More precisely, if $2\nu - 2\mu = 0$ we are in the BEC limit, if $2\nu - 2\mu = \infty$ we are in the BCS limit.

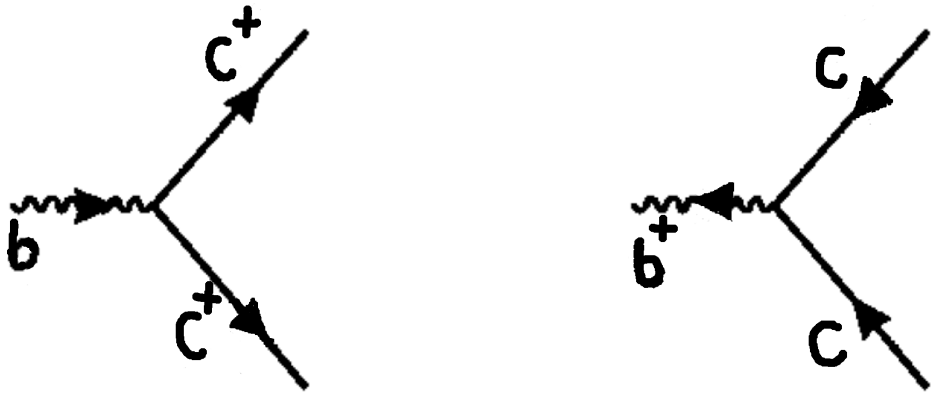

Figure 5.2: Coupling processes between fermions (straight lines) and bosons (wavy lines) in Eq. (5.6).

5.2 Attractive spin-1/2 fermions in a lattice

The above scenario is a bit different in an optical lattice. While in the weak coupling regime the radius of a Cooper-pair is much larger than the lattice spacing and the presence of the lattice makes no difference, in the strong coupling regime local pairs behave as hard-core bosons. The latter is due to the Pauli exclusion principle. This motivates us to study a model in an optical lattice which comprises tunneling of fermions, attractive interaction between fermions (leading to the formation of bosonic molecules) and tunneling of bosonic molecules. There should be no direct interaction between bosonic molecules, because at low temperatures the s-wave scattering is prohibited due to exclusion principle (see the discussion in section 2.2). In Eq. (5.6), the bosons are not hard-core bosons and the model does not describe well the BCS-BEC crossover in a lattice. Thus, a spin-1/2 Fermi gas in a d-dimensional optical lattice superimposed by the trapping potential $V_r = -\gamma(x^2 + y^2)$, where γ is the strength of the trap, can be described via the following Hamiltonian [36, 111]

$$\begin{aligned}\hat{H}_f = -\frac{\bar{t}}{2d}\sum_{\langle r,r'\rangle}\sum_{\sigma=\uparrow,\downarrow}\hat{c}^\dagger_{r\sigma}\hat{c}_{r'\sigma} \;&-\; \frac{J}{2d}\sum_{\langle r,r'\rangle}\hat{c}^\dagger_{r\uparrow}\hat{c}_{r'\uparrow}\hat{c}^\dagger_{r\downarrow}\hat{c}_{r'\downarrow} - \bar{U}\sum_r \hat{c}^\dagger_{r\uparrow}\hat{c}_{r\uparrow}\hat{c}^\dagger_{r\downarrow}\hat{c}_{r\downarrow} \\ &-\; \sum_r V_r \sum_{\sigma=\downarrow,\uparrow}\hat{c}^\dagger_{r\sigma}\hat{c}_{r\sigma} - \sum_r\sum_{\sigma=\uparrow,\downarrow}\bar{\mu}_\sigma\hat{c}^\dagger_{r\sigma}\hat{c}_{r\sigma},\end{aligned} \tag{5.7}$$

where $\hat{c}^\dagger_{r\sigma}$ creates a fermion with spin σ on lattice site r. The first term describes aforementioned tunneling of fermions between neighboring sites

with the rate $\bar{t}/2d$, while the second term describes tunneling of local fermionic pairs with the rate $J/2d$. The third term accounts for local s-wave interaction between fermions with strength $\bar{U}$, where $\bar{U} > 0$ is an attractive interaction. Here we also include a parabolic trapping potential V_r. The latter can be combined with the chemical potential $\bar{\mu}_\sigma$ to $\mu_{r\sigma} = \bar{\mu}_\sigma + V_r$, which controls the number of particles in a grand-canonical ensemble. The chemical potential can be different for different σ, $\bar{\mu}_{\uparrow/\downarrow} = \bar{\mu} \pm h$ with an effective magnetic field $H_z = h$. For the limiting case $\bar{t} = 0$ only bosonic molecules can appear and this model is called paired fermions model and has been studied in the previous chapter. We may thus regard the strong interacting regime (when molecules form) to prevail when the tunneling J is larger than the interaction $\bar{U}$. In the opposite case we have the weak interacting regime, e.g. in the limiting case $J = 0$ we get usual BCS type of model of weakly interacting fermions.

A formal connection between Eq. (5.7) and Eq. (5.6) is explored in Appendix B.3. The relation is the following

$$J = \frac{g^2 \tilde{J}}{(2\nu - 2\mu)^2}, \quad \bar{U} = U_{\mathrm{bg}} + \frac{g^2}{2\nu - 2\mu}. \tag{5.8}$$

It is interesting to notice that in the BCS regime, i.e. if $2\nu - 2\mu \to \infty$, the tunneling $J = 0$ and $\bar{U} = U_{\mathrm{bg}}$. In the BEC regime, i.e. if $2\nu - 2\mu \to 0$, the tunneling J diverges as well as the interaction $\bar{U}$, which means that they are much larger than the tunneling of fermions $\bar{t}$ (so that $\bar{t}$ can be neglected and we arrive again at the paired fermion model). Thus, Eq. (5.7) describes qualitatively correctly the physics of BCS-BEC crossover in a lattice. We notice here that while deriving the above relations given in Eq. (5.8) we have neglected quantum dynamics of bosons in Eq. (5.6). This leads to some qualitative differences between Eq. (5.6) and Eq. (5.7). We will explore this in Sec. 5.6.1.2.

5.3 Hubbard-Stratonovich transformation

The partition function can be written in the form of a functional integral as it is shown in Eq. (4.5) with the action

$$A = \int_0^\beta d\tau \left[\sum_r (\bar{\psi}_{r\tau\uparrow} \partial_\tau \psi_{r\tau\uparrow} + \bar{\psi}_{r\tau\downarrow} \partial_\tau \psi_{r\tau\downarrow}) + H_f(\bar{\psi}_{\tau+\delta}, \psi_\tau) \right], \tag{5.9}$$

where δ should be sent to $+0$ at the end of calculations, τ is the imaginary time, the symbol $\partial_\tau \psi_\tau$ denotes the formal $\lim_{\delta \to +0}(\psi_{\tau+\delta} - \psi_\tau)$, $\beta \equiv (k_B T)^{-1}$ is the inverse temperature.

We perform a Hubbard-Stratonovich transformation to decouple the fourth order terms at the expense of introducing new complex fields. Depending on the relation between the parameters J and $\bar{U}$, there are two ways of how we perform the decoupling. If $|\bar{U}| < J$ we need to introduce two complex fields in order to preserve convergence of the Gaussian integration. In the opposite case, $|\bar{U}| > J$, we need only one complex field. We use the identity

$$\begin{aligned}
&\exp\left(\frac{J}{2d}\sum_{\langle r,r'\rangle}\bar{\psi}_{r\tau+\delta\uparrow}\psi_{r'\tau\uparrow}\bar{\psi}_{r\tau+\delta\downarrow}\psi_{r'\tau\downarrow}+\bar{U}\sum_{r}\bar{\psi}_{r\tau+\delta\uparrow}\psi_{r\tau\uparrow}\bar{\psi}_{r\tau+\delta\downarrow}\psi_{r\tau\downarrow}\right)\\
&= \int\mathcal{D}[\phi,\chi]\exp\left(-\sum_{r,r'}\bar{\phi}_{r\tau}\hat{v}^{-1}_{r,r'}\phi_{r'\tau}-\frac{\mathcal{I}}{S-\bar{U}}\sum_{r}\bar{\chi}_{r\tau}\chi_{r\tau}\right.\\
&- \left.\sum_{r}(i\phi_{r\tau}+\mathcal{I}\chi_{r\tau})\bar{\psi}_{r\tau+\delta\uparrow}\bar{\psi}_{r\tau+\delta\downarrow}-\sum_{r}(i\bar{\phi}_{r\tau}+\mathcal{I}\bar{\chi}_{r\tau})\psi_{r\tau\uparrow}\psi_{r\tau\downarrow}\right), \qquad (5.10)
\end{aligned}$$

where $\mathcal{I}=\theta(J-|\bar{U}|)$ and the matrix $\hat{v}^{-1}$ is given in Eq. (4.8).

Plugging Eq. (5.10) into Eq. (5.9) and integrating out Grassmann fields lead to

$$A_{\text{eff}}=\int_0^\beta d\tau\left\{\sum_{r,r'}\bar{\phi}_{r\tau}\hat{v}^{-1}_{r,r'}\phi_{r'\tau}+\frac{\mathcal{I}}{S-\bar{U}}\sum_{r}\bar{\chi}_{r\tau}\chi_{r\tau}-\log\det\hat{\mathbf{G}}^{-1}\right\} \qquad (5.11)$$

with

$$\hat{\mathbf{G}}^{-1}=\begin{pmatrix}-i\phi-\mathcal{I}\chi & \partial_\tau+\mu_1+\hat{t}\\ \partial_\tau-\mu_2-\hat{t} & i\bar{\phi}+\mathcal{I}\bar{\chi}\end{pmatrix}. \qquad (5.12)$$

Here $\hat{t}=\bar{t}\hat{\omega}$,where $\hat{\omega}_{r,r'}=1/2d$ when r,r' are nearest neighbors, $\mu_1=\bar{\mu}+h, \mu_2=\bar{\mu}-h$.

So far everything is exact. In order to proceed we apply the saddle-point approximation by minimizing the effective action in Eq. (5.11) with respect to the complex fields and arrive at two equations (cf. Eq. (4.12))

$$\delta A_{\text{eff}}=0 \;\Rightarrow\; \begin{cases}\phi=(J+S)G(\phi-i\chi)\\ \chi=-i(S-\bar{U})G(\phi-i\chi)\end{cases}, \qquad (5.13)$$

where $G=\int_{-1}^{1}dx\rho(x)F(x)$ with $F(x)$ given in Appendix B.2 and $\rho(x)$ is the density of states. The nontrivial solution reads

$$G=\frac{1}{J+\bar{U}},\;\; \chi=-\frac{(S-\bar{U})i\phi}{J+S}. \qquad (5.14)$$

The two auxiliary fields appear at $J \geq \bar{U}$. As it is explained above we can perform a formal mapping to the continuum model by regarding $\bar{J}/2d = 1/2M$, where M is the boson mass. The Fermi energy is fixed as $\epsilon_F = (3\pi^2 n)^{3/2}/M$. As it has been shown in [80], for $n = 1, U = 0.3\epsilon_F, g = 0.6\epsilon_F$ stable long-lived bosons exist for $\nu \leq 0.22\epsilon_F, \mu = 0$. This was regarded as an onset of the BEC regime in the crossover. When we put these numbers to $J \geq \bar{U}$ and using Eq. (5.8), we get similarly $\nu \leq 0.227\epsilon_F$. Inspired by this observation we may formally regard the appearance of two auxiliary fields as the entrance to the strongly interacting BEC regime within our model. Later on, we will explore the fate of the quantum fluctuations in both regimes and we will see that they are consistent with the conclusion that auxiliary fields may serve as the hallmark of the BEC regime, while their absence the one of the BCS regime.

5.3.1 Densities of molecules and fermions

Here we calculate the density of condensed molecules, total density of molecules and density of single fermions (see also Ref. [111] for alternative derivations). In the paired fermion model we simple took derivatives of the free energy with respect to the chemical potential by arguing that all fermions were paired up. Now the situation is a bit different and calculation of densities is not an easy task. In order to facilitate consideration we suppose we are in the strong interacting regime, such that the size of molecules is less than the spacing between lattice sites and we treat our bosons as point-like objects. The weak interacting regime is not interesting, since it would reproduce well-known results from the BCS theory. Then, since for point-like bosons their internal structure is irrelevant, Eq. (5.4) reduces to Eq. (4.1) and the density of molecules can be calculated as $n_r^{\mathrm{m}} = \langle \hat{b}_r^\dagger \hat{b}_r \rangle$. The condensed density is given in Eq. (4.17) and the density of fermions is given by $n_{r\sigma} = \frac{1}{\beta}\frac{\partial \ln Z}{\partial \mu_{r\sigma}}$. In terms of the Grassmann fields these quantities are related to one-particle propagators:

$$n_{r\sigma} = \frac{1}{\beta}\int_0^\beta d\tau \lim_{\delta\to 0^+} \langle \bar{\psi}_{r\tau+\delta\sigma}\psi_{r\tau\sigma}\rangle. \tag{5.15}$$

Analogously, the density of bosonic molecules can be measured as a two-particle propagator:

$$n_r^m = \frac{1}{\beta}\int_0^\beta d\tau \lim_{\delta\to 0^+} \langle \bar{\psi}_{r\tau+\delta\uparrow}\psi_{r\tau\uparrow}\bar{\psi}_{r\tau+\delta\downarrow}\psi_{r\tau\downarrow}\rangle. \tag{5.16}$$

The densities of dissociated atoms can be calculated by subtracting n^m from the total numbers of fermions of one species

$$n^f_{r\sigma} = n_{r\sigma} - n^m_r. \tag{5.17}$$

The condensed density reads in terms of Grassmann fields as

$$n_0 = \lim_{|r-r'|\to\infty} \frac{1}{\beta} \int d\tau \lim_{\delta\to 0^+} \langle \bar{\psi}_{r\tau+\delta\downarrow} \bar{\psi}_{r\tau+\delta\uparrow} \psi_{r'\tau\uparrow} \psi_{r'\tau\downarrow} \rangle. \tag{5.18}$$

Using calculations in Appendix B.1 we can relate densities to the Green's matrix from Eq. (5.12):

$$n_{r\uparrow} = \frac{1}{\beta} \sum_n G^{12}_{rr}(\omega_n), \;\; n_{r\downarrow} = -\frac{1}{\beta} \sum_n G^{21}_{rr}(\omega_n) \; . \tag{5.19}$$

Within the mean-field approximation (cf. Ref. [111]) this gives

$$n^f_{r\uparrow} = n_{r\uparrow} - n_{r\uparrow} n_{r\downarrow} - n_{0,r}, \;\; n^f_{r\downarrow} = n_{r\downarrow} - n_{r\uparrow} n_{r\downarrow} - n_{0,r}. \tag{5.20}$$

Here $n_{r\sigma}$ measures the presence of a fermion and absence of a pair of fermions. $n_{r\uparrow} n_{r\downarrow}$ gives the probability to find two fermions on lattice site r. Finally, $n_{0,r}$ is the product of anomalous averages $\sim \langle \psi_\uparrow \psi_\downarrow \rangle \langle \bar{\psi}_\downarrow \bar{\psi}_\uparrow \rangle$ and thus

$$n_{0,r} = \frac{1}{\beta} \sum_n G^{11}_{rr}(\omega_n) \frac{1}{\beta} \sum_n G^{22}_{rr}(\omega_n). \tag{5.21}$$

The condensed density is directly related to the correlation of complex fields, which reads

$$\begin{aligned} \langle \phi_r \bar{\phi}_{r'} \rangle &\sim \int \mathcal{D}[\phi, \psi] \phi_r \bar{\phi}_{r'} e^{-\sum_{r,r'} \bar{\phi}_r \hat{v}^{-1}_{r,r'} \phi_{r'} - \sum_r i\phi_r \psi_{r\uparrow} \psi_{r\downarrow} - \sum_r i\bar{\phi}_r \bar{\psi}_{r\uparrow} \bar{\psi}_{r\downarrow}} \\ &\sim \hat{v}_{r,r'} + \sum_{r_1 r_2} \hat{v}_{r,r_1} \hat{v}_{r',r_2} \langle \psi_{r_1\downarrow} \psi_{r_1\uparrow} \bar{\psi}_{r_2\uparrow} \bar{\psi}_{r_2\downarrow} \rangle. \end{aligned} \tag{5.22}$$

The matrix $\hat{v}$ decays fast for large separations. This implies $n_0 \sim \langle \phi_r \bar{\phi}_{r'} \rangle$ for large spatial separations.

5.3.2 The case of small tunneling rate $\bar{t}$

Here we would like to consider the case of small fermionic tunneling $\bar{t}$ to observe how the inclusion of the latter effects the results of the previous chapter 4, where $\bar{t} = 0$. From Eq. (5.14) we obtain for $T = 0$

$$\int_{-1}^{1} dx \frac{\rho(x)}{\sqrt{(\mu + \bar{t}x)^2 + |\Phi|^2}} = \frac{2}{J + \bar{U}}, \tag{5.23}$$

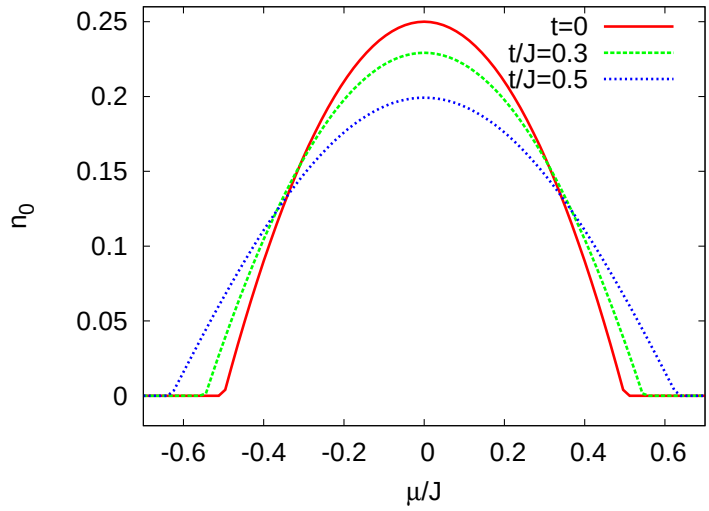

Figure 5.3: The condensed density for several $\bar{t}/J$. The tunneling rate $\bar{t}$ causes the condensate to broaden.

where $|\Phi|^2$ is introduced in Appendix B.2. For small $\bar{t} \neq 0$ we write $|\Phi|^2/9 = |\Phi_0|^2/9 + \delta\Delta = \Delta_0 + \delta\Delta$. Here $|\Phi_0|^2/9$ is the value of the order parameter for $\bar{t} = 0$. Expanding Eq. (5.23) to the second order and using $\int_{-1}^{1} dx\rho(x)x = 0$ we arrive at (here we denote $J_U = J + \bar{U}$)

$$\delta\Delta = -\frac{\bar{t}^2}{2J_U^2}(J_U^2 - 8\mu^2). \tag{5.24}$$

Hence, the contribution is negative for $|\mu| < J_U/\sqrt{8}$ and positive for $|\mu| > J_U/\sqrt{8}$. The same is valid for the condensate density. This means when working within the local density approximation, then the condensed density in the trap tends to squeeze for smaller $\bar{t}$. In other words, in the strongly interacting regime the width of the condensate is smaller than in the weakly interacting gas. An exact mean-field result is shown in Fig. 5.3. This qualitative feature is in agreement with the experiment [15].

The total density of fermions can be obtained using Eq. (5.24) as

$$n_\sigma \approx \frac{1}{2} + \frac{\mu}{J_U} - \frac{\mu}{J_U^3}\bar{t}^2. \tag{5.25}$$

Then the density of dissociated atoms reads (see Eq. (5.20))

$$n_\sigma^f \approx \frac{\bar{t}^2}{2J_U^4}(J_U^2 - 4\mu^2) \equiv \frac{2\bar{t}^2}{J_U^2}n_0, \tag{5.26}$$

where n_0 denotes the density of condensate at $\bar{t} = 0$. The above equation is consistent with the fact that the tunneling $\bar{t}$ supports the dissociation of the molecules.

If we fix the total number of fermions in the system, then we can express the chemical potential through the latter using Eq. (5.25) as

$$\mu \approx \mu_0 + \mu_0 \frac{\bar{t}^2}{J_U^2}, \tag{5.27}$$

where $\mu_0 = J_U(n - 1/2)$. In these terms, the condensate density reads

$$n_0 \approx \frac{J_U^2 - 4\mu_0^2}{4J_U^2} - \frac{\bar{t}^2}{2J_U^2}(J_U^2 - 4\mu_0^2). \tag{5.28}$$

We notice that for the fixed number of fermions $n_0 \rightarrow n_0 - n^f$, $n^{\mathrm{m}} \rightarrow n^{\mathrm{m}} - n^f$. This suggests that the dissociation occurs in the condensate phase. In other words, the Mott insulating state is robust with respect to the dissociation. Here, the two quantum mechanical processes compete with each other, the tunneling and the Pauli exclusion principle. The former forces molecules to dissociate, while the latter prohibits this, since there is no place for fermions to tunnel in a filled optical lattice.

5.4 Pairing with unequal spin populations

Here we consider the influence on pairing with unequal spin populations. This problem was important in the early 1960's to study the influence of a uniform exchange field acting on the spins of the conducting electrons in a superconductor [93]. With the developments on cold atom traps, fermionic systems composed of two particle species with different densities have been also considered [16, 52]. Here we will explore the fate of such unequal spin populations along the BCS-BEC crossover in a lattice.

Unequal spin populations can be described within the grand canonical ensemble as if there is an effective magnetic field acting on fermions. The chemical potentials are different for the two species and their contribution to the Hamiltonian reads

$$\sum_{r\sigma} \mu_\sigma \hat{c}^\dagger_{r\sigma} \hat{c}_{r\sigma} = \mu \sum_{r\sigma} \hat{c}^\dagger_{r\sigma} \hat{c}_{r\sigma} + h \sum_{r\sigma\sigma'} \hat{c}^\dagger_{r\sigma} \hat{\sigma}^z_{\sigma\sigma'} \hat{c}_{r\sigma'}, \tag{5.29}$$

where $\hat{\sigma}^z$ is the Pauli matrix. It is thus seen that the effective magnetic field acting on $1/2$-spin fermions is $2h$.

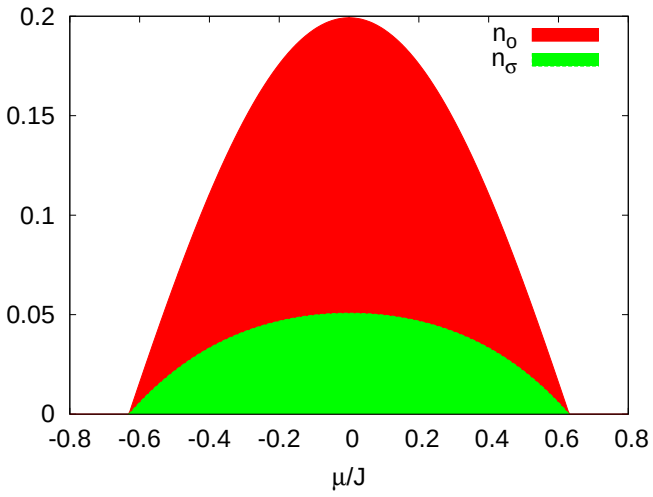

Figure 5.4: A mixture of two attracting Fermi gases with equal spin populations and $\bar{t}/J = 2$, $\bar{U} = 0$, $h = 0$. A part of fermions is paired up and condensed (n_0), while another fermions are still unpaired (n_σ).

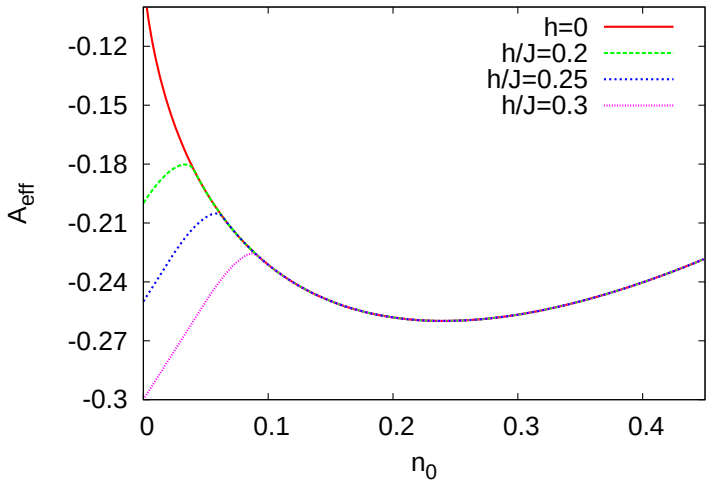

Figure 5.5: The action A_{eff} for $\bar{t}/J = 0.2, \bar{U} = 0$ and various exchange fields h.

In the case of balanced Fermi gases in the presence of an attractive force between the species, a part of them is paired and creates a superfluid state

and another part is still unpaired which is depicted in Fig. 5.4. Here we calculated the densities on the mean-field level, the chemical potential μ can be related to the trap via $\mu \sim r^2$.

Now we turn to the consideration of unequal and attractive spin populations [38]. To this end we need to calculate the action and derive all necessary quantities through it. In the Thomas-Fermi approximation the action reads (see Appendix B.4)

$$A_{\text{eff}} \sim \frac{|\Phi|^2}{J+\bar{U}} - \frac{1}{\beta}\int_{-1}^{1} dx\rho(x)\left(\ln\left[\cosh\left(\frac{x_1\beta}{2}\right)\cosh\left(\frac{x_2\beta}{2}\right)\right] + \beta[\bar{t}x+\mu]\right), \tag{5.30}$$

where x_1 and x_2 are given by Eq. (B.13). Solving Eqs. (5.14), one has also to check whether the action (5.30) is minimal for the solutions obtained.

For finite $\bar{t}$ we resort to numerical calculations. We plot the action for $\bar{t}/J = 0.2, \bar{U} = 0$ for various exchange fields h in Fig. 5.5. It is seen that at $h/J = 0.2$ the action has a minimum at $n_0 \approx 0.25$ but at $h/J = 0.3$ it is minimal at $n_0 = 0$. According to the Ehrenfest classification scheme at some sufficiently large h/J, there is a first order phase transition from finite condensate density $n_0 \approx 0.25$ to $n_0 = 0$.

In order to calculate densities at $\bar{t} \neq 0$ we use Eq. (5.30) at $T = 0$. We can calculate the derivatives with respect to the chemical potentials μ_1 and μ_2 and obtain the total densities of fermions :

$$n_{\uparrow/\downarrow} = \frac{\partial}{\partial\mu_{\uparrow/\downarrow}}(-A_{\text{eff}}) = \frac{1}{4}\int_{-1}^{1} dx\rho(x)\left[\frac{\partial x_1}{\partial\mu_{\uparrow/\downarrow}} + \text{sgn}(\zeta)\frac{\partial x_2}{\partial\mu_{\uparrow/\downarrow}}\right] - \frac{1}{2}, \tag{5.31}$$

where $\frac{\partial x_\alpha}{\partial\mu_{\uparrow/\downarrow}} = \frac{\mu+\bar{t}x}{\sqrt{|\Phi|^2+(\mu+\bar{t}x)^2}} \mp (-1)^\alpha$, $\zeta = \sqrt{|\Phi|^2+(\mu+\bar{t}x)^2} - h$. We calculate numerically the densities of dissociated atoms and condensed densities. The results are shown in Figs. 5.6, 5.7, 5.8. For sufficiently large population imbalance the atoms can overcome a paring barrier and this leads to the appearance of unpaired excess atoms. This leads to phase separation between paired and unpaired atoms due to their mutual repulsion. In the BCS regime the unpaired atoms are more mobile than paired atoms, and thus have enough kinetic energy to climb the trapping potential to create a shell around the superfluid paired fermions as depicted in Fig. 5.6. On the other hand, in the BEC regime the paired atoms are more mobile and the unpaired shell migrates to the center of the trap as depicted in Fig. 5.8.

Experimentally, the unpaired shell of fermions has been observed in [83], where weakly attracting Fermi gas has been considered. Beyond a critical polarization, the gas separated into a phase that is consistent with a superfluid paired core surrounded by a shell of normal unpaired fermions

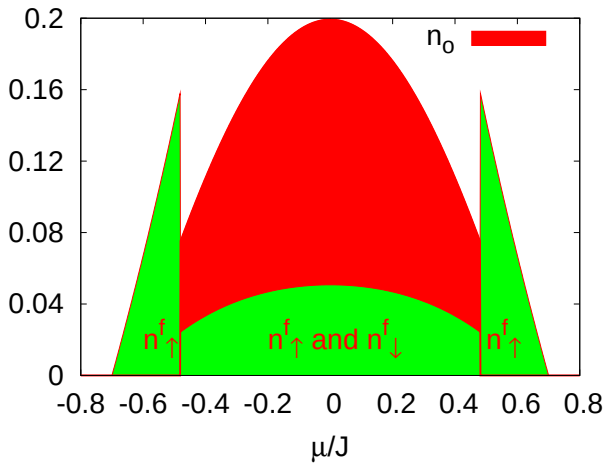

Figure 5.6: A mixture of two attracting Fermi gases with unequal spin populations and $\bar{t}/J = 2$, $\bar{U} = 0$, $h/J = 0.2$. For weak attraction, i.e. if the ratio $\bar{t}/J$ is large, an excess of $\uparrow$ spins creates a shell around superfluid core.

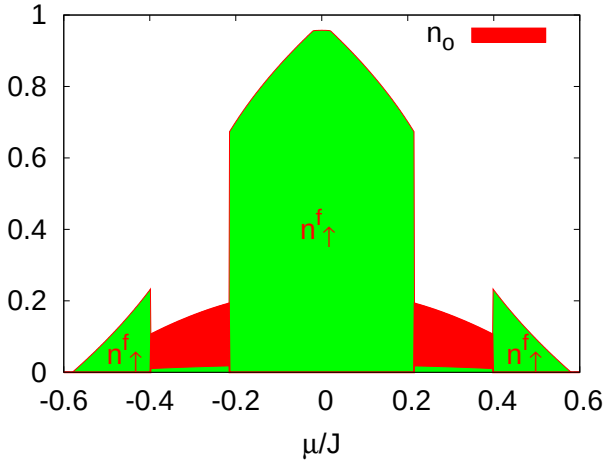

Figure 5.7: A mixture of two attracting Fermi gases with unequal spin populations and $\bar{t}/J = 1.2$, $\bar{U} = 0$, $h/J = 0.28$. For increasing attraction, i.e. weakening of $\bar{t}/J$, the superfluid region creates a shell.

similar to that depicted in Fig. 5.6. We thus predict what may happen in the strongly interacting regime. Similar theoretical studies were per-

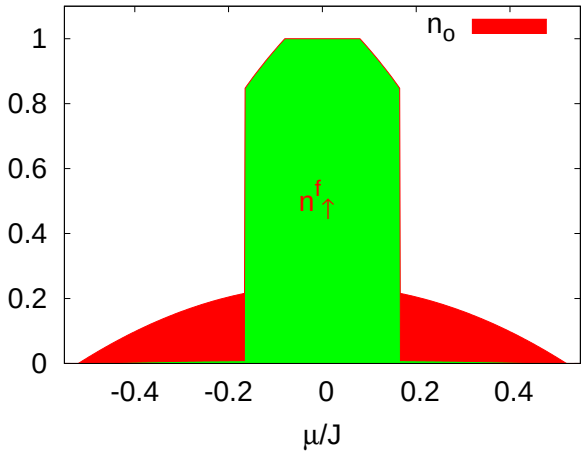

Figure 5.8: A mixture of two attracting Fermi gases with unequal spin populations and $\bar{t}/J = 0.8$, $\bar{U} = 0$, $h/J = 0.28$. For large enough attraction a superfluid phase creates a shell surrounding a spin polarized core.

formed recently in Ref. [57]. The above observation may serve as a hallmark of approaching the BEC regime and can be possible observed in future experiments.

5.5 Trapping potential

In this section we would like to consider attractive fermions in an optical lattice that is superimposed by a trapping potential and to calculate the inhomogeneous densities of fermions and condensed molecules at zero temperature. The observable signature of a superfluid phase near the Feshbach resonance was discussed in Ref. [23]. It was found that the onset of superfluidity leads to a density bulge in the center of the trap. Here we study another feature which may arise when the BEC regime is approached in an optical lattice rather than in the vicinity of the resonance. The hard-core molecules in an optical lattice are expected to reside in the center of the trap, since they are heavier than unpaired fermions. Due to strong Pauli exclusion they will repel dissociated fermions and expel them from the center of the trapping potential. To study this possibility in the following we calculate densities of unpaired fermions in a trap.

The ground state of the system is obtained as the saddle point of the action in Eq. (5.11) with respect to the fields (by solving the equation $\delta A_{eff} =$

0). Here we assume that the solution is static (i.e., independent of τ). Moreover, we also use the fact that a slowly varying field ϕ in space of a trapped condensate can be approximated via Eq. (4.43). Here we generalize it to the the present case and write it compactly (see Appendix B.5):

$$\sum_{r'} \hat{v}^{-1}_{r,r'} \phi_{r'} \approx b\phi_r + Jb^2/a^2 \sum_{r'} \left(\delta_{rr'} - \hat{J}_{rr'} \right) \phi_{r'}, \tag{5.32}$$

where $b^{-1} = (S - \bar{U})\mathcal{I} + \bar{U} + J/a^2, \mathcal{I} = \theta(J/a^2 - \bar{U})$. Then we obtain from $\delta A_{eff} = 0$ the following equations for the fields ϕ, $\bar{\phi}$

$$-\frac{Jb^2}{2d} \sum_{j=1}^{d} \frac{\bar{\phi}_{r+ae_j} - 2\bar{\phi}_r + \bar{\phi}_{r-ae_j}}{a^2} = -b\bar{\phi}_r - i\frac{1}{\beta} \sum_n G^{11}_{rr}(\omega_n), \tag{5.33}$$

$$-\frac{Jb^2}{2d} \sum_{j=1}^{d} \frac{\phi_{r+ae_j} - 2\phi_r + \phi_{r-ae_j}}{a^2} = -b\phi_r + i\frac{1}{\beta} \sum_n G^{22}_{rr}(\omega_n) \, , \tag{5.34}$$

where e_j is the Cartesian lattice unit vector in direction j. $\omega_n = \pi(2n + 1)/\beta$ is a Matsubara frequency originating from the Fourier transformation $\partial_\tau \to -i\omega_n$. The equations of the other complex field χ read

$$\bar{\chi}_r = -\mathcal{I}(S - \bar{U})\frac{1}{\beta} \sum_n G^{11}_{rr}(\omega_n), \;\; \chi_r = \mathcal{I}(S - \bar{U})\frac{1}{\beta} \sum_n G^{22}_{rr}(\omega_n) \, . \tag{5.35}$$

In these equations the Green's matrix $\mathbf{G}^{-1}$ is given in Eq. (5.12). A method to sum over the Matsubara frequencies is given in Appendix B.6. Eqs. (5.33) and (5.34) are analogous to the Gross-Pitaevskii equation for a Bose gas and provide a macroscopic wave function of the condensate molecules. The left-hand side of Eqs. (5.33) and (5.34) can be understood as a lattice Laplacian acting on the field:

$$\Delta\phi_r = \sum_{j=1}^{d} \frac{\bar{\phi}_{r+ae_j} - 2\bar{\phi}_r + \bar{\phi}_{r-ae_j}}{a^2} \, . \tag{5.36}$$

Thus, these equations are similar to the Poisson equation $0 = \nabla^2\Phi - \rho$. It should also be noticed that the additional condition $\Delta\phi = 0$ gives the Thomas-Fermi approximation.

5.5.1 Relaxation method

Eqs. (5.33) and (5.34) are similar to the Poisson equation $0 = \nabla^2\phi - \rho$. An elementary technique to solve Poisson equation is by relaxation, i.e.

to add an artificial time dependent term and write Poisson equation as $\partial\phi/\partial t = \nabla^2\phi - \rho$, provided the right-hand side is positive, and to evolve it for long time until ϕ no longer changes ($\partial\phi/\partial t = 0$) and thus the Poisson equation is satisfied. Relaxation techniques description can be found in Chapter 16 of [88]. This technique is also used to solve Schrödinger and NLS equations and the Poisson form is obtained by the Wick transformation in time $\tau = it$ obtaining $-\partial\psi/\partial\tau = (-1/2\nabla^2 + V)\psi$. In the latter, the relaxation technique is commonly called imaginary time propagation.

Let us consider the case $d = 2$. The Poisson equation can be written as $\partial\phi/\partial t = A + B$, where $A = \partial^2\phi/\partial x^2 + \partial^2\phi/\partial y^2$ and $B = -\rho$. Thus this equation can be evolved according the split-step operator technique, i.e. we evolve $\partial\phi/\partial t = A$ and $\partial\phi/\partial t = B$ in successive time steps Δt, which corresponds formally to $\exp[(A + B)\Delta t] = \exp(A\Delta t) * \exp(B\Delta t) + \mathcal{O}(\Delta t^2)$ This introduces an error of Δt^2. Further improvement can be done by the splitting $\exp[(A + B)\Delta t] = \exp(A\Delta t/2)\exp(B\Delta t)\exp(A\Delta t/2) + \mathcal{O}(\Delta t^3)$. Thus we evolve A by half time step, B by one time step and A by half time step successively. We can make the splitting error as small as we can by diminishing the time step.

The nabla square evolution corresponds to numerical solution of the heat equation in two dimensions, well described in textbooks. In this case one can apply explicit method that recover the form of the discretization Eq. (5.36). However the Crank-Nicolson (CN) algorithm is well known to be more accurate and more stable. Generalizations of the CN algorithm in two dimensions can be either the Peaceman-Rachford or the Mitchel-Fairweather splitting direction schemes, or simple split step as applied to operators A and B discussed.

Since the function has periodic boundary condition it is easier to use the CN split step in the two directions CN_x and CN_y, where each CN has periodic boundary conditions. The final evolution algorithm has the form

$$\bar{\phi} \leftarrow CN_y\bar{\phi}, (\Delta t/2) \tag{5.37}$$

$$\bar{\phi} \leftarrow CN_x\bar{\phi}, (\Delta t/2) \tag{5.38}$$

$$\phi \leftarrow CN_y\phi, (\Delta t/2) \tag{5.39}$$

$$\phi \leftarrow CN_x\phi, (\Delta t/2) \tag{5.40}$$

calculate $\frac{1}{\beta}\sum_n G_{rr,11}(\omega_n)$ and $\frac{1}{\beta}\sum_n G_{rr,22}(\omega_n)$ through summation tricks described in Appendix B.6 and using LAPACK package for eigenvalues and eigenvectors. Then

$$\bar{\chi_r} \leftarrow \bar{\chi_r} + \Delta t[-\bar{\chi_r} - (S - \bar{U})\frac{1}{\beta}\sum_n G_{rr,11}(\omega_n)], \tag{5.41}$$

$$\chi_r \leftarrow \chi_r + \Delta t[-\chi_r + (S-\bar{U})\frac{1}{\beta}\sum_n G_{rr,22}(\omega_n)], \tag{5.42}$$

$$\bar{\phi}_r \leftarrow \bar{\phi}_r + \Delta t[-4/(Jb)\bar{\phi}_r + i4/(Jb^2(S-\bar{U}))\bar{\chi}_r], \tag{5.43}$$

$$\phi_r \leftarrow \phi_r + \Delta t[-4/(Jb)\phi_r + i4/(Jb^2(S-\bar{U}))\chi_r], \tag{5.44}$$

$$\bar{\phi} \leftarrow CN_y\bar{\phi}, (\Delta t/2) \tag{5.45}$$

$$\bar{\phi} \leftarrow CN_x\bar{\phi}, (\Delta t/2) \tag{5.46}$$

$$\phi \leftarrow CN_y\phi, (\Delta t/2) \tag{5.47}$$

$$\phi \leftarrow CN_x\phi, (\Delta t/2) \tag{5.48}$$

and then return to Eq. (5.37). The algorithm is started with harmonic oscillator profile loaded initially to $\bar{\phi}$,ϕ and $\bar{\chi} = \chi = i$.

The relaxation scheme sometimes can delay long time to converge to the desired solution. Convergence rate can be improved through acceleration methods. Acceleration of elementary iterative process can be found in Qinney [89]. Extension to elliptic equations (as Poisson) can be found in the same book chapter 6 and in Numerical Recipes [88], chapter 16.

Acceleration is implemented by doing after each full step (5.37-5.48)

$$\bar{\phi} \leftarrow \bar{\phi}_{old} + \omega_{acc}\cdot(\bar{\phi} - \bar{\phi}_{old}), \tag{5.49}$$

$$\phi \leftarrow \phi_{old} + \omega_{acc}\cdot(\phi - \phi_{old}), \tag{5.50}$$

$$\bar{\chi} \leftarrow \bar{\chi}_{old} + \omega_{acc}\cdot(\bar{\chi} - \bar{\chi}_{old}), \tag{5.51}$$

$$\chi \leftarrow \chi_{old} + \omega_{acc}\cdot(\chi - \chi_{old}), \tag{5.52}$$

where subscript *old* means value at previous time step, ω_{acc} is a number between 1 and 2 that must be found empirically by numerical tests.

5.5.2 Densities of fermions in a trap

We calculate numerically the densities of a two-dimensional Fermi gas in the strongly interacting regime for $J/a^2 > |\bar{U}|$ and 400 lattice sites. The length of the system is $L = 10 = Na$ and we define the energy units $E = J/L^2$. Then the condition $J/a^2 > |\bar{U}|$ corresponds to $|\bar{U}| < 400E \equiv |\bar{U}_c|$. We fix the chemical potential $\bar{\mu} = 0$ and $\gamma = 500E/L^2$. In Fig. 5.9 the condensed density as well as the density of dissociated atoms are plotted for $\bar{U} = 200E$ ($< |\bar{U}_c|$, BEC regime). We notice that there is a dip at the center of the trap in the case of the dissociated atoms. A weaker attraction of fermions ($\bar{U} = 600E > |\bar{U}_c|$, in the BCS regime, Fig. 5.10) makes this

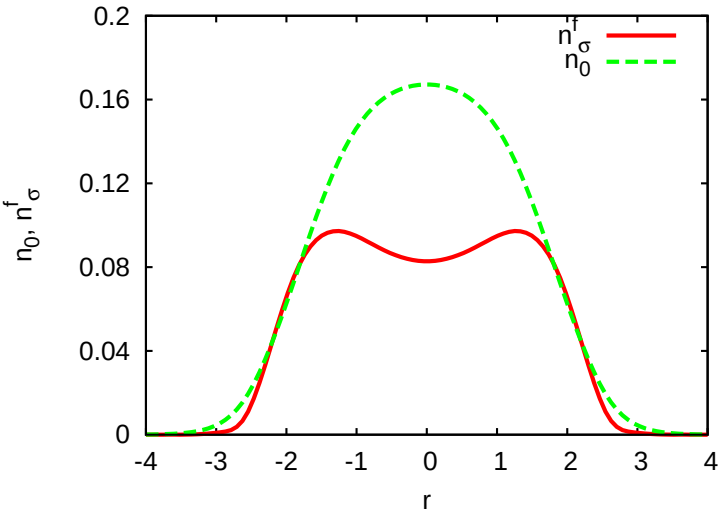

Figure 5.9: The condensate density and the density of dissociated atoms for $\bar{t}/J = 0.3$, $\bar{U} = 200E$. There is a dip at the center of the trap in the case of the dissociated atoms. It maybe explained by the Pauli exclusion principle acting between paired and unpaired fermions [36].

dip less pronounced. In Fig. 5.11 we also plot the densities in the Thomas-Fermi approximation that does not reveal the dip formations as compared to Fig. 5.9.

The dip formation can be explained by the following. In the BEC regime the nonlocal interaction in Eq. (5.7) ($\sim J$) dominates the local interaction ($\sim \bar{U}$), while in the BCS regime the latter is dominant. Thus contribution of the nonlocal nabla term in Eqs. (5.33) and (5.34) is essential for the BEC regime, and cannot be neglected. The Pauli exclusion acts between paired and unpaired fermions and causes the paired fermions to repel the dissociated ones (similar mechanism acts in the case of unbalanced Fermi mixtures, see e.g. Ref. [56]).

Eq. (5.7) describes a one band fermionic model and thus is valid for a deep optical periodic potential. For a shallow lattice, when higher bands are available, the Pauli exclusion is less efficient and we expect the dip formation to be less pronounced. We also expect that present results may be seen in the trapped system without an optical lattice. Similar mechanism of the Pauli exclusion would trigger the phase separation between paired fermions and unpaired fermions but the former is not so efficient as in the deep optical lattice.

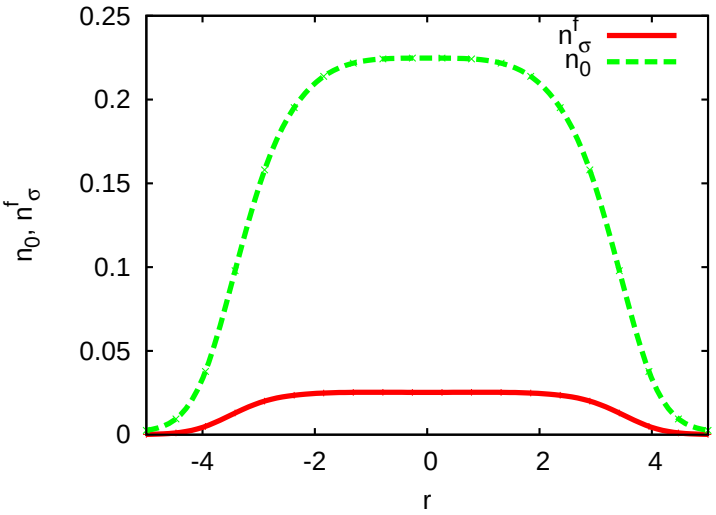

Figure 5.10: The condensate density and the density of dissociated atoms for $\bar{t}/J = 0.5$, $\bar{U} = 600E$. There is no dip at the center of the trap in the case of the dissociated atoms [36].

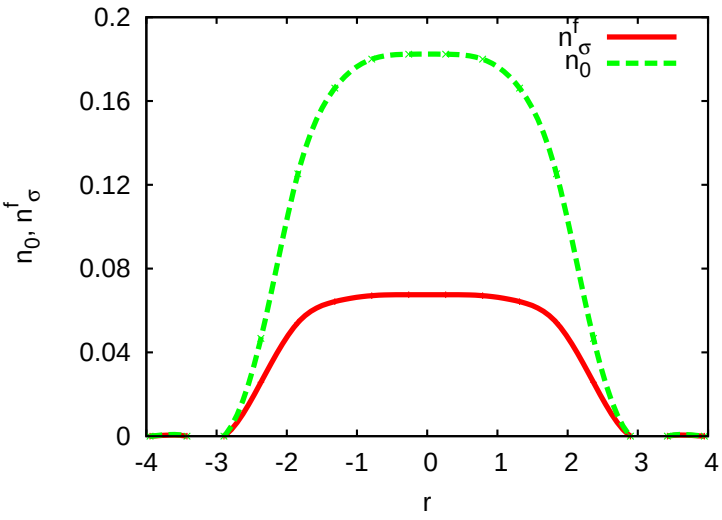

Figure 5.11: The condensate density and the density of dissociated atoms in Thomas-Fermi approximation for the same values of $\bar{t}/J$ and $\bar{U}$ as in Fig. 5.9 [36].

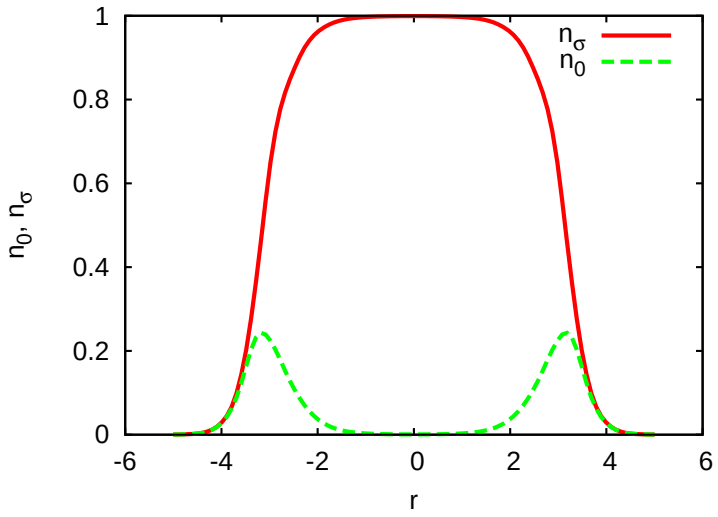

Figure 5.12: Mott state in the trap for values of $\bar{t}/J = 0$ and $\bar{U} = 0$. The chemical potential is $\mu = 1$, in contrast to all other plots where $\mu = 0$ [36].

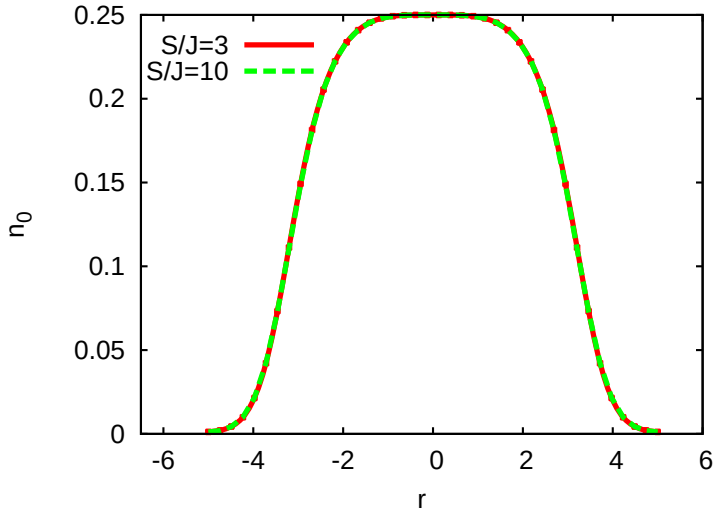

Figure 5.13: The condensate density for different values of the free parameter S. $\bar{t} = 0$, $\bar{U} = 0$. The condensate density is not sensitive to the change of the free parameter S in a wide range.

The presence of the lattice can also lead to the formation of incompress-

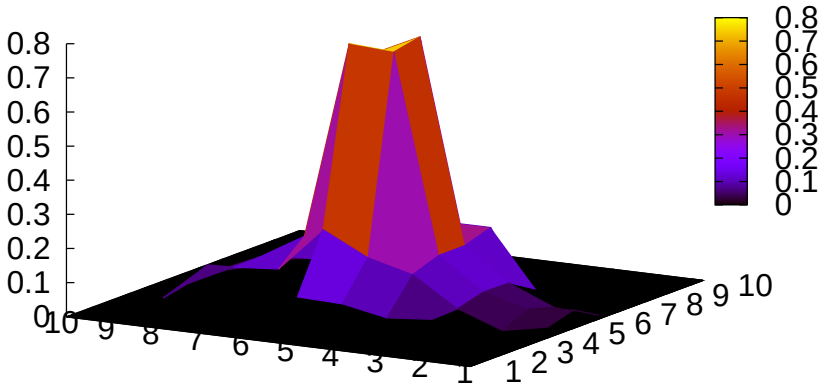

Figure 5.14: An effective single-particle potential in units of the tunneling J acting on dissociated fermions and leading to the dip in Fig. 5.9.

ible states like Mott insulating state of the bound molecules. In Fig. 5.12 a Mott plateau is formed if the number of paired molecules is increased due to a larger chemical potential. Here we present the case when all fermions are paired in the trap. The superfluid shell is also seen which resembles the bottom part of a 'wedding cake' type density profile [29].

For completeness, we plot the condensate density for different values of the free parameter S in Fig. 5.13. We see that the results are not sensitive to the change of this parameter in a wide range. Therefore, we are free to choose it at will. We have thus chosen it to be equal to $\bar{U}$ throughout this section.

5.5.2.1 Effective one-particle Hamiltonian

From Eq. (5.19) the density matrix for fermions can be written as

$$\rho_{rr'\uparrow} = \frac{1}{\beta}\sum_n G^{12}_{rr'}(\omega_n), \quad \rho_{rr'\downarrow} = -\frac{1}{\beta}\sum_n G^{21}_{rr'}(\omega_n). \tag{5.53}$$

Then, the density matrix for the dissociated atoms reads

$$\rho^{\mathrm{f}}_{rr'} = \rho_{rr'\uparrow} - \rho_{rr'\uparrow}\rho_{rr'\downarrow} - \frac{1}{\beta}\sum_n G_{rr,11}(\omega_n)\frac{1}{\beta}\sum_n G_{r'r',22}(\omega_n). \tag{5.54}$$

The diagonal elements of the density matrix give the density of particles. We compare the expression in Eq. (5.54) with an expression of the density matrix of non-interacting fermions

$$\rho^{\mathrm{f}}_{rr'} = \sum_k f_k \hat{U}^{\dagger}_{rk}\hat{U}_{kr'} \tag{5.55}$$

with the Fermi distribution function f_k. Therefore, we have gotten an eigenvalue problem. The eigenvalues f_k corresponds to an effective one-particle Hamiltonian of the dissociated atoms. The latter contains an affective potential depicted in Fig. 5.14. This potential repels fermions from the center of the trap creating the dip pattern shown in Fig. 5.9.

The effect of dip formation at the trap center for strong interactions can possibly be observed in future experiments and may serve as a signature of approaching the BEC regime of the BCS-BEC crossover in a lattice.

5.6 Quantum fluctuations

5.6.1 Second order

Quantum fields ϕ and χ fluctuate around their mean-field values. Performing similar calculations as in section 4.3 we get Eq. (4.23) with the effective action similar to that shown in Eq. (A.5). The Green's matrix (A.6) is now changed and contains different elements, represented in Appendix B.7.1.

5.6.1.1 Boson scattering length

Instead of surfing among similar calculations, as we have done for paired fermions in Chapter 4 to explore the physics of condensed molecules, here we concentrate on the effects of finite tunneling rate $\bar{t}$. Firstly, we will explore the effect of quantum fluctuations of the second order by calculating a boson scattering length a_B and look how it changes if we change the tunneling rate $\bar{t}$.

In the BEC phase we expect the excitation energy for small momenta to be linear, i.e. $\epsilon_q \approx cq$ with the sound velocity for the weakly interacting

Bose gas (see Eq. (3.7))

$$c^2 = 4\pi a_B n_0 / m_B^2. \tag{5.56}$$

Here, n_0 is the condensate density, m_B is the bare mass of bosons and a_B is the scattering length of bosons. The mass of bosons can be related to the tunneling rate J as $m_B \approx 2d/J$. The quasiparticle spectrum ϵ_q is obtained from the poles of the Green's matrix as

$$\det \mathcal{G}^{-1}(i\omega_n, q) = 0 \tag{5.57}$$

by performing analytical continuation afterwards, $i\omega_n = \omega_q + i0^+$, and setting $\epsilon_q = \omega_q$.

For small momenta q, Eq. (5.57) yields (we denote $p = \{i\omega_n, q\}$)

$$A^2(p)(\bar{U} + Jg_q)^2 = [1 - B(p)(\bar{U} + Jg_q)][1 - B(-p)(\bar{U} + Jg_q)]. \tag{5.58}$$

Here $A(p)$, $B(p)$ are given in Appendix B.7.1.

If we set $g = 0$, then we get (see Eq. (5.8))

$$A^2(p) = [1/U_{bg} - B(p)][1/U_{bg} - B(-p)]. \tag{5.59}$$

This equation has been considered in detail in Ref. [28]. The authors have performed expansion for small q and ω_n and found that the sound velocity in the weak coupling limit (small U_{bg}) is $c = v_F/\sqrt{3}$, while in the strong coupling limit (large U_{bg}) it is $c = v_F\sqrt{k_F a_s/3\pi}$. In the latter case the boson scattering length $a_B = 2a_s$, where a_s is the scattering length of the contact potential U_{bg} (see Eq. (2.11)). Here v_F is the Fermi velocity. The bare mass of fermions m_F is also related to the tunneling rate $\bar{t}$ as $m_F \approx 2d/\bar{t}$. Then the Fermi momentum k_F and the Fermi velocity $v_F = \hbar k_F/m_F$ can be calculated as $\epsilon_F = k_F^2/2m_F = (3\pi^2 n)^{2/3}/2m_F$.

For $g \neq 0$ we have a slightly modified equation:

$$A^2(p) = [1/\bar{U} - B(p)][1/\bar{U} - B(-p)] - 2Jg_q A(0)/\bar{U}^2. \tag{5.60}$$

In the weak coupling regime, the second term on the right-hand side vanishes as expected. But in the strong coupling regime it is finite and reads $-2\tilde{J}g_q A(0)/g^2 \approx -q^2 A(0)/\tilde{m}_B g^2$, where $\tilde{m}_B = 2d/\tilde{J}$. The relation between J and $\tilde{J}$ is given in Eq. (5.8).

We perform expansion in small ω_n and q. It appears that the sound velocity is reduced:

$$c^2 = 4\pi n_b a_B/m_B^2 - (16)^3\epsilon_F^2/(m_B^2 g^2 k_F) \tag{5.61}$$

with $n_b = n/2, a_B = 2a_s$. We see that the second term scales as $\sim -\bar{t}^2$ and vanishes gradually as $\bar{t}$ approaches zero. It means that the finite tunneling

rate $\bar{t}$ reduces the scattering length between bosons in the dilute regime (cf. Eq. (5.56)). Eq. (5.61) suggests that there are two contributions to the interaction, a direct and a mediated ones. The latter tries to reduce the direct one. This is caused by the dissociated fermions: a fermion placed between two paired bosons pushes them apart due to the Pauli exclusion principle and thus effectively screens the interaction between them.

5.6.1.2 Comparison with the two-channel model

The two-channel model has been introduced in Eq. (5.6). It describes the BCS-BEC crossover in free space. On the mean-field level, the lattice model in Eq. (5.7) and the two-channel model are related formally via Eq. (5.8). Physically the nature of the Hubbard-Stratonovich fields ϕ in the lattice model is of different nature than the corresponding fields originating from the two-channel model (see Eq. (B.21)). As a result, in the BEC limit the two channel model describes a non-interacting Bose gas, while the lattice model describes a hard-core Bose gas.

Here we study the quantum fluctuations in the two-channel model in order to compare it with the lattice model. The new quantum features are brought by the term $\bar{\phi}_{r\tau}\partial_\tau\phi_{r\tau}$ in the action (see Eq. (B.21)). This apparently innocent term leads to profound results. We consider the case $\bar{t} = 0$ for simplicity. Performing similar calculations as in the chapter 4, we obtain the following expression for the order parameter within the two-channel model

$$\Delta_0^2 = \frac{\bar{U}^2}{4} - \mu^2 \tag{5.62}$$

with $\bar{U} = g^2/(2\nu - 2\mu)$. Fluctuations around the mean-field result yield two modes

$$\epsilon_q^2 = \frac{1}{2}\left(a_q \pm \sqrt{a_q^2 - b_q^2}\right) \tag{5.63}$$

with $a_q = (g^4 - 4\mu\nu^3)/\nu^2 + (Jq^2+\nu)^2$ and $b_q = 2q\sqrt{J(g^4\nu - 4\mu^2\nu^3 + Jg^4q^2)}/\nu$.

We notice that within the lattice model we have obtained one mode. The second one was absent, since it is not possible to excite it due to the hard-core nature of the bosons. From Eq. (B.22) it is seen that in order to suppress the term $\bar{\phi}_{r\tau}\partial_\tau\phi_{r\tau}$, we can send $g \to \infty$. In this case one of the modes has an infinite gap, while the other one reads

$$\epsilon_q = \sqrt{Jq^2(\nu + Jq^2)}, \tag{5.64}$$

which is the Bogoliubov type of excitation similar to that in the paired fermion model.

In the vicinity of the phase transition, where $\Delta_0 \approx 0$, for small momenta Eq. (5.63) yields

$$\epsilon_q = \begin{cases} 2Jq^2|\mu|/|2\mu - \nu|, \\ \sqrt{(2\mu-\nu)^2 + 2\nu J q^2}. \end{cases} \tag{5.65}$$

We see that one mode is gapless, while the other one is gaped. The former represents phase fluctuations, while the latter represents density fluctuations. An effective field theory for the BCS-BEC crossover in free space has been derived in Ref. [66]. There, the gapless mode has been also studied in detail.

To summarize, the two-channel model in Eq. (5.6) gives a gaped and a gapless modes, while the lattice model in Eq. (5.7) gives only a gapless mode. This feature arises due to the hard-core nature of bosons in the lattice model, as it is discussed in detail in chapter 4.

5.6.2 Quartic order

So far we have expanded the effective action to the second order to observe low energy fluctuations of the order parameter. In this section we would like to make one step further and expand it to the fourth order. We carry the analysis out for $T = 0$ as well as for finite T. The effective action then can be written as the sum of three terms $\delta A_{\text{eff}} \approx A_0 + A_2 + A_4$. Here A_0 is the action originated from the saddle-point calculations, A_2 is the second order correction (which has been explored in the previous section). The third term represents the fourth order correction and can be written as (see Appendix B.7.2)

$$A_4 = \frac{1}{2} \sum_{p_1,p_2,p_3} \delta\bar{\Delta}_{p_1} \delta\Delta_{p_2} \delta\bar{\Delta}_{p_3} \delta\Delta_{-p_1-p_2-p_3} \Gamma(p_1,p_2,p_3), \tag{5.66}$$

where the so-called vertex function

$$\Gamma(p_1,p_2,p_3) = \frac{1}{\beta^2} \sum_k G^0_{12}(k) G^0_{21}(k-p_1) G^0_{12}(k-p_1-p_2) G^0_{21}(k-p_1-p_2-p_3) \tag{5.67}$$

has been introduced.

Minimizing the action δA_{eff} with respect to the fields we get (see details in Appendix B.7.2)

$$-i\omega_n d(q)\delta\phi_q + (1+(J+S-\bar{U})B(q))^2 \left[v^{-1}(q) - \frac{B(q)}{1+(J+S-\bar{U})B(q)}\right] \delta\phi_q + g_s \sum_{p_2,p_3} \delta\phi_{p_2} \delta\bar{\phi}_{p_3} \delta\phi_{-p-p_2-p_3} = 0 \tag{5.68}$$

This expression resembles the Gross-Pitaevskii equation. The first term originates from the time derivative, if we Fourier transform it to the real time domain, while the third one accounts for the interaction. The second term may depend on the free parameter S (it has been introduced in the paired fermion model), which is the shortcoming of our approximation. But the most interesting thing, what we can look at, are the first and the third terms. The interactions g_s includes an effective dimer-dimer interaction mediated by the gas of dissociated fermions. It contains the direct dimer-dimer interaction, which unlike the mediated one, does not vanish for $\bar{t} = 0$ (see Eq. B.56). We thus can write $g_s = U_{\text{direct}} - U_{\text{mediated}}$. This feature is similar to that which has been discussed at the and of the previous section. However, here the effective interaction is between bosons of the effective low energy field theory on the top of the trivial saddle-point results (we have expanded around the vanishing order parameter) culminating in the Gross-Pitaevskii equation (5.68). On the other hand, the considerations in the previous section includes nonperturbative effects of bound state formation and condensation of the nontrivial saddle-point results (the order parameter was finite).

At $T = 0$, the first term is purely imaginary, indicating that the modes are not damped on this level of approximation. It is a quit satisfactory result since it is known that the fermionic excitations have a gap in the BEC limit. We will see in the next section how this gap appears. At finite temperatures we calculate the coefficient $d(q)$ carefully at $q = 0$, since it may happen that finite temperature can cause a damping mechanism and $d(q)$ is imaginary. $d(q)$ is related to $B(p)$, so that we calculate the latter quantity first by using the Dirac identity,

$$\lim_{\delta \to +0} \frac{1}{x \pm i\delta} = \mathcal{P}\frac{1}{x} \mp i\pi\delta(x), \tag{5.69}$$

where $\mathcal{P}\frac{1}{x}$ denotes the principal part of $1/x$, and we arrive at

$$B(\omega_q + i0^+, 0) = \mathcal{P}\int_{-1}^{1} dx \rho(x) \frac{\tanh[\beta|\bar{t}x + \mu|/2]}{\omega_q - 2|\bar{t}x + \mu|} - i\pi \frac{\rho(\mu/\bar{t})}{\bar{t}} \tanh[\beta\omega_q/4]. \tag{5.70}$$

From this follows (see also Appendix B.7.2 for similar calculation done for $T = 0$) that for finite temperatures and $\omega_q \ll |\mu|$

$$d(0) = \sum_k \frac{\tanh(\beta\epsilon_k/2)}{4\epsilon_k^2} + i\frac{\pi}{4\bar{t}}\beta\rho(\mu/\bar{t}), \tag{5.71}$$

where ρ is the density of states. It is finite if its argument $x \in [-1, 1]$. Thus, for $|\mu| < \bar{t}$ modes are damped (since $d(0)$ is imaginary), while for $|\mu| >$

$\bar{t}$ they are propagating (since $d(0)$ is real). The above results have been obtained for the vanishing order parameter, i.e. near the phase boundary. Alluding to our saddle-point calculations, at the phase boundary $|\mu| \sim J$. Then using Eq. (5.8) and the considerations from above we conclude that if the ratio $\bar{t}/J$ is small, then the system is in the BEC regime and the modes are propagating. On the other hand, if $\bar{t}/J$ is comparable to one, then the system is in the BCS regime and the modes are damped. This is in agreement with the statements in Ref. [27]. The point at which these modes become propagating is regarded as a crossover point between BEC and BCS regimes. Thus, the appearance of the auxiliary fields (i.e., if $\bar{t}/J$ is small) may lead to the propagating mode and thus to the BEC regime. This point, despite being semi-qualitative, strengthens the arguments given at the end of section 5.3 that auxiliary fields represent the hallmark of the BEC phase.

5.6.3 Spectral function

In the previous section we considered the field fluctuations at small momenta. To take into account for the field fluctuations for larger momenta we have to perform properly the analytical continuation by mapping the imaginary time Green's function onto the real time Green's function in order to extract the real time dynamics of the excitation modes of the system. This is done by $i\omega_n = \omega + i0^+$. The spectral function is related to the retarded Green's function by [3]

$$A(q,\omega) = \frac{1}{\pi}\mathrm{Im}G^{11}(q,\omega + i0^+), \tag{5.72}$$

where the superscript "11" means that we are calculating the $(1,1)$ element of the inverse of the matrix in Eq. (B.44). We calculate the one-particle spectral function in the vicinity of the phase boundary, where the order parameter can be supposed to be equal to zero. Then, the straightforward calculation yields

$$A(q,\omega) = \frac{v_q^2}{\pi[\bar{U} - Jg_q]^2}\frac{\mathrm{Im}B(\omega + i0^+, q)}{\left(\frac{1}{\bar{U}-Jg_q} - \mathrm{Re}B(\omega + i0^+, q)\right)^2 + \mathrm{Im}B(\omega + i0^+, q)^2}. \tag{5.73}$$

The spectral function has a Lorentzian form with the width $\sim \mathrm{Im}B(\omega + i0^+, q)$. The prefactor depends on the free parameter S through the function $v_q = J + S - Jg_q$. It can be fixed for the current purposes from the

normalization condition

$$\int_{-\infty}^{\infty} d\omega A(q,\omega) = 1. \tag{5.74}$$

We are not interested in the exact shape of the spectral function, but rather in the points, where it vanishes. At the phase boundaries and for $h = 0$ we obtain

$$B(i\omega_n, q) = \sum_k \frac{\theta(\epsilon_k)\theta(\epsilon_{k+q})}{-i\omega_n + \epsilon_k + \epsilon_{k+q}} - \sum_k \frac{\theta(-\epsilon_k)\theta(-\epsilon_{k+q})}{-i\omega_n + \epsilon_k + \epsilon_{k+q}}. \tag{5.75}$$

We can calculate the real and imaginary parts by using Eq. (5.69)

$$\mathrm{Re}B(\omega + i0^+, q) = \mathcal{P}\sum_k \frac{\theta(\epsilon_k)\theta(\epsilon_{k+q})}{-\omega + \epsilon_k + \epsilon_{k+q}} - \mathcal{P}\sum_k \frac{\theta(-\epsilon_k)\theta(-\epsilon_{k+q})}{-\omega + \epsilon_k + \epsilon_{k+q}} \tag{5.76}$$

$$\mathrm{Im}B(\omega + i0^+, q) = \pi\sum_k [\theta(\epsilon_k) + \theta(\epsilon_{k+q}) - 1]\delta(-\omega + \epsilon_k + \epsilon_{k+q}). \tag{5.77}$$

Numerical results for $h = 0$ are presented in Fig. 5.15. We see that there are a coherent and an incoherent contributions. The coherent contribution is a delta peak in the spectral function and accounts for the quasiparticle excitation spectrum of the molecules with infinite lifetime. The incoherent contribution has a finite width, which accounts for the finite lifetime of the excitations. In this case the excitations are particle-hole excitation, which appear due to dissociation of bound pairs. It can be seen from the fact that the incoherent branch is absent for $\bar{t} = 0$.

The calculations can be extended for the case $h \neq 0$. At $q = 0$, the incoherent branch satisfies

$$\mathrm{Im}B(\omega + i0^+, 0) = \frac{\pi}{\bar{t}}\rho\left(\frac{\omega - 2\mu}{2\bar{t}}\right)\theta(\omega - 2h), \tag{5.78}$$

where ρ is the density of states. From the latter we see that the incoherent branch of the spectral function is nonzero for

$$2(\mu - \bar{t}) < \omega < 2(\mu + \bar{t}). \tag{5.79}$$

The explanation of the above result goes as follows. We create an excitation of two fermions with energy $2\mu = \mu_1 + \mu_2$ (the chemical potential corresponds to the energy necessary to add a particle to the system, therefore two fermions give the factor 2). The characteristic time for particles to tunnel, i.e. to leave this excitation formation, is $\sim 1/\bar{t}$, so that the width of

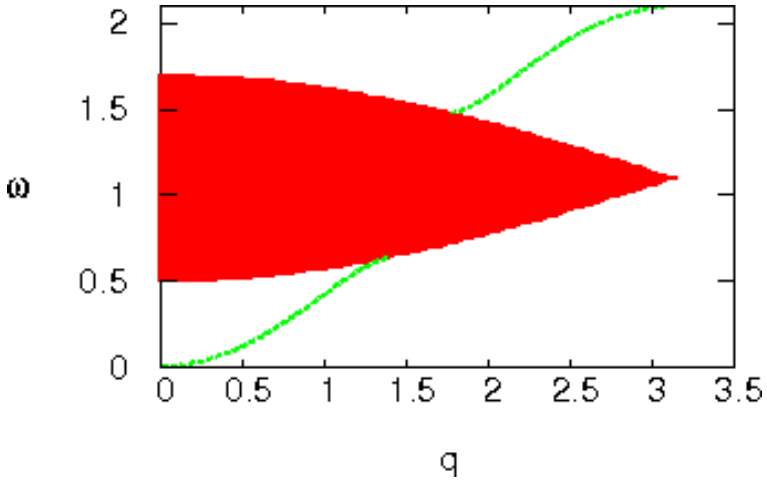

Figure 5.15: The projection of the spectral function on the ω, q plane. The green line represents the coherent branch, the red region is incoherent branch of the spectral function. $\bar{U} = 0, \mu/J = 0.6, \bar{t}/J = 0.3$.

the second branch is $\sim \bar{t}$. In case $h \neq 0$, the exchange field can be regarded as an effective magnetic field (see Eq. 5.29), such that the additional condition $\omega > 2h$ can be regarded as the Zeeman energy. Therefore, in order to create the second branch one needs also to overcome the Zeeman energy.

The coherent branch of the spectrum depicted in Fig. 5.15 has a gap and resembles the situation with nearly free electrons in a solid [11]. There, the energy has also a drop $2V_q$ near the point $q = \pi/a$. Here V_q is a Fourier component of the periodic potential. So, effectively we may map onto a model of free bosons, which feel a weak periodic potential due to unpaired fermions with the amplitude proportional to the width of the gap. We will see that similar modulation appears at the phase boundary through the so-called mechanism Peierls instability mechanism.

5.7 Decoupling in the direct channel

So far we have decoupled the fourth order terms in Eq. (5.9) via the Hubbard-Stratonovich transformation in Eq. (5.10). In fact, there is some arbitrariness with the choice of the Hubbard-Stratonovich transformation. The way we have done it is called the decoupling in the Cooper channel. There are other channels, one of which we would like to probe to see whether it provides us with new results. The correct choice of a decoupling can be

motivated only by physical reasoning. In all cases, the transformation is exact, no matter which channel is chosen. However, later on we usually make approximations and different decouplings may bring us to different results.

In this section we decouple the term responsible for the two-body interaction in Eq. (5.9) in the so-called direct channel. But we use Eq. (B.21), since it can be mapped onto Eq. (5.9) as it is shown in Appendix B.3. Let us define $\rho_{r\tau} = \sum_\sigma \bar{\psi}_{r\tau+\delta\sigma}\psi_{r\tau\sigma}$. We use the identity

$$\int d\chi_{r\tau} \exp\left[-\frac{1}{2U_{bg}}\chi_{r\tau}^2 - \chi_{r\tau}\rho_{r\tau}\right] \propto \exp\left[\frac{U_{bg}}{2}\rho_{r\tau}^2\right] \equiv \exp\left[U_{bg}\bar{\psi}_{r\tau+\delta\uparrow}\psi_{r\tau\uparrow}\bar{\psi}_{r\tau+\delta\downarrow}\psi_{r\tau\downarrow}\right], \tag{5.80}$$

with complex $\chi_{r\tau}$. Then, decoupling also the remaining fourth order terms in the Cooper channel, so that we get again two complex fields, the action in Eq. (5.9) can be written in the decomposed form

$$A = -\frac{J}{2d}\sum_{r,r'}\bar{\phi}_r\triangle_{r,r'}\phi_{r'} + \sum_r(2\nu-2\mu)\bar{\phi}_r\phi_r + \frac{1}{2U_{\rm bg}}\sum_r\chi_r^2$$

$$+\sum_r(\bar{\psi}_{r\tau\uparrow}\partial_\tau\psi_{r\tau\uparrow} + \bar{\psi}_{r\tau\downarrow}\partial_\tau\psi_{r\tau\downarrow}) + \sum_r\bar{\phi}_{r\tau}\partial_\tau\phi_{r\tau}$$

$$+\sum_r g\phi_r\bar{\psi}_{r\tau+\delta\uparrow}\bar{\psi}_{r\tau+\delta\downarrow} + \sum_r g\bar{\phi}_r\psi_{r\tau\downarrow}\psi_{r\tau\uparrow} + \sum_r\chi_r\bar{\psi}_{r\tau+\delta\uparrow}\psi_{r\tau\uparrow} + \sum_r\chi_r\bar{\psi}_{r\tau+\delta\downarrow}\psi_{r\tau\downarrow}$$

$$-\frac{\bar{t}}{2d}\sum_{\langle r,r'\rangle}(\bar{\psi}_{r\tau+\delta\uparrow}\psi_{r'\tau\uparrow} + \bar{\psi}_{r\tau+\delta\downarrow}\psi_{r'\tau\downarrow}) - \mu\sum_r(\bar{\psi}_{r\tau+\delta\uparrow}\psi_{r\tau\uparrow} + \bar{\psi}_{r\tau+\delta\downarrow}\psi_{r\tau\downarrow}). \tag{5.81}$$

Here $\triangle_{r,r'}$ is the lattice version of the nabla operator and it is explained in Appendix B.5. Integrating out Grassmann fields we get

$$A_{\rm eff} = \int_0^\beta d\tau\left\{\sum_r\bar{\phi}_r\partial_\tau\phi_r + \sum_{r,r'}\bar{\phi}_r\hat{v}^{-1}_{r,r'}\phi_{r'} + \frac{1}{2U_{\rm bg}}\sum_r\chi_r^2 - \ln\det\hat{\mathbf{G}}^{-1}\right\} \tag{5.82}$$

with

$$\hat{\mathbf{G}}^{-1} = \begin{pmatrix} g\phi & \partial_\tau+\mu+\hat{t}+\chi \\ \partial_\tau-\mu-\hat{t}-\chi & g\bar{\phi}\end{pmatrix},\ \hat{v}^{-1}_{r,r'} = -\frac{J}{2d}\triangle_{r,r'} + (2\nu-2\mu)\delta_{r,r'}. \tag{5.83}$$

Minimizing it as usual with respect to the fields, we obtain two mean-field equations:

$$\begin{aligned}\frac{2\nu - 2\mu}{g^2} &= \frac{1}{2}\sum_q \frac{1}{\sqrt{(\mu + t_q + \chi_0)^2 + g^2|\phi_0|^2}}, \\ \frac{\chi_0}{U_{bg}} &= \frac{1}{2}\sum_q \frac{\mu + t_q + \chi_0}{\sqrt{(\mu + t_q + \chi_0)^2 + g^2|\phi_0|^2}}.\end{aligned} \tag{5.84}$$

Consider a solution for small $\phi_0 \approx 0$, i.e. close to the phase boundaries, where the order parameter vanishes. Then χ_0 can be absorbed to the chemical potential and the Green's matrix can be written as

$$\ln\det\hat{\mathbf{G}}^{-1} = \mathrm{tr}\ln[\hat{\mathbf{G}}_0^{-1} + \delta\hat{\mathbf{G}}^{-1}] \tag{5.85}$$

with

$$\hat{\mathbf{G}}_0^{-1} = \begin{pmatrix} 0 & G_+^{-1} \\ G_-^{-1} & 0 \end{pmatrix}, \quad \delta\hat{\mathbf{G}}^{-1} = \begin{pmatrix} g\delta\phi & \delta\chi \\ -\delta\chi & g\delta\bar{\phi} \end{pmatrix}, \tag{5.86}$$

where $G_\pm^{-1} = \partial_\tau \pm (\mu + \hat{t} + \chi_0)$. For the vanishing order parameter, the fluctuations of ϕ and χ fields are decoupled, and we get the following contribution to the action originating from the χ fields:

$$\delta A_{\text{eff}} = \frac{1}{2U_{\text{bg}}}\sum_{q,\omega_n}|\delta\chi_{q,n}|^2 - \frac{1}{2}\sum_{q,\omega_n}|\delta\chi_{q,n}|^2(\Pi_{q,n}^{++} + \Pi_{q,n}^{--}), \tag{5.87}$$

where

$$\Pi_{q,n}^{\pm\pm} = -\frac{1}{\beta V}\sum_{p,\omega_m} G_{\pm,p,m}G_{\pm,p+q,n+m}. \tag{5.88}$$

It is easy to show that $\Pi_{q,n}^{++} = \Pi_{q,-n}^{--} = (\Pi_{q,n}^{--})^*$. By setting $\omega_n = 0$ (the stationary case), it can be seen that instability occurs at momenta, which satisfy

$$\frac{1}{2U_{\text{bg}}} < \Re[\Pi_{q,0}^{++}]. \tag{5.89}$$

This means that for these momenta the action in Eq. (5.87) becomes negative, which suggests that we have improperly chosen the mean-field value χ_0 to be spatially constant. Therefore, it has to vary in space. This is the mechanism of the Peierls instability. This spatially varying field can be absorbed by the chemical potential. This brings us to the conclusion that the order parameter, which describes molecules, feels a periodic potential via spatially modulated chemical potential. The similar conclusion has been made at the end of the previous section. Thus, in both cases the physics remains similar, regardless the way of performing the Hubbard-Stratonovich decoupling.

5.8 Fermionic degrees of freedom

Above we have explored the spectral function, which projection onto the $\{q, \omega\}$ plane is plotted in Fig. 5.15. It contains coherent and incoherent contributions. The former is a delta peak corresponding to the dissipationless elementary excitations, while the latter illustrates the damping mechanism depicted in Fig. 5.2. The width of the broadening corresponds to the inverse lifetime of these excitations. We concentrated on exploration of the bosonic fields. In this section we will study the fate of fermionic degrees of freedom. We set $\bar{U} = 0$ in order to facilitate the consideration and to ease the notations. We perform the Hubbard-Stratonovich transformation as usual by introducing the new complex fields, but do not integrate Grassmann fields subsequently. The action reads

$$A = \int_0^\beta dt \left\{ \sum_{r,r'} \bar{\phi}_r \hat{v}^{-1}_{r,r'} \phi_{r'} + \frac{1}{2J} \sum_r \bar{\chi}_r \chi_r - \begin{pmatrix} \psi^1 \\ \bar{\psi}^2 \end{pmatrix}^T \hat{\mathbf{G}}^{-1} \begin{pmatrix} \psi^2 \\ \bar{\psi}^1 \end{pmatrix} \right\}, \tag{5.90}$$

where the inverse Green's matrix $\hat{\mathbf{G}}^{-1}$ is given via Eq. (5.12). If we denote the diagonal elements of the Green's matrix as $\hat{\mathbf{\Sigma}}$, we can compute the inverse Green's matrix from the Dyson equation:

$$\hat{\mathbf{G}}^{-1} = \hat{\mathbf{G}}_0^{-1} - \hat{\mathbf{\Sigma}} \;\; \Rightarrow \;\; \hat{\mathbf{G}} = \hat{\mathbf{G}}_0 + \hat{\mathbf{G}}_\mathbf{0}\hat{\mathbf{\Sigma}}\hat{\mathbf{G}}_\mathbf{0} + \hat{\mathbf{G}}_\mathbf{0}\hat{\mathbf{\Sigma}}\hat{\mathbf{G}}_\mathbf{0}\hat{\mathbf{\Sigma}}\hat{\mathbf{G}}_\mathbf{0} + \dots \tag{5.91}$$

Let us consider now the fluctuations around the normal state with $\Delta_0 = 0$. We suppose there is no imaginary time dependence of the molecular field fluctuations. So to speak, they are heavy and thus can be treated classically. This is a poor approximation though, but nevertheless it allows us to explore basic physics without carrying all unnecessary trifles for the current consideration. We calculate the Green's function by averaging over statistical weight given in Eq. (5.90). The first order vanishes because of the Gaussian integration. To the second order we obtain

$$\langle \hat{\mathbf{G}}(k, k') \rangle \approx \langle \hat{\mathbf{G}}_0(k) \rangle \delta_{k,k'} + \frac{1}{L^d} \sum_{k''} \langle \hat{\mathbf{G}}_0(k) \hat{\mathbf{\Sigma}}(k'' - k) \hat{\mathbf{G}}_0(k'') \hat{\mathbf{\Sigma}}(k' - k'') \hat{\mathbf{G}}_0(k') \rangle + \dots \tag{5.92}$$

We are interested in the off-diagonal contributions, since they characterize the fermions (cf. Eq. (5.12)). We thus have two contributions (we omit the subscript "0")

$$G^{(1)}(k) \approx G_{12}(k) - \frac{1}{L^d} \sum_{k'} G^2_{12}(k) G_{21}(k') \langle \delta \bar{\Delta}_{k'-k} \delta \Delta_{k-k'} \rangle + \dots \tag{5.93}$$

and

$$G^{(2)}(k) \approx G_{21}(k) - \frac{1}{L^d}\sum_{k'} G_{21}^2(k) G_{12}(k') \langle \delta\bar{\Delta}_{k-k'} \delta\Delta_{k'-k}\rangle + \dots \tag{5.94}$$

The expression $\langle \delta\bar{\Delta}_p \delta\Delta_{-p}\rangle = -J(1-g_q)$ does not depend on ω_n. Here $g_q = 1 - \frac{1}{d}\sum_{i=1}^{d}\cos q_i$. These two blocks are characterized by two self-energies $\tilde{\Sigma}_1(k, i\omega_n)$ and $\tilde{\Sigma}_2(k, i\omega_n)$ respectively, which are the second terms in the above equations. This is the self-consistent Born approximation. The first order result for the self-energies is given by

$$\begin{aligned}
\tilde{\Sigma}_1(k, i\omega_n) &= \frac{J}{L^d}\sum_{k'} \frac{1 - g_{k'-k}}{i\omega_n + \mu - h + \epsilon_{k'} - \tilde{\Sigma}_2(k', i\omega_n)}, \\
\tilde{\Sigma}_2(k, i\omega_n) &= \frac{J}{L^d}\sum_{k'} \frac{1 - g_{k'-k}}{i\omega_n + \mu + h + \epsilon_{k'} - \tilde{\Sigma}_1(k', i\omega_n)}.
\end{aligned} \tag{5.95}$$

We see that in general, when exchange field $h \neq 0$, the two self-energies may differ. In the continuum limit ϵ_k becomes $-\hbar^2 k^2/2m$, $1-g_{k'-k}$ becomes $-\hbar^2(k'-k)^2/2m\bar{t}$. Here we denote $m \sim 1/\bar{t}$ as a band mass. Moreover, the summation over momenta is replaced by the integration as $\frac{1}{L^d}\sum_{k'} \to \int \frac{d\Omega_{k'}}{4\pi} d\epsilon' \rho(\epsilon')$.

We notice here that $\int \frac{d\Omega_{\mathbf{k}'}}{4\pi} \mathbf{k}\mathbf{k}' \sim \int_{-1}^{1} \cos(\theta) d\cos(\theta) = 0$, such that

$$\int \frac{d\Omega_{k'}}{4\pi} \frac{\hbar^2(k'-k)^2}{2m\bar{t}} = \frac{\hbar^2(k'^2 + k^2)}{2m\bar{t}}. \tag{5.96}$$

Consider the case $h = 0$. After performing analytic continuation and using Eq. (5.96) we see that

$$\tilde{\Sigma}(k, \omega) = a(\omega) + b(\omega)k^2, \tag{5.97}$$

where $a(\omega)$ and $b(\omega)$ are some complex function of ω and are given in Appendix B.8. Both contain real and imaginary parts. The imaginary parts constitute the damping rate.

The fermionic Green's function can be written as in Eq. (B.74):

$$\mathbf{G}(k, z) \propto \frac{1}{z - \epsilon_k + \tilde{\mu} - i1/2\tau}. \tag{5.98}$$

Therefore, the spectral function reads

$$A(k, z) \propto \frac{1/2\tau}{(z - \epsilon_k + \tilde{\mu})^2 + (1/2\tau)^2}. \tag{5.99}$$

The damping rate $1/2\tau$ is given in Eq. (B.76), and for vanishing $\bar{t}$ in 3D it is $\propto \bar{t}$, which is consistent with the conclusions of the previous section.

In this section we studied the damping mechanism from a different point of view. Above we have explored the fate of quantum fluctuations of complex fields and we have obtained the spectral function depicted in Fig. 5.15. We saw that the coherent bosonic excitations decay into incoherent branch, tentatively identified as a decay of bosonic molecules into fermions. Here we see that fermionic excitations possess similar features, namely they have finite lifetime, and the damping rate vanishes linearly with $\bar{t}$. We notice that the effective mass of fermions is not changed (see Eq. (5.98)). This can be explained by our approximation, since there is no dependence on ω_n, or, in another words, there is no exchange of quantum fluctuations with the bosonic fields. When projected onto the fermions degree of freedom, the phase coherence of the particles is not diminished, and the tunneling rate does not change.

Chapter 6

Anderson localization in a correlated fermionic mixture

In this section a mixture of two fermionic species with different masses and repulsive interaction is studied in an optical lattice. The heavy fermions are subject only to thermal fluctuations, the light fermions also to quantum fluctuations. We study the localization properties of the light fermions numerically by a transfer-matrix method. In a two-dimensional system one-parameter scaling of the localization length is found with a transition from delocalized states at low temperatures to localized states at high temperature. Original results from [39, 113] are presented.

The question of Anderson localization in an ultra cold gas has attracted considerable attention recently by a number of experimental groups [17, 82, 90]. Although the phenomenon itself has been studied in great detail over the last 50 years by many theoretical groups for various physical systems [1, 7, 101], its experimental observation has been difficult. One of the reasons is that Anderson localization is an interference effect of waves due to elastic scattering in a random environment (disorder) [98]. Real systems, however, experience also substantial inelastic scattering (e.g. absorption of electromagnetic waves by the scattering atoms, Coulomb interaction in electronic systems etc.) This may hamper the direct observation of Anderson localization significantly. Another reason is that random scattering is difficult to control in a real system. This is important in order to distinguish Anderson localization from simple trapping due to local potentials. It requires some kind of averaging over an ensemble of randomly distributed scatterers.

Ultra cold gases offer conditions, where most physical parameters are controllable. Since the atoms are neutral, there is no Coulomb interaction, and at sufficiently high dilution the interatomic collisions are negligible.

Moreover, a periodic potential (optical lattice) can be applied by counter-propagating laser fields. This enables us to control the kinetic properties of the gas atoms by creating a specifically designed dispersion. Disorder could be created by disturbing the periodicity of the optical lattice. In practice, however, this is not easy because real disorder would require infinitely many laser frequencies. A first attempt is to study the superposition of two laser fields with "incommensurate" frequencies (i.e., the ratio of the two frequencies is an irrational number) [90]. An alternative is to randomize the laser field by sending it through a diffusing plate [17].

Recent progress in atomic mixtures [78, 97, 103, 105] has offered another possibility to create disorder in an atomic system. Mixing of two different atomic species, where one is heavier than the other, creates a situation where the light atoms are scattered by the randomly distributed heavy atoms [12, 43, 61, 75]. An optical lattice is applied in order to keep the heavy atoms in quenched positions. Due to their higher mass, the heavy atoms behave classically in contrast to the light atoms, which can tunnel in the optical lattice. A crucial question is what determines the distribution of the heavy atoms. The most direct distribution is obtained by putting atoms randomly in the optical lattice "by hand", each of them with independent probability [43]. This case corresponds to uncorrelated disorder. Another possibility is to fill the optical lattice with both atomic species and consider a repulsive (local) interaction between them. Then the two species have to arrange each other such that the total atomic system presents a grand-canonical ensemble at a given temperature and a given lattice filling. In the presence of interparticle interaction within each atomic species there is a complex interplay of interaction and localization effect. This makes it difficult to isolate the effect of Anderson localization. In order to avoid interaction within each species we choose spin-polarized fermions in an optical lattice. Then only the Pauli principle controls the short-range interaction within each species, such that the remaining interaction is between the different fermionic species. It has been shown that then the light atoms are subject to a quenched average with respect to a thermal distribution of the heavy atoms, and that the distribution is related to an Ising-like model [12,75,112]. The latter implies (strong) correlations between the heavy atoms. For systems in more than one dimension there is a critical temperature T_c at which the correlation length diverges. This system provides several interesting features for studying Anderson localization. Although it is a many-body system, the light atoms behave effectively like independent (spinless fermionic) quantum particles in a random potential. The correlation of the randomness can be controlled by temperature, where the correlation length decreases with increasing tem-

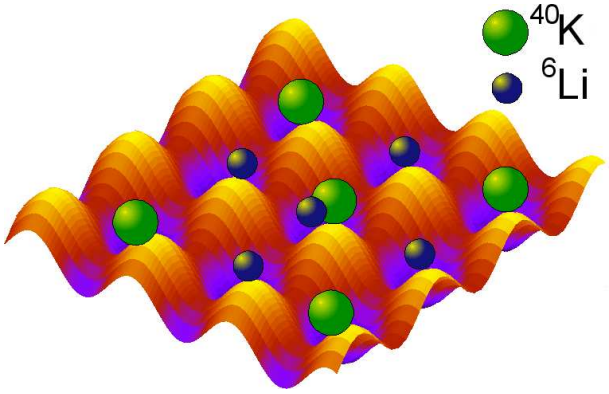

Figure 6.1: A mixture of two Fermi gases in a 2D optical lattice.

perature for temperatures $T > T_c$, or by the strength of the inter-species scattering.

In the following we shall study diffusion and Anderson localization in the grand-canonical ensemble of two spin-polarized fermionic species in one and two dimensions. Motivated by a recent experimental study on a dilute BEC in $d = 1$ [17], we first discuss a realistic scenario, in which an initial state is prepared at the center with a trapping potential and then it is released by opening (i.e., switching off) the trap. In the second part, we consider the Fermi gas in equilibrium and calculate the scaling properties of the localization length in one and two dimensions [39, 113].

6.1 Asymmetric Hubbard model

$c^\dagger$ (c) are creation (annihilation) operators of the light fermionic atoms, $f^\dagger$ (f) are the corresponding operators of the heavy fermionic atoms. This gives the formal mapping $^6\mathrm{Li} \rightarrow c_r^\dagger, c_r$ and $^{40}\mathrm{K}$ ($^{23}\mathrm{Na}$, $^{87}\mathrm{Rb}$) $\rightarrow f_r^\dagger, f_r$ (see Fig. 6.1). The physics of the mixture of atoms is defined by the asymmetric Hubbard Hamiltonian

$$H = -\bar{t}_c \sum_{\langle r,r' \rangle} c_r^\dagger c_{r'} - \bar{t}_f \sum_{\langle r,r' \rangle} f_r^\dagger f_{r'} - \sum_r \Big[\mu_c c_r^\dagger c_r + \mu_f f_r^\dagger f_r - U f_r^\dagger f_r c_r^\dagger c_r \Big]. \quad (6.1)$$

The effective interaction within each species is controlled by the (repulsive) Pauli principle, whereas the interaction strength of different atoms is U. If the f atoms are heavy, the related tunneling rate is very small. The limit $\bar{t}_f = 0$ is known as the Falicov-Kimball model, which has been

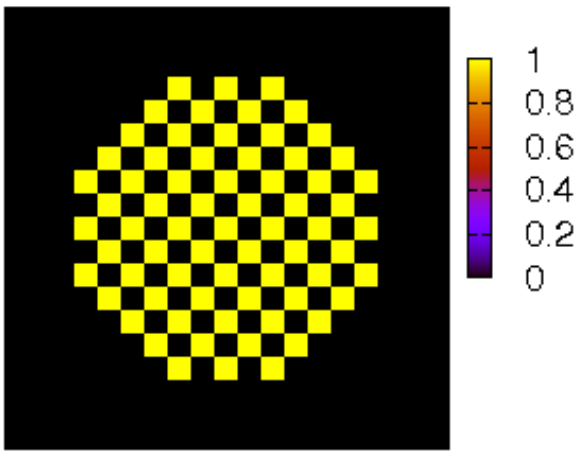

Figure 6.2: The density plot of heavy atoms placed in a harmonic trap. The chessboard pattern at the center is seen.

studied in great detail using the coherent-potential approximation (CPA) and dynamical mean-field theory (DMFT) [22, 33, 34, 42, 75]. CPA as well as DMFT are based on the infinite dimensional limit which gives a reliable description on spectral properties such as the gap opening at the metal-insulator transition. Since we are interested in properties of the wavefunctions in one- and two-dimensional realizations of the FK model, however, we cannot use these approximation schemes here but must employ a numerical scaling method.

A grand-canonical ensemble of fermions at the inverse temperature $\beta = 1/k_B T$ is defined by the partition function

$$Z = \mathrm{Tr} e^{-\beta H}.$$

In the FK limit $\bar{t}_f = 0$ the Hamiltonian of the light atoms depends only on the real numbers $\{n_r\}$ ($n_r = 0, 1$), representing the presence or absence of a heavy atom on lattice site r. Then the Hamiltonian is given by a quadratic form with respect to the c operators of the light atoms:

$$H_c(\{n_r\}) = \sum_{r,r'} h_{c;rr'} c_r^\dagger c_{r'} = -\bar{t}_c \sum_{\langle r,r' \rangle} c_r^\dagger c_{r'} + \sum_r (U n_r - \mu_c) c_r^\dagger c_r \,, \qquad (6.2)$$

where the second equation is the definition of the matrix h_c. This means that the density fluctuations $n_r = f_r^\dagger f_r$ have been replaced by classical variables $n_r = 0, 1$. Thus $H_c(\{n_r\})$ describes non-interacting fermions which

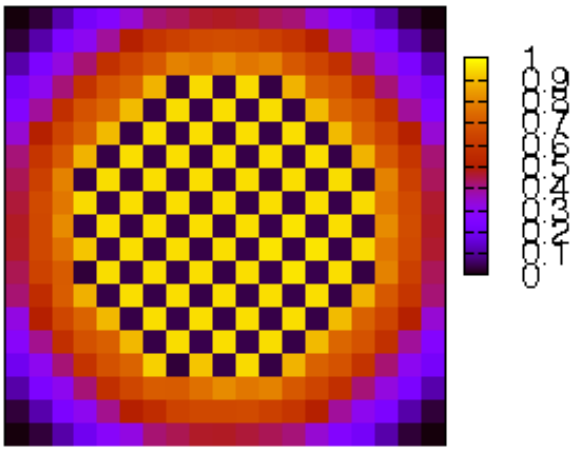

Figure 6.3: The density plot of light atoms placed in a harmonic trap: Light atoms try to avoid the heavy ones.

are scattered by heavy atoms, represented by n_r. The trace Tr_c in the partition function can be evaluated and gives a fermion determinant:

$$Z = \sum_{\{n_r\}} e^{\beta\mu_f \sum_r n_r} \mathrm{Tr}_c \left(e^{-\beta H_c(\{n_r\})} \right) = \sum_{\{n_r\}} e^{\beta\mu_f \sum_r n_r} \det \left(\mathbf{1} + e^{-\beta h_c} \right) . \quad (6.3)$$

The right-hand side is a sum over (non-negative) statistical weights. After normalization we can define

$$P(\{n_r\}) = \frac{1}{Z} e^{\beta\mu_f \sum_r n_r} \det \left(\mathbf{1} + e^{-\beta h_c} \right) \quad (6.4)$$

which gives $\sum_{\{n_r\}} P(\{n_r\}) = 1$. Thus $P(\{n_r\})$ is a probability distribution for correlated disorder and describes the distribution of the heavy atoms. In the strong-coupling regime $\bar{t}_c^2/2U \gg 1$ the distribution becomes that of an Ising model with nearest-neighbor coupling. At half-filling (i.e., $\mu_f = \mu_c = U/2$) it reads [12]

$$P(\{S_r\}) \propto \exp \left(-\beta(\bar{t}_c^2/2U) \sum_{<r,r'>} S_r S_{r'} \right) \quad (6.5)$$

where $S_r = 2n_r - 1$.

To exemplify the distribution we place the mixture in the harmonic trap $V(\mathbf{r}) \sim r^2$ at $T = 0$ and plot schematically the distributions of heavy and light atoms in Fig. 6.2 and 6.3.

6.2 Anderson localization

A trapped atomic cloud, concentrated around the center of the optical lattice, is the initial state $|i\rangle$ of our system. After switching off the trapping potential the dynamics of the light atomic cloud is described by the evolution equation $|\Psi_t\rangle = e^{-iHt}|i\rangle$. The optical lattice remains present during the evolution of the cloud. We assume that the thermal excitations are slow in comparison with the tunneling dynamics. This is the case when the tunneling energy $\bar{t}_c$ is large in comparison with thermal energy $k_B T = 1/\beta$. Moreover, a slow adiabatic expansion is studied. Now we consider a light atom inside the expanding cloud and follow its movement: Using the equilibrium state of the entire system $|0\rangle$, we add one particle to create the initial state $|i\rangle = c_0^\dagger|0\rangle$. Then the local density of particles at site r with respect to the state $|\Psi_t\rangle$ reads

$$N_r = \langle\Psi_t|c_r^\dagger c_r|\Psi_t\rangle = \langle i|e^{iHt}c_r^\dagger c_r e^{-iHt}|i\rangle. \tag{6.6}$$

The equilibrium state $|0\rangle$ can be expanded in terms of energy eigenfunctions and Boltzmann weights at the inverse temperature β as

$$\langle N_r\rangle = \frac{\sum_k e^{-\beta E_k}\langle E_k|c_0 e^{iHt}c_r^\dagger c_r e^{-iHt}c_0^\dagger|E_k\rangle}{\sum_k e^{-\beta E_k}} = \frac{1}{Z}\mathrm{Tr}\left[e^{-\beta H}c_0 e^{iHt}c_r^\dagger c_r e^{-iHt}c_0^\dagger\right]. \tag{6.7}$$

For the FK model this expression can also be written as a quenched average with respect to the distribution of heavy particles [112]

$$\langle N_r\rangle = \langle \mathcal{G}_{0r}^\dagger(t)\mathcal{G}_{r0}(t)\rangle_f \tag{6.8}$$

with the single-particle Green's function

$$\mathcal{G}_{rr'}(t) = [e^{-ith_c}(\mathbf{1} + e^{-\beta h_c})^{-1}]_{rr'}\,. \tag{6.9}$$

$\langle ...\rangle_f$ is the average with respect to the statistical weight of Eq. (6.4) or Eq. (6.5). For a given configuration $\{n_r\}$ of heavy atoms the Green's function can also be expressed by eigenfunctions of the single-particle Hamiltonian h_c in Eq. (6.2) ($h_c\phi_k = e_k\phi_k$). The spatial properties of these eigenfunctions determine the spreading of the average density particle density $\langle N_r\rangle$ through the Green's function:

$$\mathcal{G}_{r0}(t) = \sum_k e^{-ie_k t}\frac{\phi_{k,r}^*\phi_{k,0}}{1 + e^{-\beta e_k}}\,. \tag{6.10}$$

The denominator represents the Fermi function, reflecting the fact that our atoms are fermions. At low temperatures all states with $e_k > 0$ (i.e., states

with energy below the chemical potential according to Eq. (6.2)) contribute equally to the Green's function.

According to the localization theory, it can be assumed that $|\phi_{k,r}| \sim e^{-|r|/\xi_k}$, where ξ_k is the localization length. After a Fourier transformation of the time-dependent density in Eq. (6.8), the $\omega = 0$ Fourier component of $\langle N_r \rangle$ reads

$$\bar{N}_r(\omega = 0) = \sum_k \frac{|\phi^*_{k,r}\phi_{k,0}|^2}{(1 + e^{-\beta e_k})^2} \sim \frac{e^{-2|r|/\xi}}{(1 + e^{-\beta e_{k_0}})^2} \quad (r \sim \infty) \,, \tag{6.11}$$

where ξ is the largest localization length and e_{k_0} the corresponding energy level. Thus the expansion of the wave packet on large scales is controlled by ξ. This result suggests that the spatial expansion of an atomic cloud is governed by the largest length scale of the system, after having removed the characteristic size given by the trapping potential. The expansion of the cloud of light atoms is studied numerically. Depending on the temperature of the grand-canonical system, we find a spreading of the wave function at low temperatures but a localized behavior at high temperatures (cf. Fig. 6.4). Apparently, there is a critical regime with some critical temperature T_c', which separates the spreading behavior from the localized behavior.

6.3 Localization length

The localization length can be studied under the change of length scales of a finite optical lattice of length L and width M [1] with L being extremely large, representing the adiabatically expanding atomic cloud (see Fig. 6.5). The periodic boundary condition is imposed along the width of the lattice.

In particular, we analyze the change of the localization length with respect to the width M. For this purpose, we define the reduced (or normalized) localization length as $\Lambda_M = \xi/M$ and calculate this quantity by means of a numerical transfer-matrix approach [74]. A $2M$ by $2M$ transfer matrix T_i for given energy E, width M and given realization of the distribution in Eq. (6.5), picked up from the Monte-Carlo run, can be set up by mapping the wave-function amplitudes at column $i-1$ and i to column $i+1$. Then the expansion along the length is described by the product of transfer matrices:

$$T = \prod_{i=1}^{L} T_i, \tag{6.12}$$

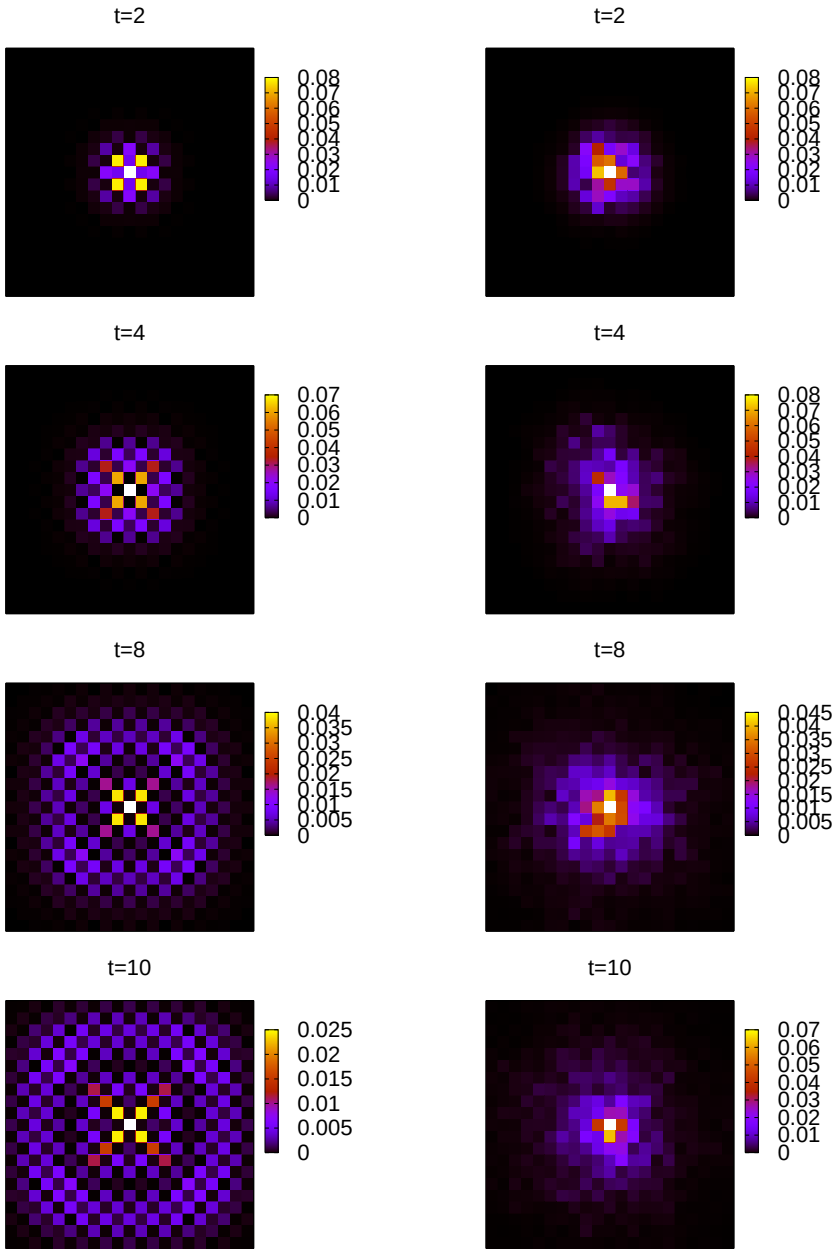

Figure 6.4: Real time evolution of a wave packet. At low temperature ($T = 0$: left panel) it propagates due to the checker-board configuration of the heavy atoms. At larger temperature ($T = 0.2$: right panel), the wave packet is localized due to a disordered configuration of heavy atoms.

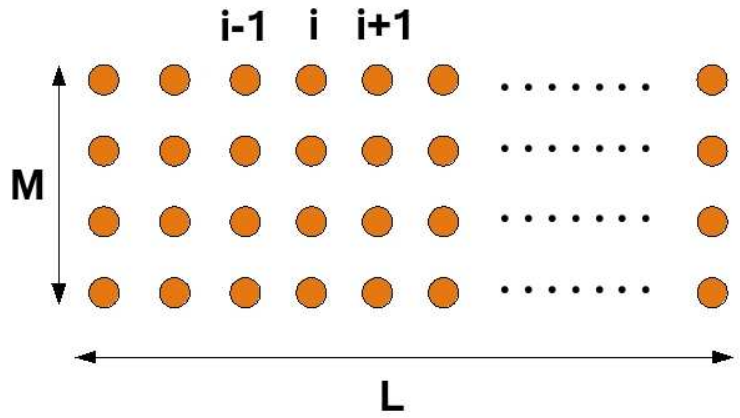

Figure 6.5: A finite optical lattice with length L and width M.

where

$$T_i = \begin{pmatrix} E - \mathbf{H}_i & -\mathbf{I} \\ \mathbf{I} & 0 \end{pmatrix} \tag{6.13}$$

with $\mathbf{H}_i$ is the Hamiltonian for column i. The logarithms of the eigenvalues of T correspond to the Lyapunov exponents of the wave functions. The largest localization length , ξ, is given by the inverse of the smallest Lyapunov exponent. In our calculations we chose $L \sim 10^8$ to take advantage of self-averaging property of the latter: there is no need for averaging over an ensemble of scatterers.

Λ_M either increases (delocalized states) or decreases (localized states) with the width M, depending on the system parameters (e.g. the inverse temperature β). There can also be a marginal behavior (e.g. for a special value β_c'), where Λ_M does not change with M. The latter indicates the existence of a phase transition from localized to delocalized states. A quantitative description of the behavior near β_c' can be based on the one parameter scaling hypothesis [1,74]. This states that $\ln \Lambda_M$ can be expanded in a vicinity of the critical point β_c' as [85,95]

$$\ln \Lambda_M = \ln \Lambda_c \pm A|\beta - \beta_c'|M^{1/\nu} \, . \tag{6.14}$$

For $A > 0$ the positive (negative) sign corresponds to delocalized (localized) behavior. Exponentiation of this equation and using $\zeta = |\beta - \beta_c'|^{-\nu}$ gives

$$\Lambda_M = \Lambda_c \exp\left[\pm A \left(\frac{\zeta}{M}\right)^{-1/\nu}\right] \equiv g\left(\frac{\zeta}{M}\right) \, , \tag{6.15}$$

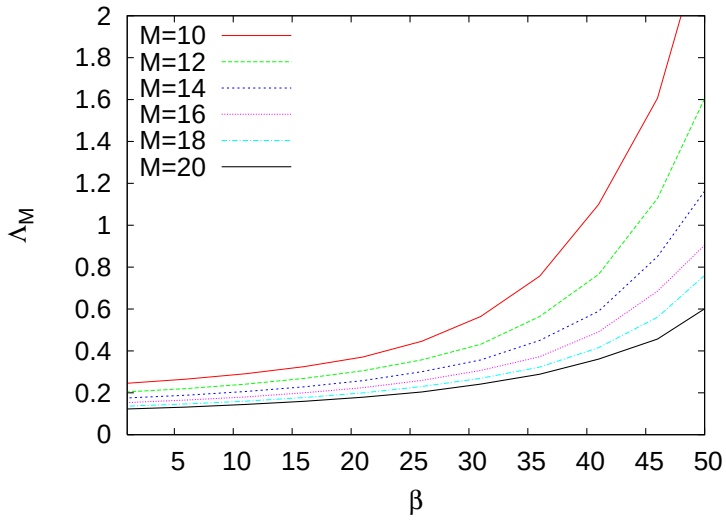

Figure 6.6: The reduced localization length Λ_M of light atoms in $d = 1$ as a function of inverse temperature for interaction strength $U = 9$. Λ_M decreases for increasing system size M, which indicates localized states [39].

where g is the scaling function. Our numerical transfer-matrix approach allows us to determine the critical point β_c' and the exponent ν, depending on the interspecies coupling parameter U.

First we analyze a one-dimensional system. In this case heavy atoms are always disordered due to thermal fluctuations. The reduced localization length Λ_M decreases with increasing length of the system (cf. Fig. 6.6) at any temperature. This reflects that all states are localized. On the other hand, the localization length decreases monotonously with temperature, as a consequence of the increasing disorder. Therefore, at sufficiently low temperature the localization length can be larger than the size of a finite system. This could be relevant in experiments, where we have a finite optical lattice.

In two dimensions the behavior is more complex. First of all, the heavy atoms can form an ordered state at low temperatures and a disordered state at high temperatures [12,75]. As long as $T > 0$, thermal excitations in the ordered state lead to correlated fluctuations of heavy atoms. There is a second-order phase (Ising) transition with a divergent correlation length at the critical temperature T_c. The corresponding distribution of heavy atoms provides a complex random environment for the light atoms. Our numerical transfer-matrix approach finds a transition from localized states

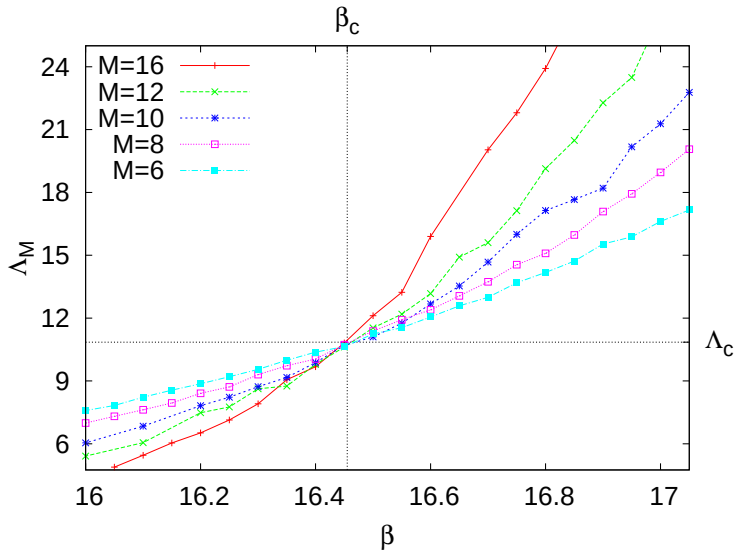

Figure 6.7: Reduced localization length of light atoms for $d = 2$ and $U = 9$. There is a critical inverse temperature $\beta_c' \approx 16.5$, where an Anderson transition occurs [39].

at high temperatures to delocalized states at low temperatures, indicated by a qualitative change of the scaling behavior (cf. Fig. 6.7). There is a critical temperature T_c', where this transition takes place. For instance, at low temperatures and half filling (i.e., for $\mu_f = \mu_c = U/2$), the heavy atoms are arranged in a staggered configuration with weak thermal fluctuations. Using the approximated distribution of Eq. (6.5), the effective spin-spin coupling $\bar{t}_c^2/2U$ leads to the critical temperature $T_c \propto \bar{t}_c^2/2U$. The result for the reduced localization length at $U = 9$ (measured in units of $\bar{t}_c$) is shown in Fig. 6.7. All curves cross at $\beta_c' \approx 16.5$, indicating a localization transition. With these parameters the Ising transition is at $\beta_c \approx 15.9$. Therefore, the localization transition occurs in the ordered phase of the heavy atoms. The one-parameter scaling function of Eq. (6.15) with

$$\Lambda_c \approx 10.9, \quad A \approx 0.09, \quad \nu \approx 0.88 \tag{6.16}$$

fits the data of the transfer-matrix calculation (cf. Fig. 6.8).

In conclusion, we have discussed a mixture of two fermionic species with different masses in an optical lattice, using the Falicov-Kimball model. The heavy atoms are represented as Ising spins and the light atoms as quantum particles. The latter tunnel in a random environment which is provided by a correlated distribution of heavy atoms. The distribution of the heavy atoms is given by an Ising-type model, which undergoes a

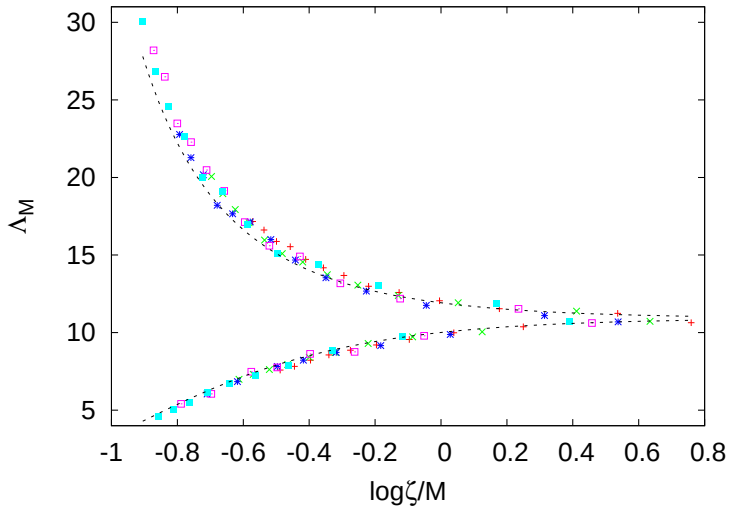

Figure 6.8: One parameter scaling for $d = 2$ and $U = 9$. The lower (upper) branch represents (de-) localized states. The data from the transfer-matrix calculation approach the scaling function of Eq. (6.15) with $\Lambda_c \approx 10.9$, $A \approx 0.09$ and $\nu \approx 0.88$ (dashed curves) [39].

second-order phase transition in $d = 2$ from staggered order to disorder. Depending on the dimensionality ($d = 1, 2$) of the atomic system and the physical parameters (e.g. temperature or interaction strength), the quantum states of the light atoms are either localized or delocalized. All states of light atoms in a one-dimensional fermionic mixture are localized. In a two-dimensional mixture these states are localized at high temperatures and delocalized at low temperatures. Such a system can be realized experimentally as a mixture with two spin-polarized fermionic species, e.g., ^{6}Li as light atoms and ^{40}K (^{23}Na, ^{87}Rb) as heavy atoms.

Chapter 7

Conclusion

In this thesis, many-particle problems of strongly interacting fermions in optical potentials have been investigated by means of functional mean-field methods. The integration over microscopic quantum fields (Grassmann fields) has been traded for an integration over degrees of freedom adjusted to the low-energy characteristic of the system (complex fields). This allowed to explore the ground state properties of the system as well as low-energy fluctuations on top of that, which are accessible in experiments.

Motivated by recent experiments on Bose-Einstein condensates (BEC) in optical lattices which have shown the existence of a Mott insulator (MI), in chapter 4 we have presented a model of strongly interacting bosons composed of two tightly bound fermions in an optical lattice. We have calculated the phase diagram, which includes the BEC and the MI. Including Gaussian fluctuations, we have found that the dispersion of quasiparticles is gapless in the BEC phase but has a gap in the MI phase. We have calculated the total density, the condensate density, and the static structure factor. We have shown that the quantum fluctuations as well as thermal fluctuations lead to a depletion of the condensate, but the former do not change the critical points. We have calculated the superfluid density and showed that at the BEC-MI transition it has a jump from a finite value in the BEC to zero in the MI. In the dilute regime we have derived an effective Gross-Pitaevskii equation for bosons. We also calculated the density-density correlation function of fermions, which can be studied in a time off flight experiment. We have shown that in the Mott phase the later has dips, while in the BEC phase peaks appears. This feature reflects the fermionic nature of the insulating phase and bosonic nature of the BEC phase via quantum statistics.

In order to study the possibility of dissociation of bosonic molecules

considered in chapter 4, we have extended the paired-fermion model by including the tunneling rate of fermions in chapter 5. We have shown that this model describes the BCS-BEC crossover in a lattice, which has become an experimental subject within last few years. We have investigated the system, which consists of unequal spin populations of fermions and calculated the densities across the BCS-BEC crossover. We showed that in the BCS regime the superfluid core is surrounded by the shell of unpaired fermions, while in the BEC regime the unpaired fermions are surrounded by the superfluid shell. Another feature, which is accessible in experiments, is the density profile of dissociated fermions in a trapping potential. To calculate the later we have derived saddle-point field equations and have developed a numerical procedure to solve them. We showed that approaching the BEC regime a characteristic dip in the density profile at the center on the trap appears and can be explained by the Pauli exclusion principle.

Dissociation of Bose molecules into fermions leads to damping processes. We have calculated the spectral function of bosonic low-energy excitations and have shown that it consists of coherent and incoherent branches. The former describes long lived bosonic excitations, while the latter describes a continuum of fermionic excitation into which bosonic excitations decay. Approaching the BEC regime is characterized by the shrinking of the incoherent branch. The spectral function is directly related to a key experimental observable, the inelastic cross-section, and thus can be measured in experiments.

In the final chapter 6 we have discussed a mixture of two fermionic species with different masses in an optical lattice. The heavy atoms are represented as Ising spins and the light atoms as quantum particles. The latter tunnel in a random environment which is provided by a correlated distribution of heavy atoms. The distribution of the heavy atoms is given by an Ising-type model, which undergoes a second-order phase transition in $d = 2$ from staggered order to disorder. Depending on the dimensionality ($d = 1, 2$) of the atomic system and the physical parameters (e.g. temperature or interaction strength), the quantum states of the light atoms are either localized or delocalized. All states of light atoms in a one-dimensional fermionic mixture are localized. In a two-dimensional mixture these states are localized at high temperatures and delocalized at low temperatures. Such a system can be realized experimentally as a mixture with two spin-polarized fermionic species, e.g., $^6\mathrm{Li}$ as light atoms and $^{40}\mathrm{K}$ ($^{23}\mathrm{Na}$, $^{87}\mathrm{Rb}$) as heavy atoms.

Appendix A

Calculations to the paired-fermion model

A.1 Gaussian fluctuations

The expression for δA_{eff} reads

$$\delta A_{\text{eff}} = \int_0^\beta d\tau \left\{ \sum_{r,r'} \delta\bar{\phi}_r \hat{v}^{-1}_{r,r'} \delta\phi_{r'} + \frac{1}{S}\sum_r \delta\bar{\chi}_r \delta\chi_r + \frac{1}{2}\text{Tr}[\hat{G}_0\Sigma\hat{G}_0\Sigma] \right\}. \quad \text{(A.1)}$$

Fourier transforming we get

$$\begin{aligned} \delta A_{\text{eff}} &= \sum_q v_p^{-1}|\delta\phi_p|^2 + \frac{1}{S}\sum_p |\delta\chi_p|^2 \\ &+ \frac{1}{2\beta}\sum_{kq} \text{tr}[\hat{G}_0(k)\Sigma(-q)\hat{G}_0(k+q)\Sigma(q)], \end{aligned} \quad \text{(A.2)}$$

where

$$\begin{aligned} \hat{G}_0(k) &= \frac{-1}{(i\omega_k + E_k)(i\omega_k - E_k)} \begin{pmatrix} \Delta_0 & i\omega_k - \mu \\ i\omega_k + \mu & -\Delta_0 \end{pmatrix}, \\ \Sigma(q) &= \begin{pmatrix} -\delta\Delta_q & 0 \\ 0 & \delta\bar{\Delta}_q \end{pmatrix}. \end{aligned} \quad \text{(A.3)}$$

We denoted $\Delta_0 = i\phi_0 + \chi_0$, $E_q = \sqrt{\mu^2 + |\Delta_0|^2}$, $v_p^{-1} = (S + J - Jg_p)^{-1}$, $g_p = 1 - 1/d\sum_{i=1}^d \cos(q_i)$.

The third term in Eq. (A.2) reads

$$\begin{aligned} &\frac{1}{2\beta}\sum_{k,q}[G_{11}(k)G_{11}(k+q)\delta\Delta_{-q}\delta\Delta_q + G_{22}(k)G_{22}(k+q)\delta\bar{\Delta}_q\delta\bar{\Delta}_{-q} \\ &\quad -G_{12}(k)G_{21}(k+q)\delta\bar{\Delta}_{-q}\delta\Delta_q - G_{21}(k)G_{12}(k+q)\delta\Delta_{-q}\delta\bar{\Delta}_q]. \end{aligned} \quad \text{(A.4)}$$

After collecting terms we get ($\mathcal{V}_p = (\delta\bar{\phi}_p, \delta\bar{\chi}_p, \delta\phi_{-p}, \delta\chi_{-p})$)

$$\delta A_{\text{eff}} = \sum_p \bar{\mathcal{V}}_p \mathcal{G}^{-1} \mathcal{V}_p, \tag{A.5}$$

with the Green's matrix

$$\mathcal{G}^{-1} = \begin{pmatrix} v_p^{-1} - B(-p) & iB(-p) & -A(p) & iA(p) \\ iB(-p) & \frac{1}{S} + B(-p) & iA(p) & A(p) \\ -A(p) & iA(p) & v_p^{-1} - B(p) & iB(p) \\ iA(p) & A(p) & iB(p) & \frac{1}{S} + B(p) \end{pmatrix}. \tag{A.6}$$

Here for $\Delta_0 \neq 0$

$$B(p) = \frac{\mu^2 + J^2 - 2i\mu\omega_p}{2J(J^2 + \omega_p^2)}, \;\; A(p) = \frac{\mu^2 - J^2}{2J(J^2 + \omega_p^2)}. \tag{A.7}$$

Such that its determinant reads

$$\det \mathcal{G}^{-1} = \frac{\omega^2 + (J^2 - \mu^2) g_p + \mu^2 g_p^2}{[2J^2(3 - g_p)]^2 (J^2 + \omega_p^2)}. \tag{A.8}$$

If $\Delta_0 = 0$

$$B(p) = \frac{1}{|\mu| - i\omega_p}, \;\; A(p) = 0 \tag{A.9}$$

and the determinant reads

$$\det \mathcal{G}^{-1} = \frac{v_p^{-1}}{2J} - B(p) \left(\frac{1}{2J} - v_p^{-1} \right). \tag{A.10}$$

The $\delta\phi_r$ and $\delta\chi_r$ fields are complex and contain both amplitude and phase fluctuations. We introduce new fields:

$$\delta\phi_r^{\text{Re}} = (\delta\phi_r + \delta\bar{\phi}_r)/2, \;\; \delta\chi_r^{\text{Re}} = (\delta\chi_r + \delta\bar{\chi}_r)/2, \tag{A.11}$$

which describe the amplitude fluctuation and

$$\delta\phi_r^{\text{Im}} = (\delta\phi_r - \delta\bar{\phi}_r)/2, \;\; \delta\chi_r^{\text{Im}} = (\delta\chi_r - \delta\bar{\chi}_r)/2, \tag{A.12}$$

which describe the phase fluctuation. In matrix form the above transformation reads

$$\begin{pmatrix} \delta\phi_r^{\text{Re}} \\ \delta\chi_r^{\text{Re}} \\ \delta\phi_r^{\text{Im}} \\ \delta\chi_r^{\text{Im}} \end{pmatrix} = \frac{1}{2} \begin{pmatrix} 1 & 0 & 1 & 0 \\ 0 & 1 & 0 & 1 \\ 1 & 0 & -1 & 0 \\ 0 & 1 & 0 & -1 \end{pmatrix} \begin{pmatrix} \delta\phi_r \\ \delta\chi_r \\ \delta\bar{\phi}_r \\ \delta\bar{\chi}_r \end{pmatrix}. \tag{A.13}$$

In terms of new fields $\mathcal{V}_p \rightarrow (\delta\phi_p^{\mathrm{Re}}, \delta\chi_p^{\mathrm{Re}}, \delta\phi_p^{\mathrm{Im}}, \delta\chi_p^{\mathrm{Im}})$ and Eq. (A.6) is replaced by

$$\mathcal{G}^{-1} = \begin{pmatrix} v_p^{-1} - M_+(p) & iM_+(p) & -i\mathrm{Im}B(p) & -\mathrm{Im}B(p) \\ iM_+(p) & \frac{1}{S} + M_+(p) & -\mathrm{Im}B(p) & i\mathrm{Im}B(p) \\ -i\mathrm{Im}B(p) & -\mathrm{Im}B(p) & v_p^{-1} - M_-(p) & iM_-(p) \\ -\mathrm{Im}B(p) & i\mathrm{Im}B(p) & iM_-(p) & \frac{1}{S} + M_-(p) \end{pmatrix}, \quad \text{(A.14)}$$

where $M_\pm(p) = \mathrm{Re}B(p) \pm A(p)$.

A.2 Renormalized Gross-Pitaevskii equation

Here we consider the case of $h = 0$, $\bar{t} = 0$, $\bar{U} = 0$ based on the results in Appendix B.7.2. For this case we have

$$g_s = \frac{1}{\beta}\sum_\omega \frac{1}{(\omega^2 + \mu^2)^2} = \frac{\mathrm{Tanh}[\beta\mu/2]}{4\mu^3} - \frac{\beta\mathrm{Sech}[\beta\mu/2]^2}{8\mu^2}, \quad \text{(A.15)}$$

$$d(q) = \frac{\mathrm{Tanh}[\beta|\mu|/2]}{4\mu^2}, \;\; B(q) = \frac{1}{2|\mu|}\mathrm{Tanh}[\beta|\mu|/2]. \quad \text{(A.16)}$$

The Gross-Pitaevskii equation reads ($T = 0$)

$$i\frac{\partial}{\partial t}\phi(r,t) = \left(-\frac{\nabla^2}{2m} + \mu_R + g_R|\phi(r,t)|^2\right)\phi(r,t), \quad \text{(A.17)}$$

where

$$\mu_R = \left(-\frac{1}{6J} + \frac{1}{2J[1 + J/|\mu|]}\right) 4\mu^2(1 + J/|\mu|)^2, \quad \text{(A.18)}$$

$$m = \frac{9dJ^2}{4\mu^2(1 + J/|\mu|)^2}, \;\; g_R = g_s(4\mu^2)^2. \quad \text{(A.19)}$$

In the dilute limit (and $T = 0$)

$$m \approx \frac{d}{J}, \;\; \mu_R \approx 2\tilde{\mu}, \;\; g_R \approx 2J. \quad \text{(A.20)}$$

Appendix B

Calculations to the BCS-BEC crossover in a lattice

B.1 Observables

We performed the Hubbard-Stratonovich transformation and treated the complex fields classically for the ground state properties. Once the solutions are chosen the action is of second order in Grassmann variables. We write

$$Z = \int \mathcal{D}[\psi, \bar{\psi}] e^{-A(\psi,\bar{\psi})}, \tag{B.1}$$

where

$$\begin{aligned} A(\psi,\bar{\psi}) &= \int_0^\beta d\tau \Bigg[\sum_{r,r'} \bar{\phi}_r \hat{v}^{-1}_{r,r'} \phi_{r'} + \frac{I}{2J-\bar{U}} \sum_r \bar{\chi}_r \chi_r \\ &+ \sum_r (\psi_{r\tau\uparrow} \partial_\tau \bar{\psi}_{r\tau\uparrow} + \psi_{r\tau\downarrow} \partial_\tau \bar{\psi}_{r\tau\downarrow}) \\ &+ \sum_r (i\phi_r + I\chi_r) \psi_{r\tau+\delta\uparrow} \psi_{r\tau+\delta\downarrow} + \sum_r (i\bar{\phi}_r + I\bar{\chi}_r) \bar{\psi}_{r\tau\uparrow} \bar{\psi}_{r\tau\downarrow} \end{aligned}$$

$$- \frac{\bar{t}}{2d} \sum_{\langle r,r' \rangle} (\psi_{r\tau+\delta\uparrow} \bar{\psi}_{r'\tau\uparrow} + \psi_{r\tau+\delta\downarrow} \bar{\psi}_{r'\tau\downarrow}) - \mu \sum_r (\psi_{r\tau+\delta\uparrow} \bar{\psi}_{r\tau\uparrow} + \psi_{r\tau+\delta\downarrow} \bar{\psi}_{r\tau\downarrow}) \Bigg]. \tag{B.2}$$

We perform a shift $\psi_{r\tau+\delta\sigma} \to \psi_{r\tau\sigma}$ and Fourier transform the second and third lines (we hide the index r to avoid extra notations):

$$\frac{1}{\beta}\sum_{\omega_n}\big[-i\omega_n e^{-i\delta\omega_n}\psi_{\omega_n\uparrow}\bar{\psi}_{-\omega_n\uparrow} - i\omega_n e^{-i\delta\omega_n}\psi_{\omega_n\downarrow}\bar{\psi}_{-\omega_n\downarrow} \\ +(i\phi + I\chi)\psi_{\omega_n\uparrow}\psi_{-\omega_n\downarrow} + (i\bar{\phi} + I\bar{\chi})\bar{\psi}_{\omega_n\uparrow}\bar{\psi}_{-\omega_n\downarrow} \\ -\hat{t}(\psi_{\omega_n\uparrow}\bar{\psi}_{-\omega_n\uparrow} + \psi_{\omega_n\downarrow}\bar{\psi}_{-\omega_n\downarrow}) - \mu(\psi_{\omega_n\uparrow}\bar{\psi}_{-\omega_n\uparrow} + \psi_{\omega_n\downarrow}\bar{\psi}_{-\omega_n\downarrow})\big]. \tag{B.3}$$

Here $\hat{t}$ is the hopping matrix. The sum over $\omega_n = \pi(2n+1)/\beta$ runs for n from $-\infty$ to ∞. We shift to the Nambu representation and write the above equation as

$$-\frac{1}{\beta}\begin{pmatrix}\psi_{\omega_n\uparrow}\\ \bar{\psi}_{\omega_n\downarrow}\end{pmatrix}^T\begin{pmatrix}-i\phi - I\chi & i\omega_n e^{-i\delta\omega_n} + \mu + \hat{t}\\ i\omega_n e^{i\delta\omega_n} - \mu - \hat{t} & i\bar{\phi} + I\bar{\chi}\end{pmatrix}\begin{pmatrix}\psi_{-\omega_n\downarrow}\\ \bar{\psi}_{-\omega_n\uparrow}\end{pmatrix}. \tag{B.4}$$

Here factors $e^{\pm i\delta\omega_n}$ are so called convergence factors.

The density of molecules after Wick contractions reads

$$\begin{aligned} n_r^m &= \frac{1}{\beta}\int d\tau \lim_{\delta\to+0}\langle\bar{\psi}_{r\tau+\delta\uparrow}\psi_{r\tau\uparrow}\bar{\psi}_{r\tau+\delta\downarrow}\psi_{r\tau\downarrow}\rangle \\ &= \frac{1}{\beta}\int d\tau \lim_{\delta\to+0}\langle\bar{\psi}_{r\tau+\delta\uparrow}\psi_{r\tau\uparrow}\rangle\langle\bar{\psi}_{r\tau+\delta\downarrow}\psi_{r\tau\downarrow}\rangle \\ &+ \frac{1}{\beta}\int d\tau\langle\bar{\psi}_{r\tau\downarrow}\bar{\psi}_{r\tau\uparrow}\rangle\langle\psi_{r\tau\uparrow}\psi_{r\tau\downarrow}\rangle. \end{aligned} \tag{B.5}$$

Since in Eq. (B.4) we shifted time we have also to shift time in these formulas. So the two terms are in order:

$$\frac{1}{\beta}\int d\tau\langle\bar{\psi}_{r\tau\uparrow}\psi_{r\tau\uparrow}\rangle\langle\bar{\psi}_{r\tau\downarrow}\psi_{r\tau\downarrow}\rangle$$

$$= \frac{1}{\beta^3}\sum_{\omega_{n1},\omega_{n2},\omega_{n3},\omega_{n4}}\int d\tau e^{i\tau(\omega_{n1}+\omega_{n2}+\omega_{n3}+\omega_{n4})}\langle\bar{\psi}_{r\omega_{n1}\uparrow}\psi_{r\omega_{n2}\uparrow}\rangle\langle\bar{\psi}_{r\omega_3\downarrow}\psi_{r\omega_4\downarrow}\rangle. \tag{B.6}$$

According to Eq. (B.4), $\omega_{n1} = -\omega_{n2}$ and $\omega_{n3} = -\omega_{n4}$. So we get

$$\frac{1}{\beta}\sum_{\omega_{n1}}\langle\bar{\psi}_{r-\omega_{n1}\uparrow}\psi_{r\omega_{n1}\uparrow}\rangle\frac{1}{\beta}\sum_{\omega_{n2}}\langle\bar{\psi}_{r\omega_{n2}\downarrow}\psi_{r-\omega_{n2}\downarrow}\rangle \equiv -\frac{1}{\beta}\sum_n G_{rr,12}(\omega_n)\frac{1}{\beta}\sum_n G_{rr,21}(\omega_n). \tag{B.7}$$

Analogously is treated the second term:

$$\frac{1}{\beta}\sum_{\omega_{n1}}\langle\bar{\psi}_{r\omega_{n1}\downarrow}\bar{\psi}_{r-\omega_{n1}\uparrow}\rangle\frac{1}{\beta}\sum_{\omega_{n2}}\langle\psi_{r\omega_{n2}\uparrow}\psi_{r-\omega_{n2}\downarrow}\rangle \equiv \frac{1}{\beta}\sum_n G_{rr,11}(\omega_n)\frac{1}{\beta}\sum_n G_{rr,22}(\omega_n). \tag{B.8}$$

The convergence factors are important for the sums to be convergent.

B.2 Calculation of the function $F(x)$

$$G = \frac{1}{\beta}\sum_{\omega_n}\int_{-1}^{1} dx \frac{\rho(x)}{|\phi|^2(J+\bar{U})^2/(J+S)^2 - (i\omega_n + \mu_1 + \bar{t}x)(i\omega_n - \mu_2 - \bar{t}x)}. \tag{B.9}$$

We perform Matsubara summation in this equation. To this end we first factorize the later to separate poles

$$\begin{aligned} F(x) = \frac{1}{\beta}\sum_{\omega_n} \frac{1}{|\phi|^2(J+\bar{U})^2/(J+S)^2 - (i\omega_n + \mu_1 + \bar{t}x)(i\omega_n - \mu_2 - \bar{t}x)} \\ = -\frac{1}{\beta}\sum_{\omega_n} \frac{1}{(i\omega_n - x_1)(i\omega_n - x_2)} \end{aligned} \tag{B.10}$$

with

$$x_{12} = \frac{-(\mu_1 - \mu_2) \pm \sqrt{(\mu_1 - \mu_2)^2 + 4[|\Phi|^2 + (\mu_1 + \bar{t}x)(\mu_2 + \bar{t}x)]}}{2}, \tag{B.11}$$

where we denoted $|\Phi|^2 = |\phi|^2(J+\bar{U})^2/(J+S)^2$. Now the summation can be performed easily by one of the standard procedures elucidated in the literature [3]:

$$F(x) = \frac{f(x_2) - f(x_1)}{\sqrt{(\mu_1 - \mu_2)^2 + 4[|\Phi|^2 + (\mu_1 + \bar{t}x)(\mu_2 + \bar{t}x)]}}, \quad f(x) = \frac{1}{e^{\beta x} + 1}. \tag{B.12}$$

By making a substitution $\mu_1 = \mu + h$, $\mu_2 = \mu - h$ we get

$$F(x) = \frac{f(x_2) - f(x_1)}{2\sqrt{|\Phi|^2 + (\mu + \bar{t}x)^2}}, \quad x_{12} = -h \pm \sqrt{|\Phi|^2 + (\mu + \bar{t}x)^2}. \tag{B.13}$$

B.3 Relation between Eq.(5.7) and Eq.(5.6)

There are at least two ways how to relate these two equations and these ways lead to the same relation.

B.3.1 First way

First we would like to integrate out bosons in Eq. (5.6). In the language of the Factional-integral representation and under the assumption that

bosonic fields are treated semi-classically from Eq. (5.6) we get the bosonic part contributing to the partition function

$$\begin{aligned}
&\int \prod_q d\bar{\phi}_q d\phi_q \exp\left\{ -\sum_q [(E_q^0 + 2\nu - 2\mu)\bar{\phi}_q\phi_q \right. \\
+ \quad & \left. g\sum_p (\bar{\phi}_q c_{-p+q/2\downarrow} c_{p+q/2\uparrow} + \phi_q c^\dagger_{p+q/2\uparrow} c^\dagger_{-p+q/2\downarrow})] \right\} \\
\sim \quad & \exp\left\{ \sum_{q,p,p'} \frac{g^2}{E_q^0 + 2\nu - 2\mu} c^\dagger_{p+q/2\uparrow} c^\dagger_{-p+q/2\downarrow} c_{-p'+q/2\downarrow} c_{p'+q/2\uparrow} \right\}. \quad \text{(B.14)}
\end{aligned}$$

Combining this with the rest of Eq.(5.6) we get the effective Hamiltonian

$$\begin{aligned}
\hat{H} \quad = \quad & \sum_{p\sigma} (\epsilon_p - \mu) \hat{c}^\dagger_{p\sigma} \hat{c}_{p\sigma} - U_{\rm bg} \sum_{p,p'} \hat{c}^\dagger_{p\uparrow} \hat{c}^\dagger_{-p\downarrow} \hat{c}_{-p'\downarrow} \hat{c}_{p'\uparrow} \\
- \quad & \sum_{q,p,p'} \frac{g^2}{E_q^0 + 2\nu - 2\mu} \hat{c}^\dagger_{p+q/2\uparrow} \hat{c}^\dagger_{-p+q/2\downarrow} \hat{c}_{-p'+q/2\downarrow} \hat{c}_{p'+q/2\uparrow}. \quad \text{(B.15)}
\end{aligned}$$

The interaction in the second line in real space has the form of screened Coulomb interaction with the Fermi screening length $\sim (2\nu - 2\mu)^{-1}$. For small temperatures when we are interested in small energies and small momenta we may expand

$$\frac{1}{2\nu - 2\mu + E_q^0} \approx \frac{1}{2\nu - 2\mu} - \frac{E_q^0}{(2\nu - 2\mu)^2}. \quad \text{(B.16)}$$

In real space in a lattice we have the correspondence $E_q^0 \to -\frac{\tilde{J}}{2d}\delta_{|r-r'|,1} + \tilde{J}\delta_{r,r'}$ with $\tilde{J}/2d \approx 1/2M$ for small momenta q, and Eq.(B.15) can be cast into the form of Eq.(5.7) with parameters

$$J = \frac{g^2\tilde{J}}{(2\nu - 2\mu)^2}, \;\; \bar{U} = U_{\rm bg} + \frac{g^2(2\nu - 2\mu - \tilde{J})}{(2\nu - 2\mu)^2}. \quad \text{(B.17)}$$

In fact, the term $g^2\tilde{J}/(2\nu - 2\mu)^2$ is the part of kinetic energy, so that the interaction between fermions is

$$\bar{U} = U_{\rm bg} + \frac{g^2}{2\nu - 2\mu}. \quad \text{(B.18)}$$

B.3.2 Second way

First, we rewrite Eq.(5.6) in real space:

$$\begin{aligned}\hat{H} &= \sum_{rr'\sigma}(-\bar{t}/2d\delta_{|r-r'|,1} - \mu\delta_{r,r'})\hat{c}^{\dagger}_{r\sigma}\hat{c}_{r'\sigma} \\ &+ \sum_{r}(-J/2d\triangle_{r,r'} + (2\nu - 2\mu)\delta_{r,r'})\hat{b}^{\dagger}_{r}\hat{b}_{r} \\ &- U_{\rm bg}\sum_{r}\hat{c}^{\dagger}_{r\uparrow}\hat{c}^{\dagger}_{r\downarrow}\hat{c}_{r\downarrow}\hat{c}_{r\uparrow} + g\sum_{r}[\hat{b}^{\dagger}_{r}\hat{c}_{r\downarrow}\hat{c}_{r\uparrow} + \hat{b}_{r}\hat{c}^{\dagger}_{r\uparrow}\hat{c}^{\dagger}_{r\downarrow}]. \end{aligned} \tag{B.19}$$

The functional-integral representation of this equation reads

$$Z = \int \mathcal{D}[\bar{\phi},\phi,\bar{\psi},\psi]e^{-\int_0^\beta d\tau A(\bar{\phi},\phi,\bar{\psi},\psi)} \tag{B.20}$$

with the action

$$\begin{aligned}A &= -\frac{J}{2d}\sum_{r,r'}\bar{\phi}_{r}\triangle_{r,r'}\phi_{r'} + \sum_{r}(2\nu - 2\mu)\bar{\phi}_{r}\phi_{r} + \frac{1}{U_{\rm bg}}\sum_{r}\bar{\chi}_{r}\chi_{r} \\ &+ \sum_{r}(\bar{\psi}_{r\tau\uparrow}\partial_{\tau}\psi_{r\tau\uparrow} + \bar{\psi}_{r\tau\downarrow}\partial_{\tau}\psi_{r\tau\downarrow}) + \sum_{r}\bar{\phi}_{r\tau}\partial_{\tau}\phi_{r\tau} \\ &+ \sum_{r}(g\phi_{r} + i\chi_{r})\bar{\psi}_{r\tau+\delta\uparrow}\bar{\psi}_{r\tau+\delta\downarrow} + \sum_{r}(g\bar{\phi}_{r} + i\bar{\chi}_{r})\psi_{r\tau\downarrow}\psi_{r\tau\uparrow} \end{aligned}$$

$$-\frac{\bar{t}}{2d}\sum_{\langle r,r'\rangle}(\bar{\psi}_{r\tau+\delta\uparrow}\psi_{r'\tau\uparrow} + \bar{\psi}_{r\tau+\delta\downarrow}\psi_{r'\tau\downarrow}) - \mu\sum_{r}(\bar{\psi}_{r\tau+\delta\uparrow}\psi_{r\tau\uparrow} + \bar{\psi}_{r\tau+\delta\downarrow}\psi_{r\tau\downarrow}). \tag{B.21}$$

We can perform unitary transformation $\phi \to -i\phi$ and $\chi \to i\chi$ as well as absorbing $g\phi \to \phi$ afterwards. We finally obtain

$$\begin{aligned}A_{\rm eff} = \int_0^\beta d\tau \Bigg\{ &\sum_{r}\frac{1}{g^2}\bar{\phi}_{r}\partial_{\tau}\phi_{r} + \sum_{r,r'}\frac{1}{g^2}\bar{\phi}_{r}\hat{v}^{-1}_{r,r'}\phi_{r'} + \frac{1}{U_{\rm bg}}\sum_{r,r}\bar{\chi}_{r}\chi_{r} \\ &- \ln\det\hat{\mathbf{G}}^{-1}\Bigg\} \end{aligned} \tag{B.22}$$

with

$$\hat{\mathbf{G}}^{-1} = \begin{pmatrix} -i\phi - \chi & \partial_{\tau} + \mu + \hat{t} \\ \partial_{\tau} - \mu - \hat{t} & i\bar{\phi} + \bar{\chi} \end{pmatrix}. \tag{B.23}$$

If we compare the above expression with Eq.(5.11) we get

$$S = \frac{g^2}{2\nu - 2\mu},\ \ \bar{U} = U_{\rm bg} + \frac{g^2}{2\nu - 2\mu},\ \ J = \frac{g^2\tilde{J}}{(2\nu - 2\mu)^2}. \tag{B.24}$$

B.4 Calculation of the action in the mean-field approximation

We denote $|\Phi|^2 = |\phi|^2(J+\bar{U})^2/(J+S)^2$ as in Appendix B.2. Then

$$A_{\text{eff}} = \beta\left(\frac{|\Phi|^2}{J+\bar{U}} - \int_{-1}^{1} dx\rho(x)\frac{1}{\beta}\sum_{\omega_n}\ln\left[(-i\omega_n + x_1)(i\omega_n - x_2)\right]\right). \quad \text{(B.25)}$$

Since (see similar calculations in [93])

$$\sum_{\omega_n}\ln(i\omega_n - a) = \ln\prod_{\omega_n}(i\omega_n - a) = \ln\cosh\left(\frac{a\beta}{2}\right) + const, \quad \text{(B.26)}$$

$$const_1 + const_2 = \beta\int_{-1}^{1} dx\rho(x)(\mu + \bar{t}x) \quad \text{(B.27)}$$

with $\omega_n = \frac{\pi(2n+1)}{\beta}$, we get Eq. (5.30).

B.5 Approximation in Eq.(5.32)

For simplicity we rescale $J \to J/a^2$. Eq.(5.32) can be written symbolically as

$$\hat{v}^{-1}\phi \approx b\phi + Jb^2(\hat{1} - \hat{J})\phi. \quad \text{(B.28)}$$

The second term, $\sim \nabla^2\phi$, is small for slowly varying fields ϕ. The above approximation is valid up to the second order. To show this we multiply the above equation by $\hat{v}$:

$$\phi \approx \left[b^{-1}\hat{1} - J(\hat{1} - \hat{J})\right]\left[b\hat{1} + Jb^2(\hat{1} - \hat{J})\right]\phi = \phi - J^2b^2(\hat{1} - \hat{J})^2\phi. \quad \text{(B.29)}$$

The second term is of the second order and our approximation is justified. Now we try to seek for the second order correction by writing

$$\hat{v}^{-1}\phi \approx b\phi + Jb^2(\hat{1} - \hat{J})\phi + x(\hat{1} - \hat{J})^2\phi \quad \text{(B.30)}$$

and calculate as in Eq.(B.29):

$$\begin{aligned}\phi &\approx \left[b^{-1}\hat{1} - J(\hat{1} - \hat{J})\right]\left[b\hat{1} + Jb^2(\hat{1} - \hat{J}) + x(\hat{1} - \hat{J})^2\right]\phi \\ &= \phi - J^2b^2(\hat{1} - \hat{J})^2\phi + xb^{-1}(\hat{1} - \hat{J})^2\phi. \end{aligned} \quad \text{(B.31)}$$

So we get $x = J^2 b^3$ and

$$\hat{v}^{-1}\phi \approx b[\hat{1} + Jb(\hat{1} - \hat{J}) + J^2 b^2 (\hat{1} - \hat{J})^2 + \ldots]\phi. \tag{B.32}$$

We proceed and obtain

$$\hat{v}^{-1}\phi = b \sum_{n=0} (Jb)^n (\hat{1} - \hat{J})^n \phi. \tag{B.33}$$

We want to calculate

$$\begin{aligned} \sum_{r,r'} \phi_r \hat{v}^{-1}_{r,r'} \phi_{r'} &= b \sum_{n=0} (Jb)^n (-1)^n \sum_{r,r'} \phi_r (\hat{J} - \hat{1})^n_{r,r'} \phi_{r'} \\ &= b \sum_{n=0} (Jb/2d)^n (-1)^n \sum_{r} \phi_r \Delta^n \phi_r, \end{aligned} \tag{B.34}$$

where

$$\Delta\phi_r = \sum_{j=1}^{d} [\phi_{r+ae_j} + \phi_{r-ae_j} - 2\phi_r] \tag{B.35}$$

is a "Nabla operator". Like in the continuum case we can "integrate by parts". Since fields vanish at the boundaries (trapped system), we arrive at

$$(-1)^n \sum_r \phi_r \Delta^n \phi_r = (-1)^n \sum_r \phi_r \nabla^{2n} \phi_r = \sum_r (\nabla^n \phi_r)^2 > 0, \tag{B.36}$$

where ∇ is a discrete "gradient operator". So all terms are positive:

$$\sum_{r,r'} \phi_r \hat{v}^{-1}_{r,r'} \phi_{r'} = b \sum_{n=0} (Jb/2d)^n \sum_r (\nabla^n \phi_r)^2. \tag{B.37}$$

B.6 Summation over Matsubara frequencies

Here we present a method to perform summation over the Matsubara frequencies in Eqs. (5.33),(5.34),(5.35). We define $z \equiv i\omega_n$. One can show that $G^{-1}(z) \cdot G^{-1}(z)$ is a Hermitian complex matrix. $G^{-1}(z) \cdot G^{-1}(z)$ is a Hermitian complex matrix ($i\Delta = i\phi + \chi \equiv i\bar{\phi} + \bar{\chi}$, ϕ is real, χ is complex):

$$\begin{aligned} &G^{-1}(z) G^{-1}(z) \\ &= \begin{pmatrix} -\Delta^2 + z^2 - \mu^2 - \hat{t}\mu - \mu\hat{t} - \hat{t}\hat{t} & \hat{t} i\Delta - i\Delta\hat{t} \\ \hat{t} i\Delta - i\Delta\hat{t} & -\Delta^2 + z^2 - \mu^2 - \hat{t}\mu - \mu\hat{t} - \hat{t}\hat{t} \end{pmatrix} \end{aligned} \tag{B.38}$$

and one can check that $(\hat{t}i\Delta - i\Delta\hat{t})^\dagger = \hat{t}i\Delta - i\Delta\hat{t}$, since Δ is real.

Any Hermitian matrix can be diagonalized by a unitary matrix:

$$(G^{-1}(z))^2 = \hat{U}\hat{\lambda}(z)\hat{U}^\dagger, \;\; U^\dagger = U^{-1}, \tag{B.39}$$

where $\hat{\lambda}$ is a diagonal (real) eigenvalue matrix. The equation for $\hat{\lambda}$ reads

$$\lambda_k = z^2 - z_k^2, \tag{B.40}$$

where z_k^2 are eigenvalues of $(G^{-1}(0))^2$. Reversing Eq. (B.39) we get

$$G(z) = \hat{U}\frac{1}{z^2 - z_k^2}\hat{U}^\dagger G^{-1}(z). \tag{B.41}$$

For the well behaved $g(x)$ (see [3])

$$-\frac{1}{\beta}\sum_n \frac{g(i\omega_n)}{\omega_n^2 + z_k^2} = \frac{1}{2\pi i}\oint dz \frac{g(z)f(z)}{z^2 - z_k^2} = \frac{g(z_k)f(z_k) - g(-z_k)f(-z_k)}{2z_k}, \tag{B.42}$$

where $f(z) = 1/(e^{\beta z}+1)$. This works for the blocks 11 and 22 of the Green's matrix in Eq. (5.12), since the function under the integral is well-behaved then. For the blocks 12 and 21 the sum is formally divergent since for large ω_n it behaves as $\sim 1/\omega_n$. To cure the problem one should introduce so called convergent factors [3,30].

Using the above formula we obtain finally

$$\frac{1}{\beta}\sum_n G_{rr}(\omega_n) = \sum_{km}\frac{\hat{U}_{rk}\hat{U}^\dagger_{km}}{2z_k}\{\tanh[-\beta z_k/2]G^{-1}_{mr}(0) - z_k i\sigma_2\}. \tag{B.43}$$

B.7 Quantum fluctuations

B.7.1 Second order

$$\mathcal{G}^{-1}$$

$$= \begin{pmatrix} \frac{1}{J+S-Jg_q} - B(-p) & -A(p) & iB(-p) & iA(p) \\ -A(p) & \frac{1}{J+S-Jg_q} - B(p) & iA(p) & iB(p) \\ iB(-p) & iA(p) & \frac{1}{J+S-U} + B(-p) & A(p) \\ iA(p) & iB(p) & A(p) & \frac{1}{J+S-U} + B(p) \end{pmatrix}. \tag{B.44}$$

$\underline{T=0}$

$$A(i\omega_n,q)=\sum_k\theta(E^-_{k+q})\frac{u_kv_ku_{k+q}v_{k+q}}{i\omega_n+E_k+E_{k+q}}+\sum_k\theta(E^-_k)\frac{u_kv_ku_{k+q}v_{k+q}}{-i\omega_n+E_k+E_{k+q}}$$
$$+\sum_k(\theta(E^-_k)-\theta(E^-_{k+q}))\frac{u_kv_ku_{k+q}v_{k+q}}{i\omega_n-E_k+E_{k+q}} \quad \text{(B.45)}$$

$$B(i\omega_n,q)=\sum_k\theta(E^-_{k+q})\frac{v_k^2v_{k+q}^2}{i\omega_n+E_k+E_{k+q}}+\sum_k\theta(E^-_k)\frac{u_k^2u_{k+q}^2}{-i\omega_n+E_k+E_{k+q}}$$
$$-\sum_k(\theta(E^-_k)-\theta(E^-_{k+q}))\frac{u_k^2v_{k+q}^2}{i\omega_n-E_k+E_{k+q}} \quad \text{(B.46)}$$

$\underline{T\neq 0}$

$$A(i\omega_n,q)=\sum_k(f^-_{k+q}-f^+_k)\frac{u_kv_ku_{k+q}v_{k+q}}{i\omega_n+E_k+E_{k+q}}+\sum_k(f^-_k-f^+_{k+q})\frac{u_kv_ku_{k+q}v_{k+q}}{-i\omega_n+E_k+E_{k+q}}$$
$$+\sum_k(f^-_k-f^-_{k+q})\frac{u_kv_ku_{k+q}v_{k+q}}{i\omega_n-E_k+E_{k+q}}+\sum_k(f^+_k-f^+_{k+q})\frac{u_kv_ku_{k+q}v_{k+q}}{i\omega_n+E_k-E_{k+q}}, \quad \text{(B.47)}$$

$$B(i\omega_n,q)=\sum_k(f^-_{k+q}-f^+_k)\frac{v_k^2v_{k+q}^2}{i\omega_n+E_k+E_{k+q}}+\sum_k(f^-_k-f^+_{k+q})\frac{u_k^2u_{k+q}^2}{-i\omega_n+E_k+E_{k+q}}$$
$$-\sum_k(f^-_k-f^-_{k+q})\frac{u_k^2v_{k+q}^2}{i\omega_n-E_k+E_{k+q}}-\sum_k(f^+_k-f^+_{k+q})\frac{v_k^2u_{k+q}^2}{i\omega_n+E_k-E_{k+q}}. \quad \text{(B.48)}$$

Here

$$E_k=\sqrt{\epsilon_k^2+|\Delta_0|^2},\ \ \epsilon_k=-t\cos(k)-\mu,$$
$$u_k=\sqrt{(1+\epsilon_k/E_k)/2},\ \ v_k=\sqrt{(1-\epsilon_k/E_k)/2}. \quad \text{(B.49)}$$

B.7.2 Quartic order

For low energies, we may regard ω_n and q to be small such that

$$B(-q,-i\omega_n)\approx B(-q,0)-i\omega_n d(q) \quad \text{(B.50)}$$

with

$$d(q)=\sum_k\left[\frac{\theta(E^-_k)\theta(E_k)\theta(E_{k-q})}{(E_k+E_{k-q})^2}-\frac{\theta(E^-_{k-q})\theta(-E_k)\theta(-E_{k-q})}{(E_k+E_{k-q})^2}\right]. \quad \text{(B.51)}$$

We notice here that

$$B(0) = \sum_k \frac{\theta(E_k^-)}{2E_k}, \;\; d(0) = \sum_k \frac{\theta(E_k^-)\mathrm{sign}(E_k)}{4E_k^2}, \;\; E_k = |\epsilon_k|. \tag{B.52}$$

The action can be expanded to the fourth order

$$\delta A_{\text{eff}} \approx A_0 + A_2 + A_4. \tag{B.53}$$

Here A_0 is the action originated from the saddle-point calculations, A_2 is the second order correction (which has been explored in the previous section). The third term is the fourth order correction and can be written as

$$A_4 = \frac{1}{2} \sum_{p_1,p_2,p_3} \delta\bar{\Delta}_{p_1}\delta\Delta_{p_2}\delta\bar{\Delta}_{p_3}\delta\Delta_{-p_1-p_2-p_3}\Gamma(p_1,p_2,p_3), \tag{B.54}$$

where the so called vertex function

$$\Gamma(p_1,p_2,p_3) = \frac{1}{\beta^2}\sum_k G_{12}^0(k)G_{21}^0(k-p_1)G_{12}^0(k-p_1-p_2)G_{21}^0(k-p_1-p_2-p_3) \tag{B.55}$$

has been introduced.

At low temperatures we may ignore momentum dependence in the vertex function (s-scattering):

$$\begin{aligned}
\Gamma(p_1,p_2,p_3) &\approx \Gamma(0,0,0) = \frac{1}{\beta}\sum_k [G_{12}^0(k)]^2[G_{21}^0(k)]^2 \\
&= \frac{1}{\beta}\int_{-1}^{1} dx \sum_{\omega_n} \frac{\rho(x)}{(i\omega_n - \mu_1 - \bar{t}x)^2(i\omega_n + \mu_2 + \bar{t}x)^2} \\
&= \int_{-1}^{1} dx\rho(x)\left[\frac{f(-\mu_2-\bar{t}x) - f(\mu_1+\bar{t}x)}{(\mu+\bar{t}x)^3}\right. \\
&+ \left. f'(\mu_1+\bar{t}x)\frac{1}{(\mu+\bar{t}x)^2} + f'(-\mu_2-\bar{t}x)\frac{1}{(\mu+\bar{t}x)^2}\right] \\
= \int_{-1}^{1} dx\rho(x)&\left[\frac{\theta(\mu_2+\bar{t}x)-\theta(-\mu_1-\bar{t}x)}{(\mu+\bar{t}x)^3} - \frac{\delta(\mu_1+\bar{t}x)}{(\mu+\bar{t}x)^2} - \frac{\delta(\mu_2+\bar{t}x)}{(\mu+\bar{t}x)^2}\right].
\end{aligned} \tag{B.56}$$

We denote $g_s \equiv \Gamma(0,0,0)$. By minimizing Eq. (B.54) with respect to the fields we get two equations:

$$\begin{aligned}
-i\omega_n d(q)\delta\phi_q - \omega_n d(q)\delta\chi_q &+ v^{-1}(q)\delta\phi_q - B(q)\delta\phi_q + iB(q)\delta\chi_q \\
&+ g_s\sum_{p_2,p_3}\delta\Delta_{p_2}\delta\bar{\Delta}_{p_3}\delta\Delta_{-p-p_2-p_3} = 0
\end{aligned} \tag{B.57}$$

and

$$i\omega_n d(q)\delta\chi_q - \omega_n d(q)\delta\phi_q \;+\; \frac{1}{J+S-\bar{U}}\delta\chi_q + B(q)\delta\chi_q + iB(q)\delta\phi_q - ig_s\sum_{p_2,p_3}\delta\Delta_{p_2}\delta\bar{\Delta}_{p_3}\delta\Delta_{-p-p_2-p_3} = 0. \quad \text{(B.58)}$$

From the second equation we eliminate $\delta\chi_q$:

$$\begin{aligned}\delta\chi_q &= \frac{1}{i\omega_n d(q) + \frac{1}{J+S-\bar{U}} + B(q)}[\omega_n d(q)\delta\phi_q - iB(q)\delta\phi_q \\ &+ ig_s\sum_{p_2,p_3}\delta\Delta_{p_2}\delta\bar{\Delta}_{p_3}\delta\Delta_{-p-p_2-p_3}] \approx \frac{\frac{1}{J+S-\bar{U}} + B(q) - i\omega_n d(q)}{(\frac{1}{J+S-\bar{U}} + B(q))^2} \\ &\times[\omega_n d(q)\delta\phi_q - iB(q)\delta\phi_q + ig_s\sum_{p_2,p_3}\delta\Delta_{p_2}\delta\bar{\Delta}_{p_3}\delta\Delta_{-p-p_2-p_3}] \\ &= \frac{\omega_n d(q)\delta\phi_q}{\frac{1}{J+S-\bar{U}} + B(q)} - \frac{iB(q)\delta\phi_q}{\frac{1}{J+S-\bar{U}} + B(q)} - \frac{\omega_n d(q)B(q)\delta\phi_q}{(\frac{1}{J+S-\bar{U}} + B(q))^2} \\ &+ \frac{ig_s}{\frac{1}{J+S-\bar{U}} + B(q)}\sum_{p_2,p_3}\delta\Delta_{p_2}\delta\bar{\Delta}_{p_3}\delta\Delta_{-p-p_2-p_3}. \quad \text{(B.59)}\end{aligned}$$

One also should substitute $\delta\Delta_q \approx 1/(1+(J+S-\bar{U})B(q))\delta\phi$. So finally

$$\begin{aligned}\delta\chi_q \;&\approx\; \frac{(J+S-\bar{U})\omega_n d(q)\delta\phi_q}{(1+(J+S-\bar{U})B(q))^2} - \frac{iB(q)\delta\phi_q}{\frac{1}{J+S-\bar{U}} + B(q)} \\ &+\; \frac{i(J+S-\bar{U})g_s}{(1+(J+S-\bar{U})B(q))^4}\sum_{p_2,p_3}\delta\Delta_{p_2}\delta\bar{\Delta}_{p_3}\delta\Delta_{-p-p_2-p_3}. \quad \text{(B.60)}\end{aligned}$$

Now we get an equation for $\delta\phi_q$:

$$\begin{aligned}&\frac{-i\omega_n d(q)}{(1+(J+S-\bar{U})B(q))^2}\delta\phi_q + \left[v^{-1}(q) - \frac{B(q)}{1+(J+S-\bar{U})B(q)}\right]\delta\phi_q \\ &+ \frac{g_s}{(1+(J+S-\bar{U})B(q))^4}\sum_{p_2,p_3}\delta\phi_{p_2}\delta\bar{\phi}_{p_3}\delta\phi_{-p-p_2-p_3} = 0. \quad \text{(B.61)}\end{aligned}$$

By absorbing prefactor in the first addant, we arrive at

$$\begin{aligned}&-i\omega_n d(q)\delta\phi_q + (1+(J+S-\bar{U})B(q))^2\left[v^{-1}(q)\right. \\ &\left.-\frac{B(q)}{1+(J+S-\bar{U})B(q)}\right]\delta\phi_q + g_s\sum_{p_2,p_3}\delta\phi_{p_2}\delta\bar{\phi}_{p_3}\delta\phi_{-p-p_2-p_3} = 0. \quad \text{(B.62)}\end{aligned}$$

B.8 Fermionic degrees of freedom

$$a(\omega) = -\frac{J}{\bar{t}}\int d\epsilon'\rho(\epsilon')\frac{\epsilon'}{\omega+\mu-\epsilon'-a(\omega)-2mb(\omega)\epsilon'/\hbar^2}, \quad \text{(B.63)}$$

$$b(\omega) = \frac{\hbar^2 J}{2m\bar{t}}\int d\epsilon'\rho(\epsilon')\frac{1}{\omega+\mu-\epsilon'-a(\omega)-2mb(\omega)\epsilon'/\hbar^2}. \quad \text{(B.64)}$$

The first integral is divergent, so we put a cut-off for momenta, $k < \Lambda_c \sim 2\pi/a$, where a is a lattice spacing.

To a good approximation

$$\begin{aligned} b(\omega_n) &\approx \frac{\hbar^2 J\rho(\tilde{\epsilon}_F)}{2m\bar{t}}\int_{-\infty}^{\infty} d\epsilon'\frac{1}{\omega_n+\mu-\epsilon'-a(\omega_n)-2mb(\omega_n)\epsilon'/\hbar^2} \\ &= -\frac{i\pi\hbar J\rho(\tilde{\epsilon}_F)}{2m\bar{t}(1+2mb(\omega_n)/\hbar^2)}\text{sgn}\left(\Im\frac{\omega_n+\mu-a(\omega_n)}{1+2mb(\omega_n)/\hbar^2}\right), \end{aligned} \quad \text{(B.65)}$$

$$a(\omega_n) \approx \frac{J}{\bar{t}}\int d\epsilon'\rho(\epsilon') - (\omega_n+\mu)\frac{2m}{\hbar^2}b(\omega_n), \;\; \tilde{\epsilon}_F = \Re\frac{\omega_n+\mu-a(\omega_n)}{1+2mb(\omega_n)/\hbar^2}. \quad \text{(B.66)}$$

Then

$$b(\omega_n) = \pm\frac{i\pi\hbar J\rho(\tilde{\epsilon}_F)}{2m\bar{t}(1+2mb(\omega_n)/\hbar^2)}. \quad \text{(B.67)}$$

From this we can calculate the real and imaginary parts

$$\Re b(\omega_n) = \pm\frac{\pi J\rho(\tilde{\epsilon}_F)}{\bar{t}}\frac{\Im b(\omega_n)}{(1+2m\Re b(\omega_n)/\hbar^2)^2+(2m\Im b(\omega_n)/\hbar^2)^2} \quad \text{(B.68)}$$

and

$$\Im b(\omega_n) = \pm\frac{\pi\hbar J\rho(\tilde{\epsilon}_F)}{2m\bar{t}}\frac{1+2m\Re b(\omega_n)/\hbar^2}{(1+2m\Re b(\omega_n)/\hbar)^2+(2m\Im b(\omega_n)/\hbar^2)^2}. \quad \text{(B.69)}$$

We introduce new variables x, y and A as

$$x = 1+2m\Re b(\omega_n)/\hbar^2, \;\; y = 2m\Im b(\omega_n)/\hbar^2, \;\; A = \pm\pi J\rho(\tilde{\epsilon}_F)/\bar{t}. \quad \text{(B.70)}$$

Then from Eq. (B.68) and (B.69)

$$x-1 = A\frac{y}{x^2+y^2}, \;\; y = A\frac{x}{x^2+y^2} \quad \text{(B.71)}$$

and thus we get two equations

$$y^2 = x^2-x, \;\; 4x^4-8x^3+5x^2-x = A^2. \quad \text{(B.72)}$$

There are two solutions to this polynomial as soon as $A^2 > 0$: $x_1 = 1 + z$, $x_2 = -z$ (for given A^2, z can be determined). In both cases $y^2 = z(z+1)$. Thus, in principle the imaginary and real parts of the self energy can be solved by solving the polynomial equation given above.

The fermionic propagator reads

$$\begin{aligned}\mathbf{G}(k,z) &= \frac{1}{z - \epsilon_{\mathbf{k}} + \mu - \tilde{\Sigma}(k,z)} = \frac{1}{z - \epsilon_k[1 + 2m/\hbar^2 b(z)] + \mu - a(z)} \\ &= \frac{1}{1 + 2m/\hbar^2 b(z)} \frac{1}{[z - \epsilon_k + \mu - \frac{J}{\bar{t}} \int d\epsilon' \rho(\epsilon')/(1 + 2m/\hbar^2 b(z))]}. \end{aligned} \quad \text{(B.73)}$$

We get

$$\mathbf{G}(k,z) \sim \frac{1}{z - \epsilon_k + \mu - yJ/A\bar{t} \int d\epsilon' \rho(\epsilon') - i(x-1)J/A\bar{t} \int d\epsilon' \rho(\epsilon')}. \quad \text{(B.74)}$$

It gives

$$\epsilon_F = \mu - yJ/A\bar{t} \int_0^{\epsilon_c} d\epsilon' \rho(\epsilon'), \quad \text{(B.75)}$$

$$\frac{1}{2\tau} = (x-1)J/A\bar{t} \int_0^{\epsilon_c} d\epsilon' \rho(\epsilon') = \frac{x-1}{y}[\mu - \epsilon_F]. \quad \text{(B.76)}$$

In these formulas $\epsilon_c = \hbar^2 \Lambda_c^2 / 2m \sim \bar{t}$ We see that the damping process does not change the mass, but rather shifts the chemical potential, which we denote as $\tilde{\mu} = \mu - yJ/A\bar{t} \int d\epsilon' \rho(\epsilon')$.

The theory should be consistent when $\bar{t} \to 0$. In this case the damping rate $1/2\tau$ vanishes. Let us check this. The density of states behaves as $\rho(\epsilon) \sim m^{d/2} \epsilon^{(d-2)/2} \sim \frac{\epsilon^{(d-2)/2}}{\bar{t}^{d/2}}$. Then we have

$$\mu - \epsilon_F \sim y \frac{\int_0^{\epsilon_c} d\epsilon' \rho(\epsilon')}{\rho(\epsilon_F)} \sim y \frac{\bar{t}^{d/2}}{\epsilon_F^{(d-2)/2}}. \quad \text{(B.77)}$$

If $\bar{t} \to 0$, we suppose $\epsilon_F \to \mu$. From this it follows

$$A \sim \bar{t}^{-d/2-1}, \;\; y \sim z \sim A^{1/2}, \;\; \mu - \epsilon_F \sim \bar{t}^{d/2-1/2}. \quad \text{(B.78)}$$

Hence, $1/2\tau$ vanishes as soon as $\bar{t} \to 0$ in dimensions higher than one.

Bibliography

[1] E. Abrahams, P. W. Anderson, D. C. Licciardello, and T. V. Ramakrishnan. Scaling theory of localization: Absence of quantum diffusion in two dimensions. *Phys. Rev. Lett.*, 42:673, 1979.

[2] O. Alon, A. Sakmann, and L. Cederbaum. Continuous configuration-interaction for condensates in a ring. *Europhys. Lett.*, 67:8, 2004.

[3] A. Altland and B. Simons. *Condensed Matter Field Theory*. Cambridge University Press, New York, 2006.

[4] E. Altman and A. Auerbach. Oscillating superfluidity of bosons in optical lattice. *Phys. Rev. Lett.*, 89:250404, 2002.

[5] E. Altman, E. Demler, and M. Lukin. Probing many-body states of ultracold atoms via noise correlations. *Phys. Rev. A*, 70:013603, 2004.

[6] M. H. Anderson, J. R. Ensher, M. R. Matthews, C. E. Wieman, and E. A. Cornell. Observation of bose-einstein condensation in a dilute atomic vapor. *Science*, 269:198, 1995.

[7] P. W. Anderson. Absence of diffusion in certain random lattices. *Phys. Rev.*, 109:1492, 1958.

[8] M. R. Andrews, M.-O. Mewes, N. J. van Druten, D. S. Durfee, D. M. Kurn, and W. Ketterle. Direct, nondestructive observation of a bose condensate. *Science*, 273:84, 1996.

[9] M. R. Andrews, M.-O. Mewes, N. J. van Druten, D. S. Durfee, D. M. Kurn, and W. Ketterle. Direct, nondestructive observation of a bose condensate. *Science*, 273:84, 1996.

[10] J. R. Anglin and W. Ketterle. Bose-einstein condensation of atomic gases. *Nature*, 416:211, 2002.

[11] N. W. Ashcroft and N. D. Mermin. *Solid State Physics*. Thomson Learning, Philadelphia, 1976.

[12] C. Ates and K. Ziegler. Quantum phases in mixtures of fermionic atoms. *Phys. Rev. A*, 71:063610, 2005.

[13] A. Auerbach. *Interacting electrons and quantum magnetism*. Springer-Verlag, New York, 1994.

[14] J. Bardeen, L. N. Cooper, and J. R. Schrieffer. Theory of superconductivity. *Phys. Rev*, 108:1175, 1957.

[15] M. Bartenstein, A. Altmeyer, S. Riedl, S. Jochim, C. Chin, J. H. Denschlag, and R. Grimm. Crossover from a molecular bose-einstein condensate to a degenerate fermi gas. *Phys. Rev. Lett.*, 92:120401, 2004.

[16] P. F. Bedaque, H. Caldas, and G. Rupak. Phase separation in asymmetrical fermion superfluids. *Phys. Rev. Lett.*, 91:247002, 2003.

[17] J. Billy, V. Josse, Z. Zuo, A. Bernard, B. Hambrecht, P. Lugan, D. Clment, L. Sanchez-Palencia, P. Bouyer, and A. Aspect. Direct observation of anderson localization of matter waves in a controlled disorder. *Nature*, 453:891, 2008.

[18] I. Bloch, J. Dalibard, and W. Zwerger. Many-body physics with ultracold gases. *Phys. Rev. Mod.*, 80:885, 2008.

[19] C. C. Bradley, C. A. Sackett, J. J. Tollett, and R. G. Hulet. Evidence of bose-einstein condensation in an atomic gas with attractive interactions. *Phys. Rev. Lett.*, 75:1687, 1995.

[20] G. M. Bruun, O. F. Syljuasen, K. G. L. Pedersen, B. M. Andersen, E. Demler, and A. S. Sorensen. Antiferromagnetic noise correlations in optical lattices. *Phys. Rev. A*, 80:033622, 2009.

[21] R. Bücker, A. Perrin, S. Manz, T. Betz, C. Koller, T. Plisson, J. Rottmann, T. Schumm, and J. Schmiedmayer. Single-particle-sensitive imaging of freely propagating ultracold atoms. *New Journal of Physics*, 11:103039, 2009.

[22] K. Byczuk and D. Vollhardt. Correlated bosons on a lattice: Dynamical mean-field theory for bose-einstein condensed and normal phases. *Phys. Rev. B*, 77:235106, 2008.

[23] M. L. Chiafalo, S. J. J. M. F. Kokkelmans, J. N. Milstein, and M. J. Holland. Signatures of resonance superfluidity in a quantum fermi gas. *Phys. Rev. A*, 88:090402, 2002.

[24] A. Cho. Insights flow from ultracold atoms that mimic superconductors. *Science*, 319:1180, 2008.

[25] K. B. Davis, M. O. Mewes, M. R. Andrews, N. J. van Druten, D. S. Durfee, D. M. Kurn, and W. Ketterle. Bose-einstein condensation in a gas of sodium atoms. *Phys. Rev. Lett.*, 75:3969, 1995.

[26] C. A. R. S. de Melo. When fermions become bosons: Pairing in ultracold gases. *Phys. Today*, 61:45, 2008.

[27] C. A. R. S. de Melo, M. Randeria, and J. R. Engelbrecht. Crossover from bcs to bose superconductivity: Transition temperature and time-dependent ginsburg-landau theory. *Phys. Rev. Lett.*, 71:3202, 1993.

[28] C. A. R. S. de Melo, M. Randeria, and J. R. Engelbrecht. Bcs to bose crossover: Broken-symmetry state. *Phys. Rev. B*, 55:15153, 1997.

[29] B. DeMarco, C. Lannert, S. Vishveshwara, and T. Wei. Structure and stability of mott-insulator shells of bosons trapped in an optical lattice. *Phys. Rev. A*, 71:063601, 2005.

[30] R. Diener, R. Sensarma, and M. Randeria. Quantum fluctuations in the superfluid state of the bcs-bec crossover. *Phys. Rev. A*, 77:023626, 2008.

[31] R. A. Duine and H. T. C. Stoof. Atommolecule coherence in bose gases. *Phys. Rep.*, 396:115, 2004.

[32] A. Einstein. Quantentheorie des einatomigen idealen gases. *Sitzungsber. Preu. Akad. Wiss.*, page 261, 1924.

[33] L. M. Falicov and J. C. Kimball. Simple model for semiconductor-metal transitions: Smb6 and transition-metal oxides. *Phys. Rev. Lett.*, 22:997, 1969.

[34] P. Farkaovsk. Ground-state properties of fermionic mixtures with mass imbalance in optical lattices. *Europhysics Letters*, 84:37010, 2008.

[35] R. Feynman. Atomic theory of the two-fluid model of liquid helium. *Phys. Rev.*, 94:262, 1954.

[36] O. Fialko, A. Gammal, and K. Ziegler. Spin-1/2 fermions with attractive interaction in an optical lattice. *arXiv:0904.4334v1 [cond-mat.quant-gas]*, 2009.

[37] O. Fialko, C. Moseley, and K. Ziegler. Interacting bosons in an optical lattice: Bose-einstein condensation and mott insulator. *Phys. Rev. A*, 75:053616, 2007.

[38] O. Fialko and K. Ziegler. Functional-integral representation of atomic mixture. In W. Janke and A. Pelster, editors, *Proceedings of the 9th International Conference "Path integrals. New trends and perspectives"*. World Scientific, 2007.

[39] O. Fialko and K. Ziegler. Anderson localization in correlated fermionic mixtures. *EPL*, 85:60003, 2009.

[40] O. Fialko and K. Ziegler. Noise correlations of a strongly attractive spin-1/2 fermi gas in an optical lattice. *J. Phys. B: At. Mol. Opt. Phys.*, 43:065304, 2010.

[41] M. P. A. Fisher, P. B. Weichman, G. Grinstein, and D. S. Fisher. Boson localization and the superfluid-insulator transition. *Phys. Rev. B*, 40:546, 1989.

[42] J. K. Freericks and V. Zlati. Exact dynamical mean-field theory of the falicov-kimball model. *Rev. Mod. Phys.*, 75:1333, 2003.

[43] U. Gavish and Y. Castin. Matter-wave localization in disordered cold atom lattices. *Phys. Rev. Lett.*, 95:020401, 2005.

[44] F. Gerbier, S. Trotzky, S. Fölling, U. Schnorrberger, J. D. Thompson, A. Widera, I. Bloch, L. Pollet, M. Troyer, B. Capogrosso-Sansone, N. V. Prokofev, and B. V. Svistunov. Expansion of a quantum gas released from an optical lattice. *Phys. Rev. Lett.*, 101:155303, 2008.

[45] F. Gerbier, S. Trotzky, S. Flling, U. Schnorrberger, J. D. Thompson, A. Widera, I. Bloch, L. Pollet, M. Troyer, B. Capogrosso-Sansone, N. V. Prokof'ev, , and B. V. Svistunov. Expansion of a quantum gas released from an optical lattice. *Phys. Rev. Lett.*, 101:155303, 2008.

[46] F. Gerbier, A. Widera, S. Fölling, O. Mandel, T. Gericke, and I. Bloch. Interference pattern and visibility of a mott insulator. *Phys. Rev. A*, 72:053606, 2005.

[47] F. Gerbier, A. Widera, S. Fölling, O. Mandel, T. Gericke, and I. Bloch. Phase coherence of an atomic mott insulator. *Phys. Rev. Lett.*, 95:050404, 2005.

[48] S. Giorgini, L. Pitaevskii, and S. Stringari. Theory of ultracold atomic fermi gases. *Phys. Rev. Mod.*, 80:1215, 2008.

[49] M. Greiner and S. Fölling. Optical lattices. *nature*, 453:736, 2008.

[50] M. Greiner, O. Mandel, T. Esslinger, T. W. Hänsch, and I. Bloch. Quantum phase transition from a superfluid to a mott insulator in a gas of ultracold atoms. *Nature*, 415:39, 2002.

[51] G. F. Gribakin and V. V. Flambaum. Calculation of the scattering length in atomic collisions using the semiclassical approximation. *Phys. Rev. A*, 48:546, 1993.

[52] M. Haque and H. T. C. Stoof. Pairing of a trapped resonantly interacting fermion mixture with unequal spin populations. *Phys. Rev. A*, 74:011602(R), 2006.

[53] M. Holland, S. J. J. M. F. Kokkelmans, M. L. Chiofalo, and R. Walser. Resonance superfluidity in a quantum degenerate fermi gas. *Phys. Rev. Lett.*, 87:120406, 2001.

[54] S. D. Huber, E. Altman, H. P. Büchler, and G. Blatter. Dynamical properties of ultracold bosons in an optical lattice. *Phys. Rev. B*, 75:085106, 2007.

[55] A. Imambekov, I. E. Mazets, D. S. Petrov, V. Gritsev, S. Manz, S. Hofferberth, T. Schumm, E. Demler, and J. Schmiedmayer. Density ripples in expanding low-dimensional gases as a probe of correlations. *Phys. Rev. A*, 80:033604, 2009.

[56] M. Iskin and C. A. R. S. de Melo. Fermi-fermi mixtures in the strong-attraction limit. *Phys. Rev. A*, 77:013625, 2008.

[57] M. Iskin and C. J. Williams. Population-imbalanced fermions in harmonically trapped optical lattices. *Phys. Rev. A*, 78:011603(R), 2008.

[58] D. Jaksch, C. Bruder, J. I. Cirac, C. W. Gardiner, and P. Zoller. Cold bosonic atoms in optical lattices. *Phys. Rev. Lett.*, 81:3108, 1998.

[59] R. Kanamoto, H. Saito, and M. Ueda. Quantum phase transition in one-dimensional bose-einstein condensates with attractive interactions. *Phys. Rev. A*, 67:013608, 2003.

[60] T. Kennedy, E. H. Lieb, and B. S. Shastry. The xy model has long-range order for all spins and all dimensions greater than one. *Phys. Rev. Lett.*, 61:2582, 1988.

[61] E. Kogan. Quasi-localization and quasi-mobility edge for light atoms mixed with heavy ones. *Eur. Phys. J. B*, 61:181, 2008.

[62] W. Kohn. Analytic properties of bloch waves and wannier functions. *Phys. Rev.*, 115:809, 1959.

[63] J. M. Kosterlitz and D. J. Thouless. Ordering, metastability and phase transitions in two-dimensional systems. *J. Phys. C*, 6:1181, 1973.

[64] L. D. Landau and E. M. Lifshitz. *Mechanics*. Pergamon, Oxford, 1977. trans. J.B. Sykes and W.H. Read.

[65] L. D. Landau and E. M. Lifshitz. *Quantum mechanics (Non-relativistic Theory)*. Pergamon, Oxford, 1977. trans. J.B. Sykes and W.H. Read.

[66] D.-S. Lee, C.-Y. Lin, and R. J. Rivers. Derivation of hydrodynamics for the gapless mode in the bec-bcs crossover from the exact one-loop effective action. *Phys. Rev. Lett.*, 98:020603, 2007.

[67] A. Leggett. The relation between the gross-pitaevskii and bogoliubov descriptions of a dilute bose gas. *New J. Phys.*, 5:103, 2003.

[68] A. Leggett. *Quantum Liquids*. Oxford University Press, Oxford, 2006.

[69] A. J. Leggett. Cooper pairing in spin-polarized fermi systems. *J. Phys. (Paris), Colloq.*, 41:7, 1980.

[70] A. J. Leggett. Bose-einstein condensation in the alkali gases: Some fundamental concepts. *Rev. Mod. Phys.*, 73:307, 2001.

[71] A. J. Leggett. Quantum liquids. *Science*, 319:1203, 2008.

[72] M. Lewenstein, A. Sanpera, V. Ahufinger, B. Damski, A. Sen, and U. Sen. Ultracold atomic gases in optical lattices: mimicking condensed matter physics and beyond. *Advances in Physics*, 56:243, 2007.

[73] J. Liang, J. Liang, and W. Liu. Quantum phase transition of condensed bosons in optical lattices. *Phys. Rev. A*, 68:043605, 2003.

[74] A. MacKinnon and B. Kramer. The scaling theory of electrons in disordered solids: Additional numerical results. *Z.Phys. B*, 53:1, 1983.

[75] M. M. Maska, R. Lemaski, J. K. Freericks, and C. J. Williams. Pattern formation in mixtures of ultracold atoms in optical lattices. *Phys. Rev. Lett.*, 101:060404, 2008.

[76] C. Moseley, O. Fialko, and K. Ziegler. Interacting bosons in an optical lattice. *Ann. Phys. (Berlin)*, 17:48, 2008.

[77] C. Moseley and K. Ziegler. N-component bose-einstein condensation in an optical lattice: Destruction of the condensate and quasiparticle properties. *Laser Physics*, 15:469, 2004.

[78] A. Mosk, S. Kraft, M. Mudrich, K. Singer, W. Wohlleben, R. Grimm, and M. Weidemller. Mixture of ultracold lithium and cesium atoms in an optical dipole trap. *Appl. Phys. B*, 73:791, 2001.

[79] P. Nozieres and S. Schmitt-Rink. Bose condensation in an attractive fermion gas: From weak to strong coupling superconductivity. *J. Low. Temp. Phys.*, 59:195, 1985.

[80] Y. Ohashi and A. Griffin. Bcs-bec crossover in a gas of fermi atoms with a feshbach resonance. *Phys. Rev. Lett.*, 89:130402, 2002.

[81] Y. Ohashi and A. Griffin. Superfluid transition temperature in a trapped gas of fermi atoms with a feshbach resonance. *Phys. Rev. A*, 67:033603, 2003.

[82] S. Ospelkaus, C. Ospelkaus, O. Wille, M. Succo, P. Ernst, K. Sengstock, and K. Bongs. Localization of bosonic atoms by fermionic impurities in a three-dimensional optical lattice. *Phys. Rev. Lett.*, 96:180403, 2006.

[83] G. B. Partridge, W. Li, R. I. Kamar, Y. Liao, and R. G. Hulet. Pairing and phase separation in a polarized fermi gas. *Science*, 311:503, 2006.

[84] C. Pethick and H. Smith. *Bose-Einstein Condensation in Dilute Gases*. Cambridge University Press, Cambridge, 2002.

[85] J. L. Pichard and G. Sarma. Finite size scaling approach to anderson localization. *J. Phys. C*, 14:L127, 1981.

[86] L. P. Pitaevskii and S. Stringari. *Bose-Einstein Condensation*. Claredron, Oxford, 2003.

[87] V. Popov. *Functional Integrals in Quantum Field Theory and Statistical Physics*. Reidel, Dordrecht, 1983.

[88] W. H. Press, S. A. Teukolsky, W. T. Vetterling, and B. P. Flannery. *Numerical Recipes in Fortran 90*. Cambridge University Press, New York, 1996.

[89] D. Quinney. *An introduction to the Numerical Solution of Differential Equations*. Wiley, Letchworth, 1997.

[90] G. Roati, C. DErrico, L. Fallani, M. Fattori, C. Fort, M. Zaccanti, G. Modugno, M. Modugno, and M. Inguscio. Anderson localization of a non-interacting boseeinstein condensate. *Nature*, 453:895, 2008.

[91] R. Roth and K. Burnett. Superfluidity and interference pattern of ultracold bosons in optical lattice. *Phys. Rev. A*, 67:031602(R), 2003.

[92] S. Sachdev. *Quantum Phase Transitions*. Cambridge University Press, Cambridge, 1999.

[93] G. Sarma. On the influence of a uniform exchange field acting on the spins of the conduction electrons in a superconductor. *J. Phys. Chem. Solids*, 24:1029, 1963.

[94] D. Shirkov. 60 years of broken symmetries in quantum physics (from the bogoliubov theory of superfluidity to the standard model). *arXiv:0903.3194v2 [physics.hist-ph]*, 2009.

[95] K. Slevin and T. Ohtsuki. Corrections to scaling at the anderson transition. *Phys. Rev. Lett.*, 82:382, 1999.

[96] D. M. Stamper-Kurn and W. Ketterle. In R. Kaiser, C. Westbrook, and F. David, editors, *Coherent Atomic Matter Waves, Les Houches 1999 Summer School, Session LXXII in 1999*. Springer, New York, 2001.

[97] C. A. Stan, M. W. Zwierlein, C. H. Schunck, S. M. F. Raupach, and W. Ketterle. Observation of feshbach resonances between two different atomic species. *Phys. Rev. Lett.*, 93:143001, 2004.

[98] D. A. Steck. Paralyzed by disorder. *Nature*, 453:12, 2008.

[99] E. Timmermans, P. Tommasini, M. Hussein, and A. Kerman. *Phys. Rep.*, 315:199, 1999.

[100] D. van Oosten, P. van der Straten, and H. T. C. Stoof. Quantum phases in an optical lattice. *Phys. Rev. A*, 63:053601, 2001.

[101] F. J. Wegner. Electrons in disordered systems. scaling near the mobility edge. *Z. Phys. B*, 25:327, 1976.

[102] F. Werner, O. Parcollet, A. Georges, and S. R. Hassan. Interaction-induced adiabatic cooling and antiferromagnetism of cold fermions in optical lattices. *Phys. Rev. Lett.*, 95:056401, 2005.

[103] E. Wille, F. M. Spiegelhalder, G. Kerner, D. Naik, A. Trenkwalder, G. Hendl, F. Schreck, R. Grimm, T. G. Tiecke, J. T. M. Walraven, S. J. J. M. F. Kokkelmans, E. Tiesinga, and P. S. Julienne. Exploring an ultracold fermi-fermi mixture: Interspecies feshbach resonances and scattering properties of ^{6}li and ^{4}0k. *Phys. Rev. Lett.*, 100:053201, 2008.

[104] C. Yang. Concept of off-diagonal long-range order and the quantum phases of liquid he and of superconductors. *Rev. Mod. Phys.*, 34:694, 1962.

[105] M. Zaccanti, C. DÉrrico, F. Ferlaino, G. Roati, M. Inguscio, and G. Modugno. Control of the interaction in a fermi-bose mixture. *Phys. Rev. A*, 74:041605(R), 2006.

[106] A. Zee. *Quantum field theory in a nutshell*. Princeton University Press, Princeton, 2003.

[107] K. Ziegler. Condensation of a hard-core bose gas. *Phys. Rev. A*, 62:23611, 2000.

[108] K. Ziegler. Phase transitions of a bose gas in an optical lattice. *Laser Physics*, 13:587, 2002.

[109] K. Ziegler. Phase transitions of a bose gas in an optical lattice. *Laser Physics*, 13:587, 2002.

[110] K. Ziegler. Two-component bose gas in an optical lattice at single-particle filling. *Phys. Rev. A*, 68:053602, 2003.

[111] K. Ziegler. Spin-1/2 fermions: crossover from weak to strong attractive interaction. *Laser Physics*, 15:650, 2005.

[112] K. Ziegler. Disorder physics in mixtures of fermionic atoms. *Laser Physics*, 16:699, 2006.

[113] K. Ziegler and O. Fialko. Anderson localization in atomic mixtures. In W. Janke and A. Pelster, editors, *Proceedings of the 9th International Conference "Path integrals. New trends and perspectives"*. World Scientific, 2007.

Acknowledgements

I would like to express my gratitude to all those who gave me the possibility to complete this thesis.

I am deeply indebted to my supervisor Prof. Dr. Klaus Ziegler for his suggestions and encouragement during this work. He enhanced my level significantly and lifted my interest in theoretical physics. I am grateful to Prof. Dr. Gert-Ludwig Ingold for acting as second referee of this thesis. Many thanks to Prof. Dr. Achim Wixforth and Prof. Dr. Liviu Chioncel for their kind agreement to act as board members during the oral exam.

I thank Dr. Christopher Moseley for fruitful collaboration and discussions, Dr. Andreas Sinner and Eder Annibale for proofreading parts of this thesis, their suggestions and friendship. I acknowledge DAAD for providing me the opportunity to visit Universitade de Sao Paulo (USP) and collaborate with Prof. Dr. Arnaldo Gammal. He provided me warm welcome at USP and introduced to me powerfull numerical tricks. I am also grateful to Dr. Ofir E. Alon for supervision of me at the Minerva summer school in Dresden.

I would like to thank also the members of TP I and TP II groups and other friends for stimulation and pleasant atmosphere, in particular Dr. S. Denisov, Dr. A. Ponomarev, Dr. L. Chotorlishvili, Dr. C. Gorini, Dr. M. Fadlallah and A. Hill.

Curriculum vitae

Name	Oleksandr Fialko
Date of birth	16.03.83
Place of birth	Tetiiv, Ukraine
2004	Bachelor in Physics, diploma with honor Taras Shevchenko National University of Kiev, Ukraine
2005	Master in Physics, diploma with honor Taras Shevchenko National University of Kyiv, Ukraine
2005-2010	Scientific researcher University of Augsburg, Germany